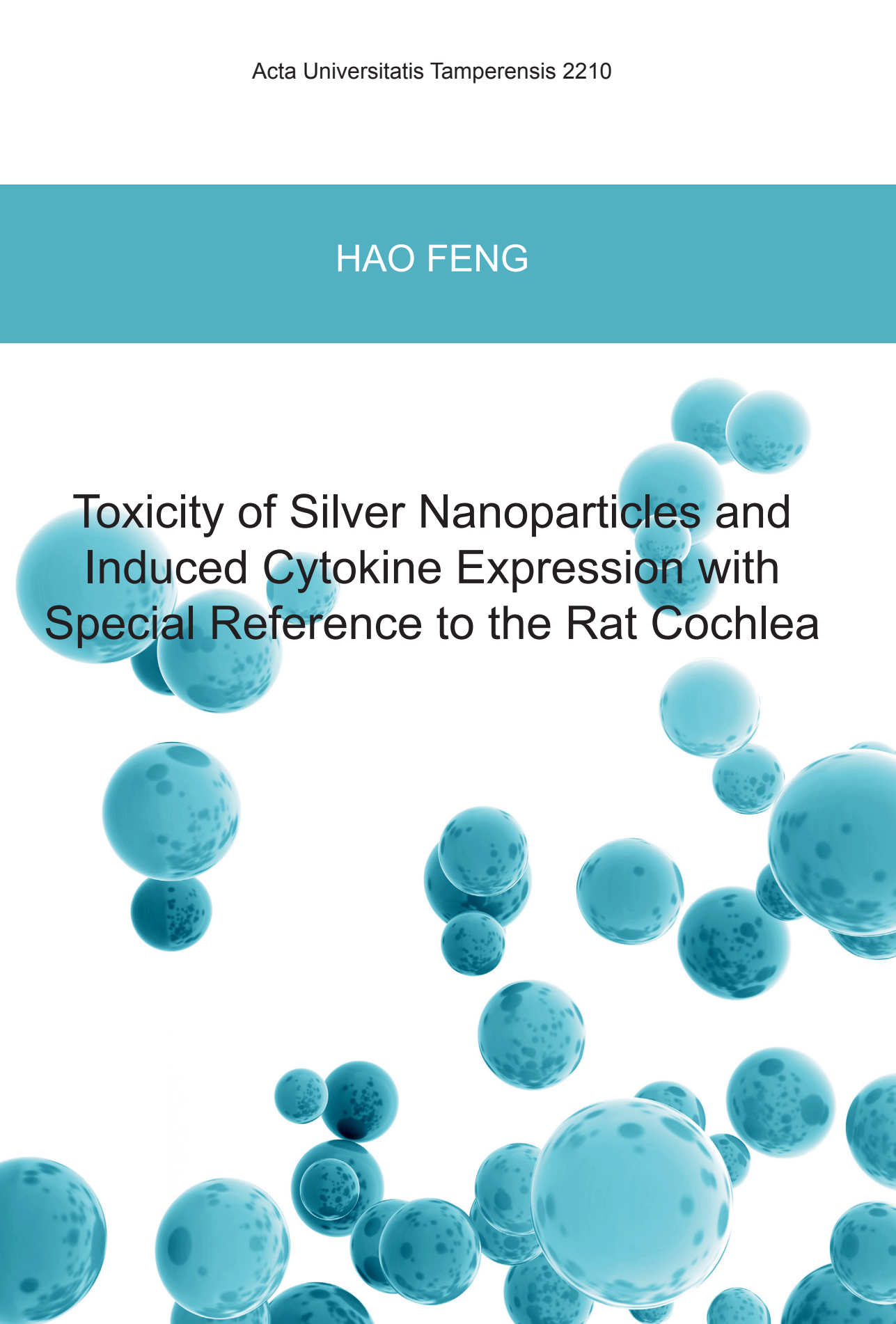


HAO FENG

Toxicity of Silver Nanoparticles and
Induced Cytokine Expression with
Special Reference to the Rat Cochlea





HAO FENG

Toxicity of Silver Nanoparticles and
Induced Cytokine Expression with
Special Reference to the Rat Cochlea



ACADEMIC DISSERTATION

To be presented, with the permission of
the Board of the School of Medicine of the University of Tampere,
for public discussion in the auditorium of Finn-Medi 5,
Biokatu 12, Tampere, on 14 November 2016, at 12 o'clock.

UNIVERSITY OF TAMPERE

HAO FENG

Toxicity of Silver Nanoparticles and
Induced Cytokine Expression with
Special Reference to the Rat Cochlea

Acta Universitatis Tamperensis 2210
Tampere University Press
Tampere 2016

ACADEMIC DISSERTATION
University of Tampere, School of Medicine
Finland

Supervised by

Docent Jing Zou
University of Tampere
Finland
Professor Emeritus Ilmari Pyykkö
University of Tampere
Finland

Reviewed by

Docent Maija Vihinen-Ranta
University of Jyväskylä
Finland
Docent Saku Sinkkonen
University of Helsinki
Finland

The originality of this thesis has been checked using the Turnitin OriginalityCheck service in accordance with the quality management system of the University of Tampere.

Copyright ©2016 Tampere University Press and the author

Cover design by
Mikko Reinikka

Acta Universitatis Tamperensis 2210
ISBN 978-952-03-0227-6 (print)
ISSN-L 1455-1616
ISSN 1455-1616

Acta Electronica Universitatis Tamperensis 1710
ISBN 978-952-03-0228-3 (pdf)
ISSN 1456-954X
<http://tampub.uta.fi>

Suomen Yliopistopaino Oy – Juvenes Print
Tampere 2016



Contents

| | |
|--|----|
| Abstract | 6 |
| Abbreviations | 7 |
| List of original publications | 8 |
| 1 Introduction | 9 |
| 2 Review of the literature | 10 |
| 2.1 Medical applications and toxicity of Ag NPs | 10 |
| 2.1.1 Applications of Ag NPs in medicine..... | 10 |
| 2.1.1.1 Ag NPs in diagnostics | 10 |
| 2.1.1.2 Ag NPs in anti-microbial therapy..... | 11 |
| 2.1.2 Interaction between Ag NPs and the immune system..... | 13 |
| 2.1.2.1 Components of the immune system | 13 |
| 2.1.2.2 Macrophage polarisation..... | 14 |
| 2.1.2.3 Response of the immune system to Ag NPs | 15 |
| 2.1.3 Toxicity of Ag NPs and the mechanism of toxicity | 17 |
| 2.1.3.1 Evaluation of toxicity of Ag NPs..... | 17 |
| 2.1.3.2 Fate of Ag NPs within the cells | 19 |
| 2.1.3.3 Toxicological mechanism of Ag NPs..... | 20 |
| 2.2 Basic knowledge of the inner ear | 21 |
| 2.2.1 Physiology of the cochlea..... | 21 |
| 2.2.2 Analogy of the blood-inner ear barrier and the blood-brain barrier..... | 23 |
| 2.2.3 Evaluation of permeability of the blood-inner ear barrier..... | 24 |
| 2.3 Inner ear immunology..... | 25 |
| 2.3.1 Deviation in understanding of the inner ear being an immunologically privileged organ..... | 25 |
| 2.3.2 Communication between the inner ear and the immune system..... | 26 |
| 2.3.3 Topical immune response in the inner ear | 27 |
| 3 Aims of the current research..... | 30 |
| 4 Material and methods | 31 |
| 4.1 Ag NPs | 31 |

| | | |
|-------|--|----|
| 4.2 | Evaluation of toxicity of Ag NPs in BALB/c 3T3 cells using NRU, WST-1, ATP measurement, and PI staining assays (I)..... | 31 |
| 4.3 | Delivery of Ag NPs <i>in vivo</i> and animal assignments..... | 32 |
| 4.4 | Distribution of Ag NPs in the rat ear shown by micro CT (II)..... | 33 |
| 4.5 | Evaluation of Ag NPs-induced permeability change of the biological barriers in the rat ear using MRI (I)..... | 33 |
| 4.6 | ABR measurements (I)..... | 34 |
| 4.7 | Sample preparation for immunostaining..... | 35 |
| 4.8 | Analysis of cytokine expression (III and IV)..... | 35 |
| 4.8.1 | Antibodies and chromogen..... | 35 |
| 4.8.2 | Immunofluorescence staining..... | 36 |
| 4.8.3 | Immunostaining visualized by DAB..... | 36 |
| 4.9 | Cell death detection (III)..... | 37 |
| 4.10 | Confocal and light microscopies..... | 37 |
| 4.11 | Data analysis and statistics..... | 38 |
| 5 | Results..... | 39 |
| 5.1 | Ag NPs toxicity in BALB/c 3T3 cells (I)..... | 39 |
| 5.2 | Transportation of Ag NPs from the rat middle ear to the inner ear (II)..... | 39 |
| 5.3 | Permeability augmentation of the biological barriers in the rat ear and hearing loss caused by Ag NPs (I)..... | 39 |
| 5.4 | Accumulation of hyaluronic acid in the rat cochlea exposed to Ag NPs (III)..... | 40 |
| 5.5 | Ag NPs elevated the levels of CD68, MCP1, TLR4, A20, and RNF11 (IV)..... | 40 |
| 5.6 | Cell death in the rat cochlea exposed to Ag NPs (III)..... | 41 |
| 6 | Discussion..... | 42 |
| 6.1 | General comments..... | 42 |
| 6.2 | Correlation of Ag NPs toxicity in BALB/c 3T3 cells and the rat cochlea (I and III)..... | 43 |
| 6.3 | Transportation of Ag NPs from the rat middle ear to the inner ear (II)..... | 44 |
| 6.4 | Ag NPs augmented the permeability of biological barriers in the rat ear and caused hearing loss (I)..... | 44 |
| 6.5 | Accumulation of hyaluronic acid in the rat cochlea exposed to Ag NPs (III)..... | 45 |
| 6.6 | Involvement of ubiquitin-editing protein A20 in modulating inflammation in the rat cochlea associated with Ag NPs-induced CD68 up-regulation and TLR4 activation (IV)..... | 45 |
| 6.7 | Future directions..... | 46 |

| | | |
|---|--|----|
| 7 | Summary and conclusions | 47 |
| 8 | Acknowledgements | 48 |
| 9 | References..... | 50 |
| | Full texts for original publications | 67 |

Abstract

Silver nanoparticles (Ag NPs) display potent anti-bacterial, anti-viral, and anti-fungal activities and are reportedly efficient in treating otitis media. However, increasing applications of Ag NPs have raised concerns as to their potential adverse effects on human health. In particular, possible toxicological mechanism in the cochlea is not well documented.

The current study aimed to: 1) show the *in vitro-in vivo* correlation of Ag NPs toxicity using BALB/c 3T3 cells and the rat cochlea; 2) demonstrate the transportation of Ag NPs from the rat middle ear to the inner ear; 3) investigate the impact of Ag NPs on the permeability of biological barriers in the rat ear; and 4) elucidate the molecular mechanism of Ag NPs-induced functional change in the biological barriers in the rat cochlea.

The results demonstrated that BALB/c 3T3 cells *in vitro* were more sensitive to Ag NPs as much as 1 000 times than the rat cochlear cells *in vivo*. After transtympanic injection, Ag NPs accessed into the rat inner ear through the round and oval windows detected with micro computed tomography (CT). Ag NPs caused significant changes to the permeability of biological barriers in the skin of the external ear canal, mucosa of the middle ear, and inner ear detected using gadolinium-enhanced magnetic resonance imaging (MRI) as well as hearing loss detected using auditory brainstem response (ABR) measurements. Ag NPs caused accumulation of hyaluronic acid in the rat cochlea and up-regulated the expressions of CD68, TLR4, MCP1, A20, and RNF11 in the striae basal cells, spiral ligament fibrocytes, and non-sensory supporting cells of Corti's organ, which was implicated in the enhanced immune activity. The rat ear model might be expanded to study other engineered nanomaterials in nanotoxicology research.

Abbreviations

| | |
|-------------------|--|
| A20 | tumour necrosis factor-alpha-induced protein 3 |
| ABR | auditory brainstem response |
| Ag NPs | silver nanoparticles |
| ATP | adenosine triphosphate |
| CD44 | cluster of differentiation 44 |
| CD68 | cluster of differentiation 68 |
| CT | computed tomography |
| DAB | 3, 3'-diaminobenzidine |
| DAPI | 4', 6-diamidino-2-phenylindole |
| dB | decibel |
| dH ₂ O | deionised water |
| Erk1/2 | extracellular signal-regulated kinases 1/2 |
| HEPES | 4-(2-hydroxyethyl)-1-piperazineethanesulfonic acid |
| IC ₅₀ | half maximal inhibitory concentration |
| JNK | c-Jun N-terminal kinases |
| M1 | classically activated macrophage |
| M2 | alternatively activated macrophage |
| MCPs | monocyte chemotactic proteins |
| MRI | magnetic resonance imaging |
| NPs | nanoparticles |
| NRU | neutral red uptake |
| PBS | phosphate buffered saline |
| PI | propidium iodide |
| Rac1 | Ras-related C3 botulinum toxin substrate 1 |
| RNF11 | RING finger protein 11 |
| ROS | reactive oxygen species |
| TGF- β | transforming growth factor-beta |
| Th1 | Type 1 T helper cells |
| Th2 | Type 2 T helper cells |
| TLRs | toll-like receptors |
| TNFRs | tumour necrosis factor receptors |
| TNF- α | tumour necrosis factor-alpha |
| TUNEL | terminal deoxynucleotidyl transferase deoxyuridine triphosphate nick end labelling |
| VCAM1 | vascular cell adhesion molecule 1 |

List of original publications

The dissertation is based on the following original publications which are referred to in the text by Roman numerals I-IV:

I. Zou J, **Feng H**, Mannerström M, Heinonen T, Pyykkö I. Toxicity of silver nanoparticle in rat ear and BALB/c 3T3 cell line. *J Nanobiotechnology* 2014; 12 (1): 52.

II. Zou J, Hannula M*, Misra S*, **Feng H***, Labrador RH, Aula AS, Hyttinen J, Pyykkö I. Micro CT visualization of silver nanoparticles in the middle and inner ear of rat and transportation pathway after transtympanic injection. *J Nanobiotechnology* 2015; 13 (1): 5.

III. **Feng H**, Pyykkö I, Zou J. Hyaluronan up-regulation is linked to renal dysfunction and hearing loss induced by silver nanoparticles. *Eur Arch Otorhinolaryngol* 2015; 272 (10): 2629-2642.

IV. **Feng H**, Pyykkö I, Zou J. Involvement of ubiquitin-editing protein A20 in modulating inflammation in rat cochlea associated with silver nanoparticles-induced CD68 up-regulation and TLR4 activation. *Nanoscale Res Lett* 2016; 11 (1): 240.

*Equal contributor

The original publications are reproduced in this dissertation with the permission from copyright holders.

1 Introduction

Nanoparticles (NPs) have been widely used in a variety of areas and Ag NPs are one of the most prevalent metal NPs due to their favourable physicochemical and biological properties (*e.g.*, high ratio of surface to volume, excellent optical features, high electrical and thermal conductivity, and extraordinary anti-microbial capability). They have been increasingly applied in health care, mechanics, optics, electronics, biomedical sciences, chemical industries, pharmacy and pharmaceuticals, and energy science. However, their potential safety issues have become a serious public health concern, and the exact toxicological mechanism is not known in detail. Currently, various methods are used to evaluate the toxicity of Ag NPs but they are quite complicated and vary from case to case when applied. Recently, alternative methods (*e.g.*, tissue equivalents) have been accepted in the *in vivo* study for regulatory purpose in Europe. Therefore, the European Union 7th framework programme large-scale integrating project NanoValid is launched and attempts to establish the new reference methods in nanotoxicology (<http://www.nanovalid.eu/>).

The rat ear was identified as an excellent multifunctional model in pharmacological and toxicological research due to its unique and sophisticated structure that houses epithelia (*e.g.*, the skin of the external ear canal and mucosa of the middle ear), sensory organs (*e.g.*, Corti's organ, crista ampullaris, saccule maculae, and utricle maculae), neurons of the cranial nerves (*e.g.*, spiral ganglion and Scarpa's ganglion), a vascular bed similar to the brain, and a biological barrier (the blood-inner ear barrier) that limit the entry of hazardous substances to avoid compromising the vulnerable homeostasis of the inner ear (Zou et al., 2011; Zou, 2012). Therefore, it is assumed that not only can the impact on the skin of the external ear canal and mucosa of the middle ear be shown but also potential hazardous effects on the sensory organs can be evaluated using gadolinium-enhanced MRI with high accuracy and sensitivity when Ag NPs cross the biological barriers and enter the inner ear. In addition, possible effects on hearing caused by Ag NPs can be studied by ABR measurements, and possible alterations in cytokine expression in the inner ear exposed to Ag NPs can be identified by immunostaining using confocal microscopy.

The current study aimed to evaluate the toxicity of Ag NPs by comparing its effects on BALB/c 3T3 and rat cochlear cells. Moreover, the transportation and distribution of Ag NPs in the rat ear after transtympanic injection was demonstrated using micro CT and the impact of Ag NPs on the permeability of biological barriers in the rat ear was shown using gadolinium-enhanced MRI. Finally, the molecular mechanism of Ag NPs-induced functional change in the biological barriers in the rat cochlea was elucidated using immunohistochemistry.

2 Review of the literature

2.1 Medical applications and toxicity of Ag NPs

The term 'NPs', also known as ultrafine particles, is used to define particles that are between 1-100 nanometres in at least one dimension (Kreuter, 1978). In this size range, their properties are altered in a distinctive manner compared with their fine and coarse particle counterparts. Due to the rapid development of state-of-the-art science and technology, the production and application of NPs have increased dramatically over the last few decades. The NPs have attracted great attention due to their unique properties (*e.g.*, small size, diverse shape, and high ratio of surface to volume). NPs exhibit tremendous significance in a large number of areas, such as health care, mechanics, optics, electronics, biomedical sciences, chemical industries, pharmacy and pharmaceuticals, and energy science. Thus, many novel interdisciplinary and frontier subjects have been established including nanomedicine, nanoelectronics, nanobiology, nanotoxicology, and nanopharmaceuticals. NPs are considered an effective and efficient solution to many challenges that we are confronted with in medicine, energy shortage, and environmental pollution (Murday et al., 2009).

2.1.1 Applications of Ag NPs in medicine

Currently, over 1 000 nano-based consumer products are being used in our daily lives, and approximately 25 % of them are related to Ag NPs (Liu and Hurt, 2010). Ag NPs are of enormous interest because of their unique physicochemical and biological properties, such as small size, diverse shape, high ratio of surface to volume, excellent optical features, high electrical and thermal conductivity, and extraordinary anti-microbial capability, in comparison with conventional silver. These traits can be incorporated into electronic components, biological transducers, cosmetics, water purification systems, and anti-microbial agents. Therefore, Ag NPs have been one of the most popular and commercialized NPs over the past few decades (Li et al., 2006; Li et al., 2011; Sintubin et al., 2012). In particular, Ag NPs are widely used in medicine including prostheses, external fixator pins, bone cement, and wound dressings (Kwakye-Awuah et al., 2008; Zheng et al., 2010).

2.1.1.1 Ag NPs in diagnostics

Nucleic acids are indispensable for gene replication, transcription, and translation. It has been reported that many diseases are associated with abnormalities of nucleic acids. Currently, nucleic acid-based detection techniques are receiving much attention because of their potential in gene expression profiling and diagnosing diseases in early stages. Routine nucleic acid-based detection techniques, such as PCR, RT-PCR, Northern and Southern blotting, rely primarily on either fluorescent or radioactive probes (Marti et al., 2007; Sassolas et al., 2008; Kolpashchikov, 2010; Lien and Lee, 2010). However, these methods are time-, labor-, and expense-consuming and have relatively poor reproducibility that is dependent on laboratory settings, protocols, and the proficiency and experience of the technicians. Therefore, using these methods, it is difficult to achieve ideal accuracy in clinical diagnosis, and there is a great need to generate highly efficient nucleic acid detection assays with good accuracy.

NPs can be modified to interact with bioactive molecules, and this can be used to develop novel nucleic acid detection assays (Niemeyer et al., 2003a; Niemeyer et al., 2003b). Ag NPs that are functionalized with polysaccharides are potential fluorescence-sensing detectors that can be used for nucleic acid identification. An oligonucleotide sequence test using human immunodeficiency virus as a model system revealed that polysaccharide-functionalized Ag NPs effectively absorbed and quenched dye-labelled single-stranded DNA through potent hydrogen bonding and weak electrostatic attraction, and this could be used to efficiently distinguish complementary nucleic acid sequences from those that were mismatched with high selectivity and good reproducibility at room temperature (Yan et al., 2015). Moreover, Ag NPs have been used as Raman scattering enhancers for nucleotide sequence analysis. Zhang et al. developed an approach to detect specific nucleotide sequences using a combination of mixed silver nanoprobe and Raman reporter molecules by a sandwich hybridization assay (Zhang et al., 2011). In addition, it has been indicated that Ag NPs are capable of boosting the fluorescence of dye-labelled DNA in the presence of the poly-cation spermine, and this can be used to detect and quantify the DNA level at sub-picomolar concentrations without any enzymatic enhancement (Annink and Gill, 2014). Ag NPs have also been used successfully to increase the sensitivity of DNA microarrays by engineering the substrate to elevate the fluorophores' radiative rate through metal-enhanced fluorescence (Sabanayagam and Lak-owicz, 2007).

2.1.1.2 Ag NPs in anti-microbial therapy

Silver and its compounds have been used to treat inflammatory diseases (*e.g.*, ulcers, burns, sepsis, and acute epididymitis) since ancient Greek and Roman times due to their anti-microbial capabilities. However, their applications are hindered by relatively poor efficacies (Egger et al., 2009). Ag NPs appear to be more active and effective than conventional silver as they may reach microbes in the closest proximity at the highest ratio of surface to volume, thus leading to extraordinary anti-microbial capability (Wigginton et al., 2010). Previous studies showed that three possible mechan-

isms were involved in Ag NPs-induced activity against a broad spectrum of microbes including Gram-negative bacteria (*e.g.*, *Escherichia coli* and *Pseudomonas aeruginosa*), Gram-positive bacteria (*e.g.*, *Bacillus subtilis* and *Staphylococcus aureus*), fungi (*e.g.*, *Aspergillus flavus* and *Aspergillus niger*), and viruses (*e.g.*, influenza virus, human-parainfluenza virus, and hepatitis B virus) (Sondi and Salopek-Sondi, 2004; Kim et al., 2007; Lu et al., 2008; Baram-Pinto et al., 2009; Rai et al., 2009; Lara et al., 2010; Sahu et al., 2014): (1) Ag NPs combine and interact with membrane structures (*e.g.*, plasma membrane, membranous organelles, and viral envelopes), alter membrane permeability and disruption transport, leading to a change in osmotic pressure, and ultimately killing microbes (Sondi and Salopek-Sondi, 2004; Morones et al., 2005; Lara et al., 2011; Park et al., 2011); (2) Ag NPs cause oxidative stress that reflects an imbalance between the generation of reactive oxygen species (ROS) (*e.g.*, superoxide anion, hydrogen peroxide, and hydroxyl radical) and the consumption of antioxidants (*e.g.*, Vitamin C and E), thus leading to lipid peroxidation, protein denaturation, mitochondrial dysfunction, and long-lasting DNA condensation (Feng et al., 2000; Sondi and Salopek-Sondi, 2004; Kim et al., 2007; Li et al., 2011; Mohammadzadeh, 2012); and (3) Ag⁺ released from Ag NPs have the ability to reduce adenosine triphosphate (ATP) production and disrupt DNA replication (Cumberland and Lead, 2009).

Microbes that adhere to an interface can accumulate to be communities and form microbial biofilms. Microbial biofilms are the structured aggregation of microbes encased in a self-produced polymeric conglomeration that is composed of polysaccharides, proteins, and extracellular DNAs. They might account for over 80 % of microbial infection and consequential damage in humans (O'Toole et al., 2000; Cos et al., 2010; Flemming and Wingender, 2010). It has been reported that microbial biofilms severely hamper the penetration of antibiotics and immune components into microbes, and thus they exhibit as much as 1 000 times higher drug resistance than microbes themselves (Davies, 2003). Ag NPs can inhibit the formation of new biofilms, disrupt the preformed biofilms, penetrate through the mature biofilms, and eliminate biofilms thoroughly (Markowska et al., 2013; Cavalieri et al., 2014). Therefore, Ag NPs are widely used in prostheses, external fixator pins, bone cement, and wound dressings (Kwakye-Awuah et al., 2008; Zheng et al., 2010).

Chronic otitis media, characterized by recurrent infection causing otalgia and purulent otorrhea, is still a significant public health issue affecting 0.5 %-43 % of any given population in developing and developed countries (Monasta et al., 2012). Usually, empirical antibiotic therapy is considered a mainstay of otitis media treatment. However, antibiotics are not always efficient due to the emergence of multidrug resistant strains of bacteria (*e.g.*, methicillin-resistant *Staphylococcus aureus*). Significantly, microbial biofilm formation has recently been reported in the middle ears of patients with chronic otitis media all over the world (Hall-Stoodley et al., 2006; Lampikoski et al., 2012; Nguyen et al., 2013; Gu et al., 2014; Wessman et al., 2015). Ag NPs may overcome some disadvantages of antibiotics (*e.g.*, drug resistance and side effects to other systems) and eliminate microbes as well as microbial biofilm with high efficacy in the ear therapy through distinctive mechanisms, such as inducing ROS generation

and modulating immune function, which are completely different from routine therapy with antibiotics (Keren et al., 2013; Xu et al., 2013; Xu et al., 2015). Therefore, Ag NPs may be useful in the treatment of diseases in the ear with microbial biofilm formation and any potential multidrug resistant strains of bacteria that represent a big challenge for conventional antibiotics.

The anti-bacterial activity of Ag NPs is affected by their physicochemical properties including size, shape, ratio of surface to volume, surface charge, dissolution rate, stability in the diluent, status of aggregation and agglomeration, and coating modification (Franci et al., 2015). Smaller Ag NPs adhere to and penetrate the cell membrane and reach the nucleus more easily due to their large surface area, compared with the larger Ag NPs (Sondi and Salopek-Sondi, 2004). In addition, smaller Ag NPs induce production of superoxide peroxide in the mitochondrial membrane and lead to a more remarkable lethal effect (Yang et al., 2012). The positively charged Ag NPs exhibit higher anti-bacterial activity because of their more potent capabilities to combine with the negatively charged plasma membrane compared with the negatively charged and neutral Ag NPs (El Badawy et al., 2011). The aggregated and agglomerated Ag NPs may cripple the anti-bacterial capabilities because the decreased surface area will disturb the efficacy of Ag NPs on bacteria (Zhou et al., 2012). Ag NPs that are stabilized by polymers (*e.g.*, poly-vinylpyrrolidone) and surfactants (*e.g.*, sodium dodecyl sulphate and Tween 80) display enhanced anti-bacterial capabilities (Huynh and Chen, 2011). Furthermore, the electronic structure, redox potential, and surface plasmon resonance of Ag NPs may influence ROS generation to affect their anti-bacterial capabilities (Fatima et al., 2015).

2.1.2 Interaction between Ag NPs and the immune system

2.1.2.1 Components of the immune system

The immune system is responsible for eliminating non-self components (*e.g.*, mutant cells), maintaining homeostasis (*e.g.*, clearance of senescent and injured cells), and defending against foreign hazardous factors (*e.g.*, lipopolysaccharides) to exert its roles in immune surveillance, immune homeostasis, and immune defence. It consists of the innate immune system and the adaptive immune system.

Innate immunity elicited by the innate immune system is non-specific, prompt, and temporary, and it acts as the first line of defence in safeguarding the body. It relies primarily on the pattern recognition receptors (*e.g.*, toll-like receptors, cytoplasmic NOD-like receptors, intracellular retinoic acid-inducible gene-I-like receptors, transmembrane C-type lectin receptors, and absent in melanoma 2-like receptors) that are expressed on the natural immunocompetent cells (*e.g.*, monocyte-macrophage system and dendritic cells) to specifically recognize and combine with the conservative molecular patterns including pathogen-associated molecular patterns (*e.g.*, lipopoly-

saccharides, peptidoglycan, mannose, nucleic acid, and lipoteichoic acid) that are correlated with microbial pathogens or cellular stressors and damage-associated molecular patterns (*e.g.*, uric acid, ATP, and heat shock protein) that are correlated with cellular components released during cell damage. Innate immunity plays a critical role in responding to stressors at the early stage (Mogensen, 2009; Chen and Nunez, 2010).

Adaptive immunity elicited by the adaptive immune system is antigen-dependent, obtuse, and permanent, and it only occurs when the body is irritated by an antigen encountered before. It is comprised of cellular immunity and humoral immunity, the former of which is controlled by T cells, while the latter is mediated by a variety of immunoglobulins that are synthesized and released by B cells. Adaptive immunity plays an indispensable role in recalling and responding to an antigen that the body encountered before (da Rocha Junior et al., 2013).

The two immune systems communicate with each other at both the cellular and molecular levels. On one hand, several immunocompetent cell populations (*e.g.*, B1 cell, $\gamma\delta$ T cell, and natural killer cell) that possess distinctively functional characteristics are known to bridge the two immune systems. On the other hand, cytokines [*e.g.*, interferon- γ and interleukins (ILs)] produced by immunocompetent cells (*e.g.*, macrophage and T cell) create crosstalk between the two immune systems in either a paracrine or an autocrine manner through cell-to-cell or cell-to-extracellular matrix contacts (Getz, 2005).

2.1.2.2 Macrophage polarisation

Leukocytes are the essential cellular components in directing the host immune defence. Among them, macrophages are the predominant cells in response to stimuli at the early stage. Macrophages were initially depicted as phagocytic cells by Metchnikoff in the 19th century (Cavaillon, 2011). Today, it is widely accepted that macrophages play an indispensable role in antigen presentation, adaptive immunity, tissue repair, and wound healing. Abundant evidence shows that macrophages are not only critical for immune function but also important for inflammation, tumorigenesis, and metabolism. Therefore, macrophages are suggested to be the cells that orchestrate numerous biological activities in the organism (Rees, 2010).

Macrophages originate and differentiate from either monocytes or myeloid progenitor cells in the peripheral blood, and they can be classified into two subpopulations: (1) infiltrating macrophages that are recruited and migrate from the systemic circulation into local tissues and (2) tissue-resident macrophages that exist in local tissues during the steady state (Geissmann et al., 2010). The innate immune response triggered by macrophages that occurs in the skin, lungs, and mucosal systems is an important defensive pathway at the early stage when the body confronts stressors. Plasticity and flexibility are the key features of macrophages and reflect their activation states. The different phenotypes of macrophages are generated to meet their div-

erse roles in multiple biological activities (Scott et al., 2014; Das et al., 2015).

Activated macrophages have distinctively functional phenotypes that are similar to the Type 1/Type 2 T helper cells (Th1/Th2) polarisation paradigm of T lymphocytes and therefore can be defined as M1 (classically activated) and M2 (alternatively activated). M1 macrophages induced by Th1 signature cytokines [*e.g.*, interferon- γ and tumour necrosis factor- α (TNF- α)], which are relevant to toll-like receptor (TLR)-dependent signaling, have the ability of up-regulating genes involved in cell-biased immunity, enhancing antigen presentation (*e.g.*, major histocompatibility complex-II), and producing a diverse array of inflammatory cytokines (*e.g.*, IL-1 β and TNF- α), while M2 macrophages induced by Th2 signature cytokines (*e.g.*, IL-4, IL-10, IL-13, and immune complexes) play an important role in immune suppression (*e.g.*, IL-10), anti-inflammation (*e.g.*, IL-6 and IL-10), and wound healing [*e.g.*, transforming growth factor- β (TGF- β) and vascular endothelial growth factor] (Mantovani et al., 2004; Murray and Wynn, 2011; Cao and He, 2013). In particular, M2 macrophages can be categorized into three subpopulations that are dependent on their diverse roles. M2a macrophages induced by IL-4 or IL-13 are implicated in advanced stages of tissue regeneration and wound healing as well as immune regulation. M2c macrophages induced by IL-10 participate in immune suppression, anti-inflammation, and tissue remodelling. Interestingly, M2b macrophages induced by immune complexes play a dual role in immune response as M2b macrophages not only release large amounts of anti-inflammatory cytokines, such as IL-10 but also secrete pro-inflammatory cytokines including IL-1 β and TNF- α (Kharraz et al., 2013).

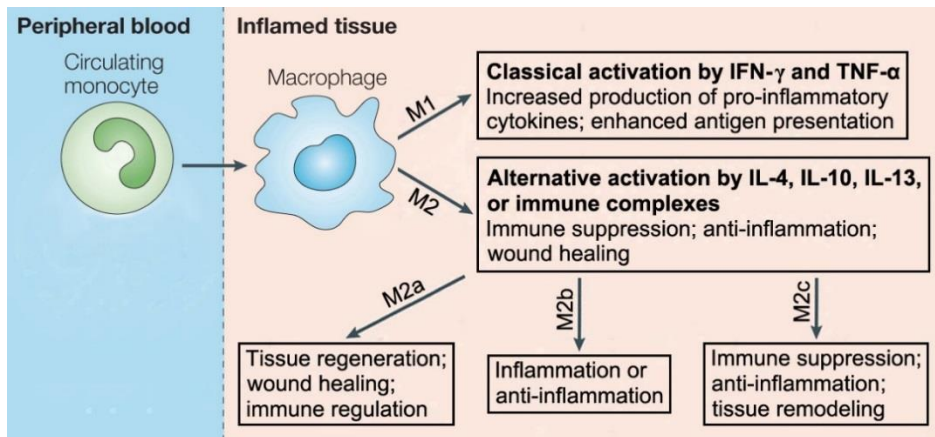


Fig. 1 Illustration of macrophage polarisation. M1: classically activated macrophage; M2: alternatively activated macrophage; IFN- γ : interferon- γ ; TNF- α : tumour necrosis factor- α ; IL-4: interleukin-4; IL-10: interleukin-10; IL-13: interleukin-13. Modified based on Gordon and Taylor (Gordon and Taylor, 2005).

2.1.2.3 Response of the immune system to Ag NPs

As a foreign material, NPs will be recognized and processed by the immune system upon entering the body, and therefore the response of the immune system to the NPs must be considered. An appropriate immune response (*e.g.*, synthesis and secretion of immunoglobulins and mobilisation of immunocompetent cells) is important for host defence against the hazardous stimulus. However, an excessive or uncontrolled immune response is clearly detrimental to the host and will result in dysregulated biological activities (*e.g.*, inflammation). At least three circumstances are ascertained during the interplay between the immune system and NPs. First, the immune stimulatory effect initiated by the NPs directly affects innate and adaptive immunity to trigger immune-mediated destruction or rejection and eliminate NPs ultimately, thus leading to the maintenance of homeostasis as a defensive behaviour. Second, the immune toxicity resulted from the NPs impairs the immune system and causes a pathological change. Third, the biocompatibility of NPs to the immune system denotes that NPs do not have influence on or interact with the immune system. It should be noted that the elemental composition and properties of NPs (*e.g.*, size, shape, hydrophobicity, and surface charge), the approach of administration and dosage of NPs, and the duration of exposure to NPs can affect the interaction between the immune system and NPs, and therefore the consequential effects vary from case to case (Dobrovolskaia and McNeil, 2007; Zolnik et al., 2010; Boraschi et al., 2012; Moyano et al., 2012).

Usually, the immune modulatory effect is used to describe a desired or an expected change of immune activity. NPs are evaluated for their immune stimulatory potential based on their multiple capabilities to affect innate and/or adaptive immunities. Specifically, NPs exhibit immune modulatory effects via different mechanisms including activation of innate immunocompetent cells, enhancement of antigen processing by antigen-presenting cells, and regulation of the network of cytokines (Xu et al., 2013). Ag NPs increased the levels of serum antigen-specific IgG and IgE remarkably, as well as the ratio of IgG1/IgG2a, indicating the role of Ag NPs in triggering the Th2-biased immune response. Also, Ag NPs had a significant immune modulatory effect, and the mechanism was primarily attributed to the recruitment and activation of local leukocytes and, in particular, macrophages (Xu et al., 2013).

Immune suppression is a reduction or a depression of the efficacy or activation of immune activity, which may be either inadvertent or desirable. Traditionally, immune suppression is reflected by immune toxicity. However, immune suppression may improve the therapeutic effect of inflammatory, allergic, and autoimmune diseases and prevent the rejection reaction in transplantation (Lettiero et al., 2012; Lappas, 2015; Luo et al., 2015). Immune suppression can be mediated by the toxicity of substances to any component of the immune system, and Ag NPs-induced immune toxicity has its own features. *In vitro* studies indicated that human peripheral blood mononuclear cells and human acute monocytic leukemia cells, as well as the murine peritoneal macrophages that were exposed to Ag NPs exhibited a remarkable decrease in cell viability and dysfunction of immunocompetence (Shavandi et al., 2011; Hayashi et al., 2012), and after cellular entry by endocytosis most of Ag NPs accumulated in

the lysosomes (Arai et al., 2015). *In vivo* study demonstrated that high dose administration of Ag NPs induced the suppression of natural killer cell activity in the spleen (De Jong et al., 2013). In addition, Ag NPs decreased the levels of T cell-derived antibodies, the counts of monocyte and neutrophil, and the distribution of natural killer T cell. Also, Ag NPs significantly inhibited proliferation of T cells and lymphocytes (Malaczewska, 2014; Arai et al., 2015). Histological evidence revealed the accumulation of Ag NPs in the spleen and lymph nodes of mice, which was observed as brown and black pigmentation (De Jong et al., 2013).

2.1.3 Toxicity of Ag NPs and the mechanism of toxicity

2.1.3.1 Evaluation of toxicity of Ag NPs

To standardize the evaluation of Ag NPs toxicity, numerous regulations (Council Directive 86/609/EEC of 24 Nov. 1986, Directive 2003/15/EEC of the European Parliament and of the Council of 27 Feb. 2003, Regulation (EC) No. 1907/2006 of the European Parliament and of the Council of 18 Dec. 2006 amending Directive 1999/45/EC and repealing Council Regulation (EEC) No 793/93 and Commission Regulation (EC) No. 1488/94 as well as Council Directive 76/769/EEC and Commission Directives 91/155/EEC, 93/67/EEC, 93/105/EC and 2000/21/EC, OJ L 396 of 30.12.2006) have been implemented in Europe. However, they are quite complicated and vary from case to case when applied. Recently, alternative methods (*e.g.*, tissue equivalents) have been accepted in the *in vivo* study for regulatory purpose in Europe. Therefore, the European Union 7th framework programme large-scale integrating project NanoValid is launched and attempts to establish the new reference methods in nanotoxicology.

Usually, the toxicity of NPs is evaluated using *in vitro* cell culture techniques. The BALB/c 3T3 cell line is originally established from murine embryonic fibroblast cells and has been widely used in toxicological studies (Todaro and Green, 1963; Aaronson and Todaro, 1968). Accordingly, BALB/c 3T3 cell-dependent cytotoxicity assays, such as the neutral red uptake (NRU) test have been developed and introduced into toxicological studies. The NRU test is developed on the principle of the capabilities of viable cells to incorporate and bind the supravital dye neutral red into the lysosome, thus reflecting membrane integrity. It is used to identify the phototoxic effect of a test substance (Repetto et al., 2008). The NRU test provides an approach for quantitative analysis of cell viability in a culture system and is one of the most prevalent cytotoxicity assays in biomedicine due to its less time-, labor-, and expense-consumption, less complexity of laboratory handling, and relatively high sensitivity. Therefore, it was accepted as a reference method by Organization for Economic Cooperation and Development in 2004 and specified to be a guideline in toxicology. However, the NRU test is only used in evaluating the toxicity of conventional chemicals, and its applicability remains unknown in nanotoxicology. Therefore, it is necess-

ary to combine the NRU test with other routine cytotoxicity assays, such as the WST-1 test and intracellular ATP measurement that have been widely used in nanotoxicological studies, to validate its availability. The WST-1 test is developed on the principle of enzymatic cleavage of the tetrazolium salt WST-1 to formazan by cellular mitochondrial dehydrogenases that are present in viable cells and used to evaluate the mitochondrial function. The WST-1 test is more stable than the conventional MTT assay (Sulić et al., 2005). ATP is the direct energy source that sustains multiple biological activities within the cells, and it is produced primarily from the mitochondria. Therefore, the level of total cellular ATP within the cells can be used as a general indicator for assessing mitochondrial activity.

Although *in vitro* cell culture-based tests have the advantages of real-time observation, homogeneity of sample, diversity of applications of techniques, no ethical concerns, it is apparent that *in vitro* studies are not equal to or cannot replace *in vivo* experiments because living cells that are incorporated into a highly organized organ behave in a totally different manner from the isolated cells that are separated from the organism due to the existence of the extracellular matrix and intimate cell-to-cell and cell-to-extracellular matrix communications (Doke and Dhawale, 2015). Therefore, animal experiments must be introduced into and included in biomedical studies to remedy the disadvantages of *in vitro* cell culture. As a mammal, the rat has a well-developed nervous system and is an important model animal in experimental medicine, pharmacology, and toxicology. Significantly, the genome of the rat possesses the approximate number of genes that humans have, and most human genes that are implicated in diseases have counterparts in the genome of the rat and appear to be highly conserved throughout evolution (Gibbs et al., 2004). More than that, the rat ear was identified as an excellent multifunctional model in pharmacological and toxicological research due to its unique and sophisticated structure that houses epithelia (*e.g.*, the skin of the external ear canal and mucosa of the middle ear), sensory organs (*e.g.*, Corti's organ, crista ampullaris, saccule maculae, and utricle maculae), neurons of the cranial nerves (*e.g.*, spiral ganglion and Scarpa's ganglion), a vascular bed similar to the brain, and a biological barrier (the blood-inner ear barrier) that limit the entry of hazardous substances to avoid compromising the vulnerable homeostasis of the inner ear. Previous observations demonstrated that the rat inner ear was an ideal organ for the evaluation of NPs' biocompatibility and toxicity (Zou et al., 2011; Zou, 2012). However, the European Union 7th framework programme large-scale integrating project NanoValid attempts to establish the new reference methods in nanotoxicology, and the reference methods follow the '3Rs' principle: replacement of a procedure that uses animals with a procedure that does not use animals, reduction of the number of animals used in a procedure, and refinement of a procedure to alleviate or minimize potential animal pain. Therefore, it is quite necessary to integrate the *in vitro* and *in vivo* study and overcome the respective disadvantage to evaluate the toxicity of Ag NPs comprehensively.

2.1.3.2 Fate of Ag NPs within the cells

Ag NPs may penetrate and invade the body through dermal contact (Korani et al., 2011; Kim et al., 2013), inhalation (Sung et al., 2009), and ingestion (Kim et al., 2010; Loeschner et al., 2011). They interact with living cells in a more distinctive manner than conventional silver compounds. Prior to contact between Ag NPs and the plasma membranes of cells, Ag NPs interact with the extracellular bioactive molecules in body fluids including proteins, carbohydrates, and lipids. This can affect the subsequent interactions between Ag NPs and cells. Among them, creation of a protein corona plays a critical role in leading to the change of interaction between Ag NPs and cells. The protein corona is defined as the complexes that form at the interface between the NPs and proteins. Irreversible binding of NPs on the proteins leads to 'hard corona', whereas reversible binding of NPs on the proteins leads to 'soft corona'. The 'hard corona' may play a more important role than the 'soft corona' in determining the behaviour of NPs and the function of proteins (Saptarshi et al., 2013; Tenzer et al., 2013; Lee et al., 2015).

The interactions between Ag NPs and cells consist of recognition, uptake, internalization, translocation, and finally accumulation or excretion by cells, which are dependent on the properties of Ag NPs, the cell types, the approach and dosage of administration, and the duration of exposure (Stensberg et al., 2011). The recognition and uptake of Ag NPs, as well as other NPs, is primarily mediated by endocytosis (Garcia-Alonso et al., 2011; Zhang et al., 2014). Positively charged Ag NPs recognize and bind to target cells that have negatively charged plasma membrane more efficiently than those that are negatively charged or neutral with the same size (Frohlich, 2012). Mesenchymal stem cells uptake the Ag NPs via macropinocytosis (Greulich et al., 2011). Monocytes uptake and internalize the Ag NPs through clathrin-dependent and actin-independent pathways (Singh and Ramarao, 2012). Macrophages uptake and internalize the Ag NPs via actin-dependent endocytosis that is mediated by scavenger receptors (Wang et al., 2012). Transmission electron microscopy studies have showed that the smaller Ag NPs are much more readily to be internalized via macropinocytosis or phagocytosis than the larger Ag NPs with the same surface properties (Zhang et al., 2015). After entering the cells, Ag NPs display a homogeneous distribution in both the cytoplasm and the nucleus and interact with the cellular membrane structures and cause their impairment including not only the plasma membrane but also the membranous organelles (*e.g.*, mitochondria, endoplasmic reticulum, lysosome, and Golgi apparatus). Actually, the membrane is considered a primary affected site in Ag NPs-induced toxicity (Lansdown, 2004; AshaRani et al., 2009; El Badawy et al., 2011; Khan et al., 2011; Joshi et al., 2012). For example, Ag NPs can induce mitochondrial dysfunction, indicated as mitochondrial membrane potential depolarisation, formation of a mitochondrial permeability transition pore, and release of apoptosis-inducing factor, endonuclease G, and cytochrome *c* (Ma et al., 2015). Ag NPs appear to either passively diffuse through nuclear pores (Godbey et al., 1999; Parfenov et al., 2006) or be actively imported into the nucleus via receptor-mediated

transport (Pante and Kann, 2002; Williams et al., 2009). The positively charged Ag NPs slow down the acidification of endosomes that are responsible for the transportation of internalized Ag NPs from the plasma membrane to lysosomes that act as the digestive system within the cells. Ag NPs finally end up in lysosome, where the cells attempt to digest or excrete them (Al-Rawi et al., 2011; Greulich et al., 2011). However, the mechanism of cellular egress is not fully understood although some evidence shows that it may be mediated by exocytosis (AshaRani et al., 2009).

2.1.3.3 Toxicological mechanism of Ag NPs

Ag NPs-induced toxicity may be mediated by the mechanisms of oxidative stress, membrane permeability alteration, ion transport disruption, cellular respiration disturbance, protein denaturation, and DNA impairment (Klaine et al., 2008). Among them, oxidative stress, protein denaturation, and DNA impairment are considered the significant mechanisms involved in Ag NPs-induced toxicity. Oxidative stress reflects the disequilibrium between the generation of ROS and the capability of a biological system to detoxify or eliminate ROS and repair the consequential damage. Usually, excessive ROS generation is considered a primary factor in determining oxidative stress. ROS are a family of chemically reactive oxidants with a short half-life including superoxide radical, hydroxyl radical, hydrogen peroxide, and singlet oxygen. They play a critical role in inflammation, carcinogenesis, and aging. Toxic substances elevate the rate of ROS generation by either blocking electron transport or accepting an electron from a respiratory carrier and transferring it to molecular oxygen (Turrens, 2003). Mitochondria are identified as the major site of ROS production within the cells. Ag NPs that are taken up by the mitochondria result in mitochondrial membrane depolarisation by damaging membrane phospholipids and generate more electrons by disrupting the electron transport chain (Lenaz, 2001). Ag NPs have been found to elevate respiration rate and impede the detoxification of antioxidants, and therefore generate excessive ROS (Carlson et al., 2008; Choi and Hu, 2008; Neal, 2008; Piao et al., 2011b; Piao et al., 2011a; Yang et al., 2012; Massarsky et al., 2013; Massarsky et al., 2014; Paino and Zucolotto, 2015). It should be noted that overproduction of ROS has been implicated in the degradation of hyaluronic acid that is capable of allowing the rapid diffusion of water-soluble molecules into the matrix (Hansell et al., 2000). The lower molecular weight fragments that interact with CD44 may up-regulate chemokines [*e.g.*, monocyte chemotactic proteins (MCPs)], adhesion molecules (*e.g.*, intercellular adhesion molecule-1 and vascular cell adhesion molecule-1), and inflammatory cytokines leading to leukocytes infiltration and consequential inflammation (Esser et al., 2012; Mirzapoiazova et al., 2015; Onodera et al., 2015). More significantly, excessive ROS may lead to secondary damages, such as protein denaturation, DNA impairment, endoplasmic reticulum stress, and lipid peroxidation (Posgai et al., 2011; Zhang et al., 2012a).

Accurate conformation is necessary for proteins to function properly. Conform-

ational changes caused by heavy metals result in irreversible protein denaturation and, consequently, impair the function of proteins. Ag NPs can induce the formation of protein corona leading to haemolysis, activation of the thrombocyte and complement system, and cell death (Saptarshi et al., 2013; Tenzer et al., 2013; Lee et al., 2015). Furthermore, protein aggregation and peptide fibrillation caused by Ag NPs will lead to the formation of amyloid-like structures that are implicated in neuro-degenerative diseases, such as Parkinson's disease and Alzheimer's disease (Colvin and Kulinowski, 2007; Wagner et al., 2010; Elsaesser and Howard, 2012). Also, Ag NPs have the capability to change the configuration of peptides into forms of aggregation and fibrillation (Aili et al., 2008; Wu et al., 2008; Wagner et al., 2010).

As a genetic vehicle, nucleic acids are vital for gene replication, transcription, and translation, many diseases are found to be associated with the aberrant nucleic acids. Ag NPs induce aneuploidy and chromosomal abnormalities, such as chromatid lesions and centromere spreading (Wise et al., 2010). The Ag NPs accumulated within the cells cause DNA impairment in a dose-dependent manner (Tomankova et al., 2015). DNA impairment is capable of activating intracellular signaling that affects cell-cycle checkpoints and DNA repair (Elsaesser and Howard, 2012). Once the damage is deprived, checkpoint-arrested cells will resume cell-cycle progression. However, it has been shown that Ag NPs induce DNA impairment, leading to cell cycle halted in the G2/M phase, and exacerbate the apoptosis rate (Carlson et al., 2008; AshaRani et al., 2009; Kim et al., 2009; Asharani et al., 2010). In addition, ROS-induced DNA impairment can activate poly (ADP-ribose) polymerase-1 that in turn triggers the translocation of apoptosis-inducing factor from the mitochondria into the nucleus, in which it triggers chromatin condensation, DNA fragmentation, and nuclear shrinkage (Dawson and Dawson, 2004).

2.2 Basic knowledge of the inner ear

2.2.1 Physiology of the cochlea

The inner ear, composed of the cochlea and vestibule, is responsible for transducing the physical signals of sound and head position into neural impulses that are recognized by the brain. It is embedded within the bulla in rodents, while it is deeply buried in the petrous temporal bone at the lateral skull base in humans. As an auditory organ, the cochlea can be separated into three compartments, the scala vestibule, scala tympani, and scala media. The former two are communicated with each other by the helicotrema and filled with perilymph that contains ~ 4 mM K^+ ions and ~ 150 mM Na^+ ions and is similar to extracellular fluid (*e.g.*, plasma and cerebrospinal fluid), while the latter one, also known as the cochlear duct, is filled with endolymph that contains ~ 150 mM K^+ ions and ~ 1 mM Na^+ ions and is similar to intracellular fluid (Ryan et

al., 1979). Corti's organ, which is located on the basilar membrane of the cochlear duct and is composed of mechano-sensory cells (inner and outer hair cells) and non-sensory supporting cells (*e.g.*, Deiters' cells and pillar cells), is responsible for the transformation of sound vibration into neural impulses that are recognized by the brain. In rodents, one row of inner hair cells releases the neurotransmitters that can interact with the receptors located in the peripheral processes of the spiral ganglion cells in response to sound vibration. Three rows of outer hair cells amplify the motion of the basilar membrane to stimulate the inner hair cells more effectively (Dallos, 2003; Lu et al., 2006; Jia et al., 2007). Sensory cells are bathed with their hair bundles in K^+ -rich endolymph, while cell bodies in K^+ -poor corticolymph (almost identical to the perilymph). When the hair bundles of hair cells are deflected on the basilar membrane that is vibrated by the sound wave, the K^+ ions enter the hair cells through the transduction channels located in their cilia and are then expelled basolaterally. These K^+ ions appear to be delivered to the spiral ligament fibrocytes via the non-sensory supporting cells that are coupled by gap junctions. After K^+ ions that are collected from the strial intermediate and basal cells influx into the intrastrial space, they are taken up by the strial marginal cells and are then excreted into endolymph, where they are ready for sensory cells to receive the mechanical stimuli of the next round (Hibino et al., 2010). Na^+ ions movement that is controlled by the epithelial sodium channels in the stria vascularis and Reissner's membrane is also important for normal functioning of the sensory cells (Mizuta et al., 1995; Couloigner et al., 2001; Pondugula et al., 2004).

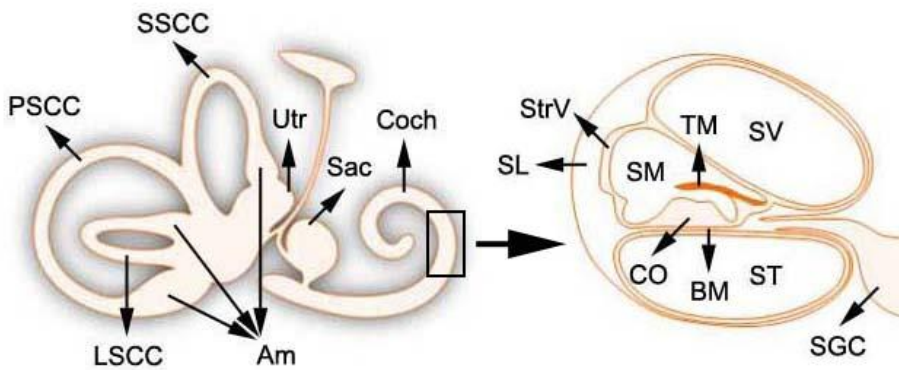


Fig. 2 Illustration of inner ear anatomy. PSSC: posterior semicircular canal; SSCC: superior semicircular canal; LSCC: lateral semicircular canal; Am: ampule; Utr: utricle; Sac: saccule; Coch: cochlea; StrV: stria vascularis; SL: spiral ligament; SV: scala media; SM: scala media; ST: scala tympani; TM: tectorial membrane; CO: Corti's organ; BM: basilar membrane; SGC: spiral ganglion cell.

A number of electrophysiological methods, such as distortion product otoacoustic emissions, electrocochleography, and ABR, are used to monitor hearing. Among them, ABR is an objective and non-invasive detection method to evaluate the function of both the peripheral and central auditory system. Therefore, using ABR measu-

rements is quite useful to determine hearing level in experimental studies as well as clinical investigations. ABR is a compound evoked potential that is extracted from ongoing electrical activity in the brain and recorded with the platinum needle electrodes placed underneath the scalp. As shown in **Fig. 3**, the resulting recording in the rat is composed of a series of vertex positive waves of which I through V are evaluated. Wave II is the most evident and stable response and can be utilized to identify the threshold that is the minimum visible and repeatable response (Alvarado et al., 2012; Ruebhausen et al., 2012). In the ABR measurements, the level of hearing loss is presented as a threshold shift, the larger the threshold shift, the more severe the hearing loss. The increase in this parameter indicates the degree of hearing loss and is expressed by decibel (dB).

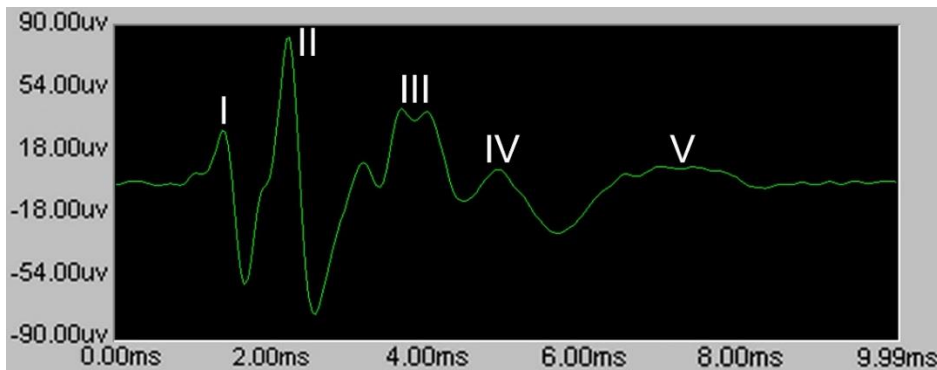


Fig. 3 A typical ABR click waveform recorded in a normal rat at a stimulus of 80 dB SPL. dB SPL: decibel sound pressure level.

2.2.2 Analogy of the blood-inner ear barrier and the blood-brain barrier

The concept of the blood-inner ear barrier was first proposed by Hawkins in 1973, and it was considered a complex of numerous endothelial cells that were coupled by tight junctions and the underlying basement membrane (Hawkins, 1973). In recent years, great progress has been achieved in elucidating the sophisticated cellular architecture of the blood-inner ear barrier. It has been indicated that abundant basal infoldings of the strial marginal cells and dendrite-like projections of the strial intermediate cells and basal cells intimately contact the capillaries, which suggests the strial cells may participate in constructing the blood-inner ear barrier (Ando et al., 1999; Spicer and Schulte, 2005a, b). In addition, pericytes are found to be intimately associated with the endothelial cells of capillaries, showing their processes tightly positioned adjacent to the endothelia (Dai et al., 2009; Shi, 2009). Significantly, pericytes contribute to remodelling the integrity of the blood-inner ear barrier via desmin because of its role in cell architecture and force transmission (Shi, 2009). Moreover, the perivascular resident macrophages that are positive for F4/80, CD68, and CD 11b, with foot processes strikingly rich in mitochondria and vesicles, are found to be int-

imately associated with the abluminal surfaces of capillaries, suggesting that they may play a similar role to that of astrocytes in the brain and glial cells in the retina in regulating the integrity of the blood-inner ear barrier (Shi, 2010; Zhang et al., 2012b; Neng et al., 2013; Zhang et al., 2013b; Zhang et al., 2013a).

The blood-inner ear barrier is not only a physical barrier that prevents the influx of toxic substances into the inner ear, thus protecting the vulnerable structures of the inner ear from systemic influences but also a selective permeable membrane that allows the transmission of small liposoluble molecules from the blood into the inner ear, whereas high molecular weight, water soluble, and charged molecules are unlikely to diffuse passively (Juhn et al., 1981; Juhn, 1988; Swan et al., 2008). On one hand, the breakdown of the blood-inner ear barrier is involved in many hearing and balance disorders, such as Ménière's disease (Tagaya et al., 2011; Zou et al., 2011; Zou, 2012). On the other hand, because of the blood-inner ear barrier, conventional approaches of drug administration, such as oral or parenteral routes, are largely not efficient or are even ineffective in treating inner ear diseases (Saito et al., 2001). Therefore, characterizing the blood-inner ear barrier is important for understanding the pathogenesis of inner ear diseases and for the innovation of novel drug delivery systems.

The inner ear is a tiny organ made up of multiple tissues that is deeply buried in the bone, leading to its inaccessibility and complexity. Thus, it is difficult to elucidate the essence of the blood-inner ear barrier. It has been suggested that the blood-inner ear barrier is functionally similar to the blood-brain barrier as well as the blood-retina barrier and the blood-testis barrier. The function of the blood-brain barrier is achieved by tight junctions, a paucity of pinocytotic vesicles in the endothelial cells, and a uniformly thin and negatively charged layer in the endothelial cells (Reese and Karnovsky, 1967; Vorbrodt et al., 1986). Histologically, both the blood-inner ear barrier and the blood-brain barrier are composed of endothelial cells that are joined together by tight junctions lining along the capillaries in which the fenestration is absent (Shi, 2011). Physiologically, both of them share the capabilities in allowing Na^+ ions and urea to cross (Sterkers et al., 1987), facilitating glucose transport (Crone, 1965; Ferrary et al., 1987), and responding to acetazolamide (Vogh and Maren, 1975; Sterkers et al., 1984). Furthermore, the permeability of both barriers can be augmented by histamine and prostaglandin E2 (Gross et al., 1981; Inamura and Salt, 1992; Schmidley et al., 1992). Significantly, Ag NPs have been shown to disrupt the blood-brain barrier and cause neural toxicity in the brain (Sharma et al., 2010). Therefore, it is theoretically possible to investigate the essence of the blood-inner ear barrier and explore the pathogenesis of the inner ear disorders using Ag NPs.

2.2.3 Evaluation of permeability of the blood-inner ear barrier

Traditional studies to evaluate the integrity of the biological barrier have used approaches, such as the dye exclusion test (*e.g.*, Evans blue and sodium fluorescein) and

radioactive tracing (*e.g.*, I¹³¹) (Rossner and Tempel, 1966; Wispelwey et al., 1988). However, the dye exclusion test is not believed to be an ideal method to evaluate the integrity of the blood-inner ear barrier because the vessels of the inner ear are in close proximity to the tissues and fluids of interest, and sectioning may displace the extravasated dye throughout the whole tissue as a result of powerful mechanical extrusion, especially in the extravascular tissues that are sparse. Therefore, it may provide inaccurate information on the location of vascular leakage (Tachibana et al., 1981; Trune, 1997; Kastenbauer et al., 2001). In addition, it has been suggested that the amount of dye detected in the tissue homogenate may only reflect the absorption capabilities of tissues but not the severity of vascular leakage indicating the augmentation of permeability. I¹³¹ is used as a tracer in identifying the bleeding site but the radioactivity limits its applicability regardless of its very short half-life. *In vitro* cell culture model has recently been established to study the blood-inner ear barrier (Zhang et al., 2013a). However, it is questionable that how functional alteration of the blood-inner ear barrier correlates to histological changes or *in vitro* findings, as there are no convincing studies combining these alterations to endocochlear potential, ion concentrations, or hearing thresholds (Hirose et al., 2014). Therefore, an objective, reliable, safe, and quantitative method to assess vascular leakage is in great need. MRI is an *in vivo* non-invasive imaging technique that can be used to visualize the sophisticated structures of the inner ear. Accumulative evidence shows that MRI is a powerful tool to investigate the blood-inner ear barrier in both animals and humans. Significantly, the applications of contrast agents (*e.g.*, gadolinium) improve the discrimination of the endolymphatic and perilymphatic compartments of the inner ear, which benefit the diagnosis of endolymphatic hydrops in the patients suffered from Ménière's disease, as well as sudden sensorineural hearing loss, and advance the development of animal models in mimicking inner ear disorders in humans (Counter et al., 2000; Counter et al., 2003; Zou et al., 2003; Zou et al., 2009a; Pyykkö et al., 2010; Zou et al., 2010a; Zou et al., 2010c; Zou et al., 2010b; Naganawa et al., 2012; Zou et al., 2012b; Counter et al., 2013; Naganawa and Nakashima, 2014).

2.3 Inner ear immunology

2.3.1 Deviation in understanding of the inner ear being an immunologically privileged organ

It was once taken for granted that the inner ear was an 'immunologically privileged organ' due to the unique blood-inner ear barrier that was similar to the blood-brain barrier, by which the cochlear duct was separated anatomically from the systemic cir-

ulation. The impermeable nature of the blood-inner ear barrier is reflected by abundant tight junctional proteins (*e.g.*, claudin-1, -3, and -4) and adhesion molecules (*e.g.*, T-cadherin, P-selectin, intercellular adhesion molecule-1, and vascular cell adhesion molecule-1) in the stria vascularis (Shi and Nuttall, 2007; Listyo et al., 2011; Yang et al., 2011). The endothelial cells in the capillary network of the stria vascularis do not have fenestrae but are joined together by tight junctions and therefore have a very low permeability to blood components under physiological conditions (Sakagami et al., 1982; Ando et al., 1999). Thus, immunocompetent cells, antigens, and immunoglobulins are thought to be excluded from the inner ear (Barker and Billingham, 1977; Harris and Ryan, 1995; Fujioka et al., 2014; Okano, 2014).

However, accumulative evidence challenges this notion. Immunocompetent cells are identified in the cochlea even under the steady state. They reside in the stria vascularis and spiral ligament of the cochlear lateral wall and exhibit certain features of macrophage (Hirose et al., 2005; Lang et al., 2006; Tornabene et al., 2006; Okano et al., 2008; Sato et al., 2008). The inner ear is subject to mounting an immune response when challenged by stressors, such as keyhole limpet haemocyanin (McCabe, 1979; Harris, 1983; Soliman, 1992; Kanzaki, 1994). On one hand, breakdown of the blood-inner ear barrier resulted from a variety of highly risky factors including noise, ototoxic drugs, senescence, and ischaemia/hypoxia allowed bone marrow-derived cells, regardless of haematopoietic or mesenchymal origin to mobilize and migrate into the harassed sites of the inner ear via the capillary system (Shi, 2011). In addition, the communication between the inner ear and the systemic lymphatic system through the cervical lymph nodes provided another route for leukocytes trafficking into the inner ear that was sensitized by keyhole limpet haemocyanin (Yimtae et al., 2001). Consequently, endolymphatic hydrops was induced (Zou et al., 2007). On the other hand, it was apparent that the inner ear itself was capable of mounting an immune response independently when pathogens, such as lipopolysaccharides, an important component of the cell wall in Gram-negative bacteria, invaded through either the middle ear or the adjacent meninges (Harris, 1983; Ma et al., 2000; Penha and Escada, 2003; Klein et al., 2007; Moller et al., 2014).

2.3.2 Communication between the inner ear and the immune system

Small blood vessels such as capillaries play an essential role in the transmigration of immunocompetent cells and the transmission of immune molecules from the systemic circulation into the local tissues (LaFerriere et al., 1974). It should be noted that the immune components that are transferred from the systemic circulation are critical for the onset and development of an immune response in the inner ear. Lymphocytes that are extravasated from the systemic circulation can enter the inner ear via draining post-capillary venules. In the inner ear, the primary draining venules refer to the spiral modiolar veins that are located at the base of the scala tympani. These collecting venules can develop high endothelial vein-like characteristics after inoculation

of living or inactivated virus into the scala tympani (Harris et al., 1990; Fukuda et al., 1992; Pawankar et al., 1998). Abundant infiltrating leukocytes can be identified at this site followed by an immunological or inflammatory challenge (Harris et al., 1990). Further study reveals that bone marrow cells donated from green fluorescent protein transgenic mice are found at the spiral ligament of lethally irradiated mice as the recipients after intravenous infusion, and these cells initially accumulate at the basal regions then progress to the whole spiral ligament, and the extent is greater than that in the modiolus regions, suggesting that vessels of the spiral ligament in the cochlear lateral wall are an important entry route for cell trafficking into the inner ear (Tan et al., 2008).

The transmigration of leukocytes from the systemic circulation into the inner ear is mediated by molecules produced by endothelial cells and receptors expressed on the leukocytes (Takahashi and Harris, 1988a; Stearns et al., 1993; Trune and Nguyen-Huynh, 2012). In response to stressors, circulating leukocytes are captured and immobilised by the endothelial cells followed by transmigration across the microvascular wall in three steps (Bachor et al., 2001). First, adhesion molecules (*e.g.*, P-selectin, intercellular adhesion molecule-1, and vascular cell adhesion molecule-1) produced by endothelial cells elicit rolling leukocytes (*e.g.*, neutrophils, monocytes, and lymphocytes) along the vessel wall at a far slower velocity to adhere to the endothelial cells (Cook-Mills, 2002). Next, receptors (*e.g.*, toll-like receptors and T cell receptors) that are expressed on the leukocytes act as an anchor site in mediating leukocytes to adhere firmly to the endothelial cells (Yuan et al., 2012). Finally, endothelial cells downregulate tight junctional proteins (*e.g.*, claudins and occludins) and facilitate actin cytoskeletal remodelling that is mediated by the phosphorylation of myosin light chain protein to regulate membrane ruffling and lamellipodia formation and alter shape characteristics, allowing leukocytes to cross the microvascular wall (Marcus et al., 1997; Iversen et al., 1999; Nieuwdorp et al., 2009). During the process, the endothelial cells synthesize and secrete chemokines (*e.g.*, MCPs) into the adjacent tissues to guide the transmigration of leukocytes (Taylor and Gallo, 2006; Shi and Nuttall, 2007).

2.3.3 Topical immune response in the inner ear

The endolymphatic sac plays an important role in sustaining endolymph homeostasis (*e.g.*, ion composition, osmotic pressure, volume, and pH) of the inner ear (Lundquist, 1976; Bagger-Sjoberg and Rask-Andersen, 1986; Wackym et al., 1987a; Couloigner et al., 2004). Interestingly, more and more studies suggest that the endolymphatic sac is also significant for immune activity in the inner ear (Rask-Andersen and Stahle, 1980; Rask-Andersen et al., 1983; Tomiyama and Harris, 1986, 1987; Wackym et al., 1987b; Tomiyama and Harris, 1989; Tomiyama, 1992; Gloddek and Arnold, 1995; Tomiyama et al., 1995; Masuda et al., 1997; Satoh et al., 2003; Moller et al., 2015a). A functional endolymphatic sac is thought to be essential for the cochlear

immune response because the T cell-mediated immune surveillance that affects the cochlea is likely to occur primarily in the endolymphatic sac (Takahashi and Harris, 1988b; Kawauchi et al., 1992). It has been reported that the endolymphatic sac may be mimetic to mucosa-associated lymphoid tissue (Tomiyama and Harris, 1987; Gloddek and Arnold, 1995, 1998). The human endolymphatic sac is capable of synthesizing the components of the humoral innate immune system and therefore potentiates a prompt defence against the foreign pathogens that invade the inner ear (Moller et al., 2015b). The capability of the endolymphatic sac to recognize and process the antigen so as to activate the cellular adaptive immune response is supported by a distinctive array of immune molecules in the human inner ear including the toll-like receptor, Fc receptor, and chemokine ligand and receptor (Moller et al., 2015b). Antigen presentation in the endolymphatic sac may mediate the diapedesis and infiltration of leukocytes from the fenestrated capillaries (Rask-Andersen and Stahle, 1980; Altermatt et al., 1992; Moller et al., 2013). In particular, perisaccular connective tissue that contains blood and lymphatic vessels around the endolymphatic sac is considered a host site for resident lymphocytes and a primary 'trigger point' for immune surveillance in the inner ear and probably contributes to the augmentation of adaptive immunity and induced inflammation (Yeo et al., 1995; Satoh et al., 2003). Secondary endolymphatic sac challenging with inner ear proteins induces hearing loss in the guinea pigs although the incidence is lower than that of secondary systemic immunisation (Zou et al., 1996). Taken together, the endolymphatic sac does play a key role in inner ear immune surveillance and immune response.

The highly vascularized cochlear lateral wall is another immune site in the inner ear, which has the capability of recruiting and mobilising immunocompetent cells from the systemic circulation. More than that, the stria vascularis and spiral ligament themselves are implicated in the immune-mediated activity in the inner ear (Lang et al., 2006; Lang et al., 2008). Perivascular resident macrophage-like melanocytes in the intrastrial space of the stria vascularis, which express F4/80, CD68, and CD11b, contribute to the repair of impaired vessels in the context of a local inflammatory response in order to maintain the integrity of the blood-inner ear barrier (Shi, 2010; Zhang et al., 2012b). Increased levels of CD68 and major histocompatibility complex class II that are associated with the macrophages and dendritic cells are identified in the stria vascularis of *Slc26a4* knockout mice (Jabba et al., 2006). In addition, the highly-expressed glucocorticoid receptors in the stria vascularis suggest their roles in immune modulation in the inner ear (Shimazaki et al., 2002). Actually, the 'resting' cochlea contains macrophages within the spiral ligament and the spiral ligament type I fibrocytes are specialized for expressing inflammatory cytokines as part of their normal functions (Adams, 2002). Macrophages are recruited and activated in the spiral ligament in response to hazardous stimulus (*e.g.*, gene mutation) (Jabba et al., 2006; Okano et al., 2008; Sato et al., 2010). In particular, the spiral ligament type IV fibrocytes are likely to be the initiators of the local inflammatory response caused by noise (Tan et al., 2008). Moreover, the spiral ligament fibrocytes produce inflammatory cytokines, such as TNF- α and IL-1 β when challenged by lipopolysaccharides

(Moon et al., 2007; Woo et al., 2010) or exposed to noise (Hirose et al., 2005; Fujioka et al., 2006; Tornabene et al., 2006). Steroids can decrease the levels of MCP1 and macrophage inflammatory protein-2 that are secreted from the spiral ligament fibrocytes activated by TNF- α , which is supported by the fact that glucocorticoid receptors are remarkably distributed in the spiral ligament fibrocytes (Zuo et al., 1995; Shimazaki et al., 2002; Maeda et al., 2005). These findings suggest that the stria cells and spiral ligament fibrocytes may have capabilities to acquire certain features that are similar to those of immunocompetent cells.

Immune activity is also identified in the Corti's organ exposed to noise and ototoxic drugs, especially in the avian cochlea (Warchol, 1997; Bhawe et al., 1998; Warchol et al., 2001; Warchol et al., 2012). Non-sensory supporting cells of Corti's organ can act as microglia-like cells and may determine the fate of the auditory sensory epithelium because microglia are believed to be macrophages in the central nervous system and play an irreplaceable role in immune surveillance (Rio et al., 2002; Ladrech et al., 2007; Sun et al., 2015). Deiters' cells phagocytose the injured outer hair cells and eliminate the cellular debris in Corti's organ and, subsequently, repair the defect of the reticular lamina with their processes after exposure to noise (Forge, 1985; Abrashkin et al., 2006). Among the various cellular mediators detected, toll-like receptors are demonstrated as one of the most important molecules in triggering an immune response in Corti's organ (Oh et al., 2011). Furthermore, complement subcomponents (*e.g.*, Cfi and C1s) have been implicated in immune-related pathology of Corti's organ compromised by noise (Patel et al., 2013; Cai et al., 2014). In particular, a remarkable increase in the expression of major histocompatibility complex class II along with its trans-activator protein, class II trans-activator, is identified followed by monocyte infiltration and differentiate into macrophage at the basal section of the basilar membrane in the inner ear after exposure to noise, as well as the infiltration of CD4⁺ T cells (Gloddek et al., 2002; Yang et al., 2015).

3 Aims of the current research

The current study focused on the following specific topics:

1. To show the *in vitro-in vivo* correlation of Ag NPs toxicity using BALB/c 3T3 cells and the rat cochlea (**I** and **III**).
2. To demonstrate the transportation of Ag NPs from the rat middle ear to the inner ear using micro CT (**II**).
3. To investigate the impact of Ag NPs on the permeability of biological barriers in the rat ear using gadolinium-enhanced MRI (**I**).
4. To elucidate the molecular mechanism of Ag NPs-induced functional change in the biological barriers in the rat cochlea using immunostaining (**III** and **IV**).

4 Material and methods

4.1 Ag NPs

Ag NPs were supplied by Colorobbia (Firenze, Italy) and the original concentration was 4 % (w/v). The hydrodynamic size was 117 ± 24 nm and the zeta potential was -20 ± 9 mV when suspended in deionised water (dH₂O) using dynamic light scattering in a Malvern Zeta Sizer Nano Z System (Malvern Instruments Ltd., Malvern, UK). The size distribution of Ag NPs was not affected by the artificial perilymph [145.5 mM NaCl, 2.7 mM KCl, 2.0 mM MgSO₄, 1.2 mM CaCl₂, and 5.0 mM 4-(2-hydroxyethyl)-1-piperazineethanesulfonic acid (HEPES) with the pH adjusted to 7.4] (Take-mura et al., 2004) at 4 h after incubation up until 25 h.

4.2 Evaluation of toxicity of Ag NPs in BALB/c 3T3 cells using

NRU, WST-1, ATP measurement, and PI staining assays (I)

The murine embryo fibroblast BALB/c 3T3 cells (clone 31, CCL-163™, American Type Culture Collection, LGC Promochem AB, Boras, Sweden) were cultured in DMEM containing 4 mM L-glutamine and supplemented with 10 % newborn calf serum at 37 °C with 5 % CO₂; they were then seeded into 96-well plates at a density of ~3000 cells/well and allowed to form a 50 %-70 % confluent monolayer after 24 ± 2 h. After replacing the medium with 90 µl DMEM containing 4 mM L-glutamine and 5 % newborn calf serum, 10 µl Ag NPs dilutions (prepared in dH₂O immediately prior to use) were added to the wells to reach 8 different final concentrations (0.67-10.0 µg/ml) with 6 replicates. The medium containing 10 % dH₂O was used as a vehicle control. The plates were then incubated for 24 h. The exposure time was defined according to the results showing that Ag NPs remained in the rat cochlea for at least 24 h after transtympanic injection using micro CT. Four different assays, NRU, WST-1, the total cellular ATP, and propidium iodide (PI) staining, were used to study the viability of BALB/c 3T3 cells after Ag NPs exposure. The cell viability was expressed as a percentage of the viability of treated cells relative to that of the untreated (vehicle) control wells. Dose-response curves were drawn, and the half maximal inhibitory concentration (IC₅₀) was calculated using SigmaPlot® Version 12.5 (Systat Software, Inc., San Jose, USA).

4.3 Delivery of Ag NPs *in vivo* and animal assignments

Sprague-Dawley rats weighing 250-524 g were maintained at an ambient temperature of 20-22 °C with a relative humidity of 50±5 % under a 12/12 h light/dark cycle in the experimental animal unit, the University of Tampere, and Biomedicum Helsinki, Laboratory Animal Centre, the University of Helsinki, Finland. All procedures complied with local ethics committee standards (permission number: ESAVI/3033/04.10.03/2011) and were conducted in accordance with European Legislation.

Rats were anaesthetized generally by Ketalar® in combination with Domitor®. Norocarp® was used to alleviate pain. Baytril® was used to prevent potential infection. Viscotears® was used to protect eyes from dryness. Anti-sedan® was used to accelerate resuscitation. More details on the medications used in the rats are shown in **Table 1**.

Table 1 Medication used in the rats

| Brand name | Generic name | Orig. con. | Dilution | Dose | Manufacturer |
|-------------------------|----------------------------|-----------------|-------------------|------|-------------------|
| Ketalar ^a | Ketamine hydrochloride | 50 ^d | - | 0.15 | Pfizer, Finland |
| Domitor ^a | Medetomidine hydrochloride | 1 ^d | - | 0.05 | Orion, Finland |
| Norocarp ^a | Karprofen | 50 ^d | 1:10 ^f | 0.1 | ScanVet, Finland |
| Baytril ^b | Enrofloxacin | 50 ^d | - | 0.01 | Orion, Finland |
| Viscotears ^c | Carbomer | 2 ^e | - | - | Novartis, Denmark |
| Anti-sedan ^a | Atipamezole | 5 ^d | 1:10 ^f | 0.2 | Pfizer, Finland |

^aThe medication was administered intraperitoneally.

^bThe medication was administered intramuscularly.

^cThe medication was administered for ocular use.

^dmg/ml.

^emg/g.

^fDiluted in saline.

Orig. con.: original concentration; dose: ml/100 g body weight.

After anaesthesia, either 40 or 50 µl of Ag NPs at defined concentrations were injected unilaterally into the middle ear cavity by tympanic membrane penetration under an operating microscope (OPMI1-F, Carl Zeiss, Jena, Germany) according to a previously reported procedure (Zou et al., 2010a). After injection, the animals were kept in the lateral position with the injected ear oriented upward for 15 min to ensure that a sufficient amount of Ag NPs would remain in the middle ear cavity. For the animal assignments, ten rats were used for the micro CT scanning; fourteen rats were used for the MRI; twelve rats were used for the ABR measurements and ten of them were used for histological observations. More details on the animal assignments are shown in **Table 2**.

Table 2 Assignments of the rats that received CT, MRI, and ABR measurements

| Measurements | Number of rats exposed to various concentrations of Ag NPs at different time points ($\mu\text{g/ml}$) | | | | | | | | | | | | |
|--------------|--|------|-------|-----|----------------|----------------|----------------|-----|-----|----------------|----------------|----------------|----------------|
| | 40 000 | | 4 000 | | | | 2 000 | | 200 | | | | |
| | 4 h | 24 h | 4 h | 5 h | 2 d | 4 d | 7 d | 5 h | 7 d | 5 h | 2 d | 4 d | 7 d |
| CT | 2 | 2 | 2 | - | - | - | 2 ^a | - | - | - | - | - | 2 ^a |
| MRI | - | - | - | 2 | - | - | 2 | 5 | 5 | 7 ^b | - | - | - |
| ABR | - | - | - | - | 6 ^c | 6 ^c | 6 ^c | - | - | - | 6 ^c | 6 ^c | 6 ^c |

^aOne of them received ABR measurements.

^bThree rats exposed to 400 $\mu\text{g/ml}$ Ag NPs were pooled in the 200 $\mu\text{g/ml}$ group in MRI study.

^cThe rats received ABR measurements prior to Ag NPs exposure and at 2 d, 4 d, and 7 d post-transtympanic injection.

4.4 Distribution of Ag NPs in the rat ear shown by micro CT (II)

At defined observation time points post-injection, the temporal bone was fixed via cardiac perfusion with 0.01 M phosphate buffered saline (PBS) pH 7.4 containing 0.6 % (v/v) heparin (LEO Pharma A/S, Ballerup, Denmark) followed by 4 % paraformaldehyde (Merck, Espoo, Finland). After decapitation, the cadaveric head was immersed in the same fixative solution for a 2 h-fixation. Next, the head was covered with Parafilm M[®] film (Bemis Company, Inc., Oshkosh, USA) and firmly installed on the specimen stage of the micro CT. During scanning, three objectives were used, 1 \times for the large field of view images, 4 \times for the images that focused on the cochlea, and 10 \times for imaging the round and oval windows. The voltage varied from 60 to 120 kV, the source distance was adjusted to 60-100 mm, and the detector distance was 38-40 mm. The pixel size ranged from 1.7 to 35.4 μm according to different setup parameters. The images were acquired with a 4 \times objective, source voltage of 40 kV, current 200 μA , and pixel size of 5.6 μm . Images were collected using the Xradia TXMController software and reconstructed using the Xradia TXMR econstructor software.

4.5 Evaluation of Ag NPs-induced permeability change of the biological barriers in the rat ear using MRI (I)

In this section, a 4.7 T MR scanner with a bore diameter of 155 mm (PharmaScan, Bruker BioSpin, Germany) was used for the evaluation of the biological barrier function in the ear. The maximum gradient strength was 300 mT/m with an 80- μs rise time. Animals were anaesthetized with a 5 % isoflurane-oxygen mixture for induction and 3 % for maintenance at a flow rate of 1.0 L/min via a facemask. The body temperature of the rat was maintained by circulating warm water, and the respiration

rate was recorded with the Physio Tool-1.0.b.2 programme (Bruker Cor., Germany). Either 40 or 50 μl of Ag NPs at defined concentrations were delivered into the middle ear cavity using the same method as described above. A gadolinium-tetra-azacyclododecane-tetra-acetic acid (Gd-DOTA, 500 mM, DOTAREM, Guerbet, Cedex, France) solution was injected into the tail vein at a dosage of 0.725 mM/kg 2 h prior to the MRI measurement. Afterwards, the rats were placed in the magnet with their ears positioned at the isocenter. MRI scanning commenced at several time points post-injection. The first imaging time of 5 h was determined by taking the penetration time of liposome NPs from the middle ear to the inner ear as a reference (Zou et al., 2010b). The final imaging time of 7 d was selected according to the course of acute inflammation. For imaging protocols, T2-weighted 2D images were acquired using a rapid acquisition with relaxation enhancement (RARE) sequence (TR/TE_{eff} 2500/40 ms, RARE factor 8, matrix size 256 \times 256, slice thickness [ST] 0.8 mm, field of view [FOV] 5.0 \times 5.0 cm², resolution 0.195 \times 0.195 mm², and number of averages [NEX] 3) to set up the geometry. T1-weighted 2D images were acquired using a RARE sequence (TR/TE_{eff} 500/10 ms, RARE factor 4, matrix size 256 \times 192, ST 0.5 mm, FOV 2.5 \times 2.5 cm², resolution 0.098 \times 0.13 mm², and NEX 33). A 2D fluid-attenuated inversion-recovery (FLAIR) sequence (TR/TE_{eff} 8000/40 ms, inversion time 1 800 ms, RARE factor 16, matrix size 256 \times 192, ST 0.5 mm, FOV 3.0 \times 3.0 cm², resolution 0.117 \times 0.156 mm², and NEX 7) was used to confirm the signal of gadolinium. ParaVision PV 4.0 software (Bruker Cor., Germany) was used for post-processing and quantification of MR images.

4.6 ABR measurements (I)

Hearing acuity was evaluated by ABR measurements before treatment and at 2 d, 4 d, and 7 d post-injection in a soundproof chamber using BioSig32 (Tucker-Davis Technologies, Alachua, USA). Evoked ABRs were recorded as described previously with the minor modification that the ground electrode was inserted subcutaneously into the ipsilateral thigh (Zou et al., 2009). Clicks at a duration of 50 μs and a repetition rate of 21.1 $\cdot\text{s}^{-1}$ were transmitted into the external ear canal through a pipette tip connected to a silica and plastic ear speculum that was mounted to an earphone (TDH-39P, Telephonics, New York, USA). For frequency-specific ABR assessment, tone bursts at a duration of 47.619 ms and a repetition rate of 21 $\cdot\text{s}^{-1}$ were generated via an FF1 speaker (Tucker-Davis Technologies, Alachua, USA) 5 cm away from the tympanic membrane. The contralateral external ear canal was plugged with a rubber insert. Responses from 1 000 sweeps were averaged with a gain of 20 at each intensity level using a 0.3-3 kHz filter. The stimuli were presented as 80 to 0 dB sound pressure levels in descending-5-dB increments. The auditory threshold was determined by evoking a minimum visible and repeatable wave II at the lowest intensity.

4.7 Sample preparation for immunostaining

Rats were anaesthetized using the same method as described above, the temporal bone was fixed via cardiac perfusion with 0.01 M PBS pH 7.4 containing 0.6 % (v/v) heparin (LEO Pharma A/S, Ballerup, Denmark) followed by 4 % paraformaldehyde (Merck, Espoo, Finland). After decapitation, the bullae were isolated and immersed in the same fixative solution overnight, and decalcified using 10 % ethylenediamine-tetraacetic acid (Sigma, Steinheim, Germany) in the following 4 weeks with weekly solution changes. A standard procedure for paraffin embedding (70 % alcohol 1 h, 80 % alcohol 1 h, 94 % alcohol 2 h+1 h, absolute alcohol 1 h+1 h 30 min+2 h, xylene 2 h+1 h, and paraffin 3×1 h) was performed using a Tissue-Tek® VIP™ 5 Vacuum Infiltration Processor (Sakura Finetek, Torrance, USA) and a Tissue-Tek® TEC™ 5 Tissue Embedding Console System (Sakura Finetek, Torrance, USA). The tissue block was sectioned at a thickness of 4 µm using a LEICA SM2000R-Sliding Microtome (Leica, Heidelberg, Germany).

4.8 Analysis of cytokine expression (III and IV)

4.8.1 Antibodies and chromogen

The primary antibodies used in the assay were anti-CD68 (1:200, Abcam, UK), anti-CD44 (1:400, Abcam, UK), anti-hyaluronic acid (1:400, AbD Serotec, Germany), anti-TLR2 (1:250, Novus Biologicals, UK), anti-TLR4 (1:200, Novus Biologicals, UK), anti-MCP1 (1:4 000, Novus Biologicals, UK), anti-MCP2 (1:200, GeneTex, USA), anti-Rac1 (1:800, Abcam, UK), anti-myosin light chain (1:100, Cell Signaling Technology, USA), anti-VCAM1 (1:50, Proteintech, USA), anti-Erk1/2 (1:400, Abcam, UK), anti-JNK (1:100, Cell Signaling Technology, USA), anti-p38 (1:100, Cell Signaling Technology, USA), anti-TNF- α (1:800, Abcam, UK), anti-TNFR1 (1:500, Abcam, UK), anti-TNFR2 (1:50, Abcam, UK), anti-IL-1 β (1:400, Novus Biologicals, UK), anti-IL-10 (1:400, Abbiotec, USA), anti-TGF- β (1:500, Abcam, UK), anti-A20 (1:200, Sigma-Aldrich, USA), and anti-RNF11 (1:100, Abcam, UK). Among them, anti-hyaluronic acid was hosted in sheep and the rest of the antibodies were hosted in rabbit.

For the immunofluorescence staining, secondary antibodies including fluorescein isothiocyanate-labelled goat anti-rabbit IgG (1:200, Life Technologies™, New York, USA) and Cy™ 3-conjugated rabbit anti-sheep IgG (1:400, Jackson Immuno-Research Laboratories Inc., West Grove, USA) were used depending on the host of the primary antibodies. For the immunostaining visualized by 3, 3'-diaminobenzidine (DAB), a VECTASTAIN® ELITE ABC Kit (Vector Laboratories Ltd., Peterborough, UK) that contained biotinylated goat anti-rabbit IgG and Reagent A (Avidin DH solution) and B (biotinylated enzyme) was used to combine the formed immune

complex with the secondary antibody. All the primary and secondary antibodies diluted in 0.1 % BSA (Sigma, St. Louis, USA, dissolved in 0.01 M PBS pH 7.4). A DAB Peroxidase Substrate Kit (Vector Laboratories Ltd., Peterborough, UK) that contained DAB Stock Solution and Hydrogen Peroxide Stock Solution was used to visualize antibody binding.

4.8.2 Immunofluorescence staining

After deparaffinization and hydration, the cochlear slices were digested with 0.1 % Trypsin (Sigma, St. Louis, USA, dissolved in 0.01 M PBS pH 7.4) at 37 °C for 30 min. After rinsing with 0.1 % PBS-Tween® 20 for 3×2 min (Sigma, St. Louis, USA, diluted in 0.01 M PBS pH 7.4), the slices were incubated with either 10 % heat-inactivated normal rabbit (KPL Inc., Gaithersburg, USA) or goat serum (Invitrogen, Paisley, UK) depending on the host of the secondary antibodies at room temperature for 30 min. After discarding the remnant serum, the slices were incubated with the primary antibodies listed above at 4 °C overnight, respectively. After rinsing with 0.1 % PBS-Tween® 20 for 3×2 min, the slices were incubated with fluorescent secondary antibodies mentioned above depending on the primary antibodies at room temperature for 1 h. Finally, the nuclei were counterstained with 10 µg/ml 4', 6-diamidino-2-phenylindole (DAPI) (Life Technologies™, New York, USA) at room temperature for 10 min, and the slides were mounted for confocal microscopy with Fluoromount (Sigma, St. Louis, USA). In the negative control slices, the primary antibodies were replaced with 0.1 % BSA.

4.8.3 Immunostaining visualized by DAB

After deparaffinization and hydration, the cochlear slices were immersed in 3 % H₂O₂-methanol at room temperature for 30 min. After rinsing with PBS for 2×2 min, the slices were digested with 0.1 % Trypsin (Sigma, St. Louis, USA, dissolved in 0.01 M PBS pH 7.4) at 37 °C for 30 min. After rinsing with 0.1 % PBS-Tween® 20 for 3×2 min, the slices were incubated with 10 % normal goat serum (Invitrogen, Paisley, UK) at room temperature for 30 min. After discarding the remnant serum, the slices were incubated with the primary antibodies listed above at 4 °C overnight, respectively. After rinsing with 0.1 % PBS-Tween® 20 for 3×2 min, the slices were incubated with biotinylated goat anti-rabbit IgG at a dilution of 1:100 (Vector Laboratories Ltd., Peterborough, UK) at room temperature for 1 h. After rinsing with 0.1 % PBS-Tween® 20 for 3×2 min, the slices were incubated with the streptavidin-biotin-peroxidase complex (Vector Laboratories Ltd., Peterborough, UK) at 37 °C for 1 h. After rinsing with 0.1 % PBS-Tween® 20 for 3×5 min, antibody binding was visualized using a DAB Peroxidase Substrate Kit (Vector Laboratories Ltd., Peterborough, UK)

at room temperature for 5 min. Alternatively, the nuclei were counterstained using haematoxylin (Merck, Darmstadt, Germany). Dehydration and vitrification were completed with a standard protocol (70 % alcohol 10 s, 94 % alcohol 2×10 s, absolute alcohol 2×1 min, and xylene 3×3 min). The slides were mounted for light microscopy with Clarion™ Mounting Medium (Sigma, St. Louis, USA). In the negative control slices, the primary antibodies were replaced with 0.1 % BSA. Staining intensities (shown by the greyscale value that was inversely correlated with the staining intensity) in the strial basal cells, spiral ligament fibrocytes, and spiral ganglion cells were measured and semi-quantified using ImageJ 1.45S software (NIH, Bethesda, USA).

4.9 Cell death detection (III)

Apoptosis was evaluated using the terminal deoxynucleotidyl transferase deoxyuridine triphosphate nick end labelling (TUNEL) assay and an *In Situ* Cell Death Detection Kit TMR Red (Roche Diagnostics, Basel, Switzerland). After deparaffinization and hydration, the cochlear slices were incubated with Proteinase K (Fermentas, Vantaa, Finland, 20 µg/ml in 10 mM Tris/HCl, pH 7.4) at 37 °C for 30 min and, subsequently, an apoptosis mixture (5 µl of enzyme solution and 45 µl of label solution [1:9]) at 37 °C for 1 h in a dark environment. The nuclei were stained with 10 µg/ml DAPI (Life Technologies™, New York, USA) at room temperature for 10 min, and the slides were mounted for confocal microscopy with Fluoromount (Sigma, St. Louis, USA). Slices exposed to label solution instead of reaction mixture were used as negative controls, and slices exposed to recombinant DNase I (Fermentas, Vantaa, Finland, 100 U/ml in 50 mM Tris/HCl, pH 7.5, 1 mg/ml BSA) at 37 °C for 10 min, which induced DNA strand breaks prior to the previous labelling procedures, were used as positive controls.

4.10 Confocal and light microscopies

The samples from immunofluorescence staining were observed and images obtained under an inverted microscope (ECLIPSE Ti, Nikon, Tokyo, Japan) combined with an Andor confocal system installed with Andor iQ 2.8 or 3.0 software (Andor Technology, Belfast, UK). The excitation lasers were 405 nm (blue excitation), 488 nm (green excitation), and 568 nm (red excitation) from an Andor laser combiner system, and the corresponding emission filters were 450-465 nm (DAPI), 525/50 nm (fluorescein isothiocyanate), and 607/45 nm (Cy™3 and TMR Red), respectively. The immunostained samples visualized by DAB were observed under a light microscope (LEICA DM 2000, Espoo, Finland), and images were digitally photographed by a camera video (Olympus DP 25, Tokyo, Japan) with the cellSens Dimension 1.6 Olympus software (Olympus Corporation, Tokyo, Japan) installed.

4.11 Data analysis and statistics

Statistical analyses were performed using the IBM® SPSS® Statistics Version 20 or 23 software package (SPSS Inc., Chicago, USA). Independent-samples *t*-test was used to compare the signal ratio of different locations in the rat ear for evaluation of the permeability change of the biological barriers using MRI and ABR threshold shifts that were dependent on the frequencies at the defined time points.

One-way analysis of variance was used to compare the IC₅₀ for Ag NPs using different assays in BALB/c 3T3 cells and the intensities of immunostaining visualized by DAB for CD68, TLR2, TLR4, MCP1, MCP2, A20, and RNF11 in the designated structures of different turns among the cochleae exposed to 4 000 µg/ml Ag NPs, 200 µg/ml Ag NPs, and dH₂O. The LSD *post-hoc* test was used to evaluate the pairwise difference. A value of $p < 0.05$ indicated that the difference was statistically significant.

5 Results

5.1 Ag NPs toxicity in BALB/c 3T3 cells (I)

The IC₅₀ for Ag NPs was 2.8 µg/ml in the NRU assay, which was lower than that in the WST-1 assay (3.0 µg/ml) and higher than that in total cellular ATP measurement (2.6 µg/ml) and nuclear membrane integrity that was assessed by the PI staining assay (2.2 µg/ml) ($p < 0.05$, one-way ANOVA). These findings imply that Ag NPs demonstrate variable IC₅₀ in BALB/c 3T3 cells when different assays are used and PI staining is the most sensitive assay to evaluate the toxicity of Ag NPs.

5.2 Transportation of Ag NPs from the rat middle ear to the inner ear (II)

At 4 h after transtympanic injection of 40 000 µg/ml Ag NPs (40 µl), the NPs were distributed in the external ear canal, the middle ear mucosa, Eustachian tube, the ossicular chain, the stapes artery, the annular ligament, the round window membrane, and the mesothelia of the scala tympani as detected by the micro CT. At 24 h, Ag NPs were visible in the round window membrane and oval window, as well as the cochlea. At 7 d after transtympanic injection of 4 000 µg/ml Ag NPs (40 µl), Ag NPs were visualized in both the middle ear and cochlea. However, transtympanic injection of 200 µg/ml Ag NPs (40 µl) did not produce any signal. No Ag NPs were detected in the ear of non-treated control. These results suggest that the distribution of Ag NPs in the rat ear is a dynamic process, and the round and oval windows may exert roles in transporting Ag NPs from the middle ear to the inner ear.

5.3 Permeability augmentation of the biological barriers in the rat ear and hearing loss caused by Ag NPs (I)

Using gadolinium-enhanced MRI, significant changes in the permeability of biological barriers were demonstrated in the skin of the external ear canal, mucosa of the

middle ear, and inner ear at 5 h post-transtympanic injection ($p < 0.01$, independent-samples t -test). The induced alteration showed a dose-dependent manner (20-4 000 $\mu\text{g}/\text{ml}$) and recovered to the base line at 7 d ($p > 0.05$, independent-samples t -test).

Transtympanic injection of 4 000 $\mu\text{g}/\text{ml}$ Ag NPs (40 μl) caused irreversible hearing loss at 4, 8, 16, and 32 kHz ($p < 0.01$ and $p < 0.05$, independent-samples t -test), while transient hearing loss occurred at click and 2 kHz. However, 200 $\mu\text{g}/\text{ml}$ Ag NPs (40 μl) only induced hearing loss at 32 kHz at 2 d and 4 d ($p < 0.01$, independent-samples t -test), which recovered at 7 d.

These findings imply that Ag NPs disrupt the permeability of biological barriers in the skin of the external ear canal, mucosa of the middle ear, and inner ear in a dose-dependent manner, which cause cochlear functional change.

5.4 Accumulation of hyaluronic acid in the rat cochlea exposed to Ag NPs (III)

In the cochleae exposed to 4 000 $\mu\text{g}/\text{ml}$ Ag NPs, positive staining for hyaluronic acid was enhanced in the basilar membrane, spiral ligament fibrocytes, spiral ganglion cells, and strial basal cells. The spiral ligament fibrocytes and basilar membrane showed a gradient reduction in staining intensity from the first to third turn, while the strial basal cells demonstrated a gradient increase in staining intensity from the first to third turn. These results suggest that Ag NPs may augment the permeability of biological barriers in the rat cochlea and alter mechanical properties of the cochlea through the accumulation of hyaluronic acid, leading to hearing loss.

5.5 Ag NPs elevated the levels of CD68, MCP1, TLR4, A20, and RNF11 (IV)

Ag NPs at a concentration of 0.4 % rather than 0.02 % up-regulated the expressions of CD68, TLR4, MCP1, A20, and RNF11 in the strial basal cells, spiral ligament fibrocytes, and non-sensory supporting cells of Corti's organ. Meanwhile, 0.4 % Ag NPs had no effect on CD44, TLR2, MCP2, Rac1, myosin light chain, VCAM1, Erk1/2, JNK, p38, IL-1 β , TNF- α , TNFR1, TNFR2, IL-10, or TGF- β . The levels of molecules in the rat cochlea exposed to Ag NPs were summarized in **Table 3**.

Table 3 The levels of molecules in the rat cochlea exposed to Ag NPs

| Functions/Properties | Molecules |
|---|---|
| Innate immunity | CD68 (↑), TLR2 (-), TLR4 (↑) |
| Chemotaxis | MCP1 (↑), MCP2 (-) |
| Ubiquitination | A20 (↑), RNF11 (↑) |
| Cell recruitment | CD44 (-) |
| Tight junction-associated proteins | VCAM1 (-), Rac1 (-), MLC ^a (-) |
| Cellular signaling transduction | Erk1/2 (-), JNK (-), p38 (-) |
| Inflammation | IL-1 β (-), TNF- α (-), TNFR1 (-), TNFR2 (-) |
| Anti-inflammation | IL-10 (-), TGF- β (-) |

↑: enhanced; -: unchanged; MLC^a: myosin light chain.

These findings suggest that Ag NPs might confer macrophage-like functions on the stria basal cells and spiral ligament fibrocytes and enhance the immune activities of non-sensory supporting cells of Corti's organ through the up-regulation of CD68 that is mediated by TLR4 activation. Meanwhile, A20 and RNF11 played roles in maintaining cochlear homeostasis via negative regulation of the expressions of inflammatory cytokines. In summary, these results verify that non-sensory cells in the rat cochlea may attain immune feature in response to Ag NPs and support the notion that the inner ear may not be an 'immunologically privileged organ'.

5.6 Cell death in the rat cochlea exposed to Ag NPs (III)

In the cochleae exposed to 4 000 $\mu\text{g}/\text{ml}$ Ag NPs, TUNEL-positive cells were detected primarily in Corti's organ, mesothelial cells of the scala tympani, stria vascularis, spiral ligament, Reissner's membrane, and spiral limbus. The majority of positive cells in the cochlear lateral wall were demonstrated in the first turn, and clearly less positive cells in the third turn. In the cochleae exposed to 200 $\mu\text{g}/\text{ml}$ Ag NPs, a few positive cells were identified in the stria marginal cells, and sparse ones were distributed in Corti's organ and osseous spiral lamina. In the cochleae exposed to dH₂O, occasional positive cells were visualized in the bony wall. These findings suggest that Ag NPs impair the cochlear cells and the mitochondrial dysfunction may be involved in the mechanism.

6 Discussion

6.1 General comments

In the current research, first of all, we demonstrated that Ag NPs-induced toxicity was implicated in the mitochondrial dysfunction and BALB/c 3T3 cells *in vitro* were more sensitive to Ag NPs as much as 1 000 times than the rat cochlear cells *in vivo*. Secondly, to validate the role of biological barriers in resisting Ag NPs penetration into the inner ear, we exposed the rat inner ear to Ag NPs through transtympanic injection and using micro CT found that Ag NPs were detected in the middle ear, ossicular chain, round window membrane, oval window, and scala tympani. The transportation pathways were shown to be the round and oval windows. After accessing into the inner ear, Ag NPs caused significant changes to the permeability of biological barriers in the inner ear as demonstrated using gadolinium-enhanced MRI as well as hearing loss using ABR measurements. Significantly, the alterations were partially reversible and revealed a dose-dependent manner. Thirdly, to elucidate possible molecular mechanism of Ag NPs-induced functional change in the biological barriers in the rat cochlea, we thoroughly analysed the levels of molecules involved in the TLR signaling pathways and potential recruitment of macrophages and found that Ag NPs not only caused accumulation of hyaluronic acid in the rat cochlea but also up-regulated the expressions of CD68, TLR4, MCP1, A20, and RNF11 in the stria basilar cells, spiral ligament fibrocytes, and non-sensory supporting cells of Corti's organ. However, Ag NPs had no effect on CD44, TLR2, MCP2, Rac1, myosin light chain, VCAM1, Erk1/2, JNK, p38, IL-1 β , TNF- α , TNFR1, TNFR2, IL-10, or TGF- β .

In the *in vitro* study, AgNO₃ was used as a control to evaluate the toxicity of ionic Ag⁺. It has been reported that Ag NPs and ionic Ag⁺ are both toxic to the cells and ionic Ag⁺ are considered as primary components to mediate the toxicity of Ag NPs (McShan et al., 2014). However, this is quite questionable, because ionic Ag⁺ does not exist in either animal or human body after reacting with the Cl⁻ and forming AgCl. The IC₅₀ for AgCl was much higher than that for Ag NPs. Furthermore, our unpublished data demonstrated that AgCl did not cause any hearing loss even though at the saturated concentration. Therefore, it is concluded that the biological effects shown in the current research are resulted from intact Ag NPs rather than the dissociated ionic Ag⁺.

CT and MRI are the most popular imaging techniques in basic and clinical investigations. However, the biological effects caused by radiation are largely unclear when received a CT scanning, although a recent study showed that radiation might lead to decelerated growth and delayed maturity, and the typical pathologies were atrophy

and fibrosis (Miyahara et al., 2016). Meanwhile, transtympanic injection of contrast agent gadolinium-containing compounds has been shown to cause inflammatory response in the inner ear (*e.g.*, infiltration of lymphocytes into the scala tympani), degeneration of the stria vascularis, and morphological change of the outer hair cells (Kakigi et al., 2008; Katahira et al., 2013; Park et al., 2016). Therefore, the adverse effects of X-rays and gadolinium should be considered. Miniature size of the inner ear tissue may limit the applications of tissue abundance-dependent assays because it is not that easy to yield high-quality of RNAs and proteins (Cai et al., 2013). Moreover, diversity of cell populations within the inner ear may cripple the purity of targeted cells obtained, which compromise reproducibility and reliability of the results. Thus, immunostaining has been used in this study, not only can the locations and distributions of molecules in various cells within the inner ear be shown but also quantification analysis is possible.

6.2 Correlation of Ag NPs toxicity in BALB/c 3T3 cells and the rat cochlea (I and III)

Both NRU and PI staining assays are used to evaluate membrane integrity, and thus reflect the viability of cells. However, the substrates that neutral red and PI bind are lysosomes and nucleic acids, respectively, and they are distributed in different subcellular locations. The results demonstrated that nuclear membrane were more likely prone to be penetrated by Ag NPs than lysosome membrane. The differential susceptibility of cell populations to the mitochondrial toxin relied on the cellular activity-related energy consumption (Zou et al., 2011; Zou et al., 2013). Mitochondria are the central site of oxidative phosphorylation and yield ATP to sustain various biological activities within the cells. Meanwhile, glycolysis is also a significant energy source to produce ATP, especially when the mitochondria are impaired (Loesberg et al., 1990). Therefore, it is concluded that intracellular ATP measurement is more objective to reflect intracellular gross energy consumption, while WST-1 test is more specific to show the activity of the mitochondria.

In general, the IC_{50} of Ag NPs in the *in vivo* studies were higher as much as 1 000 times than that in the *in vitro* tests, suggesting that the individual cells *in vitro* were more sensitive to Ag NPs than the inner ear cells *in vivo*. This was in accordance with the previous study showing that cells in the primary cochlear cell culture were more sensitive to the mitochondrial toxin 3-nitropropionic acid than the cochlear cells of guinea pigs (Zou et al., 2013). It is most likely attributed to the highly regulated double layer of the biological barriers in the inner ear that prevents the penetration of toxins and the extracellular matrix that has a powerful capability of buffering.

6.3 Transportation of Ag NPs from the rat middle ear to the inner ear (II)

Ag NPs encountered different biological fluids in the external ear canal, middle ear, and inner ear. The plentiful perilymph in the inner ear might interact with Ag NPs to form a compound immediately after entry. However, the unchanged size distributions after incubation with artificial perilymph suggested that the bright signal in the ear represented the Ag NPs.

The oval window pathway was verified to be more efficient than the round window to transport gadolinium from the middle ear to the inner ear in animals and humans using MRI (Zou et al., 2012a; Shi et al., 2014). Differential distributions of Ag NPs in the middle and inner ear implicated that the entry of Ag NPs from the middle ear into the inner ear was a dynamic process. It should be noted that the undetectable signal after 4 000 $\mu\text{g}/\text{ml}$ Ag NPs administration might be attributed to the low sensitivity of micro CT since the layer of Ag NPs formed on the tissue is too thin to raise the value of the voxel as a result of the partial volume effect.

6.4 Ag NPs augmented the permeability of biological barriers in the rat ear and caused hearing loss (I)

The Ag NPs that penetrated through the round and oval windows entered the inner ear and disrupted the blood-perilymph and blood-endolymph barriers. Although Ag NPs might directly compromise the inner ear cells by impairing mitochondrial function as shown in the *in vitro* study, complete recovery of hearing loss after 200 $\mu\text{g}/\text{ml}$ Ag NPs exposure suggested that the sensorineural cells were well-preserved and the integrity of the blood-endolymph barrier was critical to maintain hearing (Zou et al., 2009; Zou et al., 2011; Zou, 2012). It might be speculated that the transient auditory dysfunction was mainly due to the destabilized ion homeostasis. In general, hearing loss was in line with cell death in histological observations. However, only partial hearing loss, rather than complete hearing loss, occurred at frequencies above 4 kHz. Our explanation for this discrepancy was that tone burst ABR underestimated the thresholds in individuals with steeply sloping hearing loss attributed to the relatively broad spectra of the tone burst eliciting a response from a region of better hearing that was distant from the nominal stimulus frequency (Johnson and Brown, 2005). Therefore, the stimuli higher than 4 kHz elicited nerve fibres at higher turns (corresponding to lower frequencies) where the hair cells were not affected by Ag NPs.

6.5 Accumulation of hyaluronic acid in the rat cochlea exposed to Ag NPs (III)

The accumulation of hyaluronic acid caused by Ag NPs might directly interfere with potassium transport from the supporting cells of Corti's organ towards spiral ligament fibrocytes as hyaluronic acid attracts water and allows the rapid diffusion of water-soluble molecules into the matrix (Hansell et al., 2000). On the other hand, its accumulation might disturb the function of $\text{Na}^+\text{-K}^+\text{-ATPase}$ and $\text{Na}^+\text{-K}^+\text{-2Cl}^-$ cotransporter-1 that are responsible for ion transport. Moreover, the potential between spiral ligament Type I fibrocytes and striae basal cells that are involved in the formation of endocochlear potential would be crippled by the accumulation of the negatively charged hyaluronic acid (Nin et al., 2008). In addition, it should be noted that hyaluronic acid accumulation in the basilar membrane might disorganize the tuned resonant frequency map because mass, thickness, and stiffness of the basilar membrane are essential to create a response to sound wave (Wenzel et al., 2007).

6.6 Involvement of ubiquitin-editing protein A20 in modulating inflammation in the rat cochlea associated with Ag NPs-induced CD68 up-regulation and TLR4 activation (IV)

It was reported that macrophages were capable of being recruited into murine cochlea when challenged by noise and ototoxic drugs (Hirose et al., 2005; Tornabene et al., 2006; Sato et al., 2010; Hirose et al., 2014). In the current study, only a few ramified CD68-positive cells were identified in the spiral ligament after Ag NPs administration, implying that the unchanged CD44, Rac1, myosin light chain, and VCAM1 might be the reason for failure in recruiting abundant macrophages into the cochlea even though MCP1 was elevated (Matheny et al., 2000; Sun et al., 2011; Rom et al., 2012). Moreover, the unchanged levels of Erk1/2, JNK, and p38 implicated that MAPK signaling pathway was ineffective in fulfilling the adhesion and migration of monocytes (So et al., 2007). These findings demonstrated that striae basal cells, spiral ligament fibrocytes, and non-sensory supporting cells of Corti's organ might attain certain features that are similar to macrophages.

It is conceivable that CD68 might be implicated in TLR4 activation via caveolae trafficking operated by lipid rafts and caveolin-1 phosphorylation because CD68 was reportedly involved in vesicular trafficking (Ashley et al., 2011; Jiao et al., 2013). Theoretically, TLR4 activation triggers the $\text{NF-}\kappa\text{B}$ signaling pathway and finally elevates

the levels of inflammatory cytokines including IL-1 β , TNF- α , and its receptors TNFR1 and TNFR2. However, the up-regulations of A20 and RNF11 have been shown to inhibit the TLR-mediated inflammatory response and its induced NF- κ B signaling pathway (Gon et al., 2004; Guedes et al., 2014). Therefore, neither the downstream cytokines of macrophages nor TLR4 activation was up-regulated after Ag NPs administration although it was predictable that certain cytokines might be up-regulated once, suggesting that A20 and RNF11 played an important role in maintaining cochlear homeostasis, and thus preserving hearing. Nevertheless, the protective effects of A20 and RNF11 might be limited since only partial hearing recovery occurred in the high-frequency range.

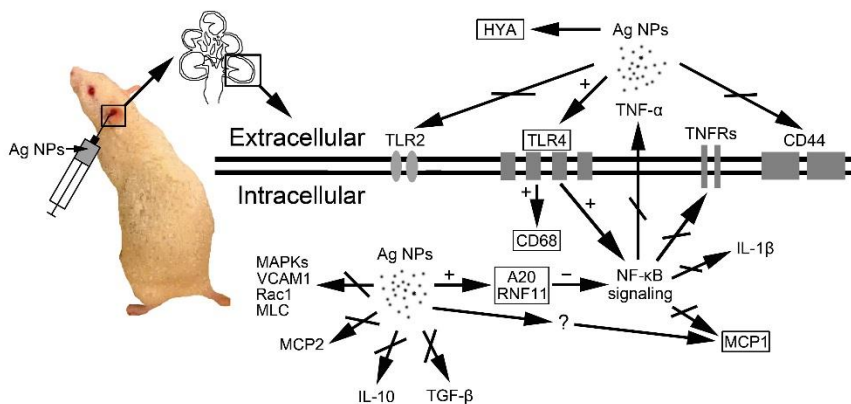


Fig. 4 Illustration of different molecules alterations in the rat cochlea exposed to Ag NPs. Ag NPs caused accumulation of hyaluronic acid and up-regulated the expressions of CD68, TLR4, MCP1, A20, and RNF11 (highlighted in square) but had no effect on CD44, TLR2, MCP2, Rac1, myosin light chain, VCAM1, Erk1/2, JNK, p38, IL-1 β , TNF- α , TNFR1, TNFR2, IL-10, or TGF- β . '+' : positive effect; '-' : negative effect; '↔' : no effect; '?' : unidentified molecules. MAPKs: mitogen-activated protein kinases; MLC: myosin light chain; HYA: hyaluronic acid.

6.7 Future directions

The current research focus on the evaluation of toxicity of Ag NPs, and the elimination of Ag NPs and the mechanism involved are not studied. Therefore, further studies should be concentrated more on the excretion of Ag NPs. In addition, it will be interesting to investigate the roles of physicochemical properties (especially the size, stability in the diluent, status of aggregation and agglomeration, and coating modification) in determining the biological behavior of Ag NPs. By doing this, it may be possible to explore the strategies on how to exert the anti-microbial activity of Ag NPs while avoiding the adverse effect of Ag NPs to the utmost extent.

7 Summary and conclusions

The following conclusions can be refined from the results of the current research:

1. Mitochondrial dysfunction was involved in the Ag NPs-induced toxicity. BALB/c 3T3 cells *in vitro* were more sensitive to Ag NPs as much as 1 000 times than the rat cochlear cells *in vivo*.
2. After transtympanic injection, the distribution of Ag NPs in the middle and inner ear could be visualized using micro CT. The pathways for Ag NPs to be transported from the rat middle ear to the inner ear were the round and oval windows.
3. Ag NPs caused significant changes to the permeability of biological barriers in the skin of the external ear canal, mucosa of the middle ear, and inner ear in a dose-dependent manner. The functional change in the inner ear was in line with the histological observations.
4. Ag NPs caused accumulation of hyaluronic acid, which might induce changes in the permeability of biological barriers and mechanical properties of the cochlea in response to vibration that are important for hearing. Also, Ag NPs might confer macrophage-like functions on the striae basal cells and spiral ligament fibrocytes and enhance the immune activities of non-sensory supporting cells of Corti's organ through the up-regulation of CD68, which might be involved in TLR4 activation. A20 and RNF11 played roles in maintaining cochlear homeostasis via negative regulation of the expressions of inflammatory cytokines.

The outlined results suggest that the delivery concentration of Ag NPs in possible future clinical application should be tightly controlled. The rat ear model might be expanded to study other engineered nanomaterials in nanotoxicology research.

8 Acknowledgements

This study was conducted at the Hearing and Balance Research Unit (HBRU), Field of Otolaryngology, School of Medicine, the University of Tampere, Finland during the years of 2012-2015.

Herein, I wish to express my sincere and deepest gratitude to my supervisors, Docent Jing Zou and Emeritus Professor Ilmari Pyykkö, for accepting my application to work and study in Finland. Their sustainable support, invaluable suggestion, and gentle generosity encourage me to accomplish my postgraduate study and scientific research efficiently and effectively at HBRU, Field of Otolaryngology, School of Medicine, the University of Tampere. In the past three years, Docent Jing Zou guided me to be a skillful scientific researcher in hearing and balance science. Above all, he mentored me how to think freely in a scientific and logical way, which benefited me tremendously. In addition, his infinite enthusiasm about science impressed me and let me understand that it is impossible to make scientific discovery without constant and persistent work. Emeritus Professor Ilmari Pyykkö always encouraged me in an open-minded, patient, and tolerant way, which motivated me to achieve the goals of my scientific research.

I would like to thank Professor Jussi Jero, Head and Neck Center, Otorhinolaryngology-Head and Neck Surgery, Helsinki University Hospital for his kindness being my opponent.

I am very grateful to official reviewers Docent Maija Vihinen-Ranta, Nanoscience Center, the Department of Biological and Environmental Science, the University of Jyväskylä and Docent Saku Sinkkonen, Head and Neck Center, Otorhinolaryngology-Head and Neck Surgery, Helsinki University Hospital, for their invaluable suggestion on the dissertation.

I wish to acknowledge the members of the follow-up group, Professor Tuula Heinonen, Director of Finnish Centre for Alternative Methods (FICAM), School of Medicine, the University of Tampere and Professor Seppo Parkkila, the Department of Anatomy, School of Medicine, the University of Tampere, for their invaluable suggestion on the dissertation. Both of them devoted and dedicated in the supervisory of this dissertation.

I am very lucky to work with so many outstanding co-workers in the University of Tampere and out of it. They helped me quite a lot during these years.

I would like to express my deepest gratitude to Professor Tuula Heinonen, Marika Mannerström, and Mirja Hyppönen, FICAM, School of Medicine, the University of Tampere, for their collaboration in the *in vitro* study.

I am very grateful to Professor Jari Hyttinen, Markus Hannula, Kalle Lehto, Ilm-

ari Tamminen, and Antti S. Aula, the Department of Electronics and Communications Engineering, Tampere University of Technology, for their collaboration in the micro CT study.

I wish to express my deepest gratitude to Minna Leppänen, Anne Hartin-Gathuo, Sanna Lehti, Tarja Tulonen, and Tuija Hartin, Animal Workshop, School of Medicine, the University of Tampere, for their great effort to take good care of the rats, without their assistance, the *in vivo* study cannot be done.

I am very grateful to Marja-Leena Koskinen for her kind help on the histology work.

I would like to thank Teemu Ihalainen and Outi Paloheimo, Neuro Group in Regenerative Medicine affiliated to BioMediTech, the University of Tampere, for their great effort to assist me on the employment of confocal microscopy.

I am indebted to the academic team under the leadership of Professor Seppo Parkkila, the Department of Anatomy, School of Medicine, the University of Tampere for providing me an opportunity to share the knowledge in the different area in the Journal Club.

I wish to appreciate Leena Honkaniemi, Arja Ahola, Satu Luhtasela, Hanna-Liisa Kojo, Ulla Kala, Salla Hyttinen, and Kari Mattila for their effort on placing the order of experiment reagents and coordination of the laboratory equipment.

I would like to thank Kristiina Tolvanen, Nastasia Prähl, and Sari Orhanen for their great effort on the coordination of my postgraduate study.

I wish to thank Kristiina Lehti and Merja Ahonen-Sihvola for their effort on the preparation of my work contract.

I would like to express my great gratitude to my predecessors Weikai Zhang and Ya Zhang and Chinese friends Jun Liu, Cai Li, Lihua Sun, Peiwen Pan, Shanjun Chen, Tingji Chen, Xiaoying Zhang, and Yuemei Fan for their kind help and nice care both physically and mentally.

I would like to thank my parents for their support.

This study was financially supported by the European Union 7th framework programme large-scale integrating project NanoValid (contract number: 263147) and NANOCI (contract number: 281056).

Tampere, March 2016

Hao Feng

9 References

- Aaronson, S.A., Todaro, G.J., 1968. Basis for the acquisition of malignant potential by mouse cells cultivated *in vitro*. *Science* 162, 1024-1026.
- Abrashkin, K.A., Izumikawa, M., Miyazawa, T., Wang, C.H., Crumling, M.A., Swiderski, D.L. et al., 2006. The fate of outer hair cells after acoustic or ototoxic insults. *Hear Res* 218, 20-29.
- Adams, J.C., 2002. Clinical implications of inflammatory cytokines in the cochlea: a technical note. *Otol Neurotol* 23, 316-322.
- Aili, D., Enander, K., Rydberg, J., Nesterenko, I., Bjorefors, F., Baltzer, L. et al., 2008. Folding induced assembly of polypeptide decorated gold nanoparticles. *J Am Chem Soc* 130, 5780-5788.
- Al-Rawi, M., Diabate, S., Weiss, C., 2011. Uptake and intracellular localization of submicron and nano-sized SiO₂ particles in HeLa cells. *Arch Toxicol* 85, 813-826.
- Altermatt, H.J., Gebbers, J.O., Muller, C., Arnold, W., Laissue, J., 1992. Functional morphology of the human endolymphatic sac. A review. *ORL J Otorhinolaryngol Relat Spec* 54, 173-178.
- Alvarado, J.C., Fuentes-Santamaria, V., Jareno-Flores, T., Blanco, J.L., Juiz, J.M., 2012. Normal variations in the morphology of auditory brainstem response (ABR) waveforms: a study in Wistar rats. *Neurosci Res* 73, 302-311.
- Ando, M., Kakigi, A., Takeuchi, S., 1999. Elongated pericyte-like cells connect discrete capillaries in the cochlear stria vascularis of gerbils and rats. *Cell Tissue Res* 296, 673-676.
- Annink, C., Gill, R., 2014. Nanoparticle Aggregate-Based Fluorescence Enhancement for Highly Sensitive and Reproducible Detection of DNA. *Part Part Syst Charact* 31, 943-947.
- Arai, Y., Miyayama, T., Hirano, S., 2015. Difference in the toxicity mechanism between ion and nanoparticle forms of silver in the mouse lung and in macrophages. *Toxicology* 328, 84-92.
- AshaRani, P.V., Low Kah Mun, G., Hande, M.P., Valiyaveetil, S., 2009. Cytotoxicity and genotoxicity of silver nanoparticles in human cells. *ACS Nano* 3, 279-290.
- Asharani, P.V., Xinyi, N., Hande, M.P., Valiyaveetil, S., 2010. DNA damage and p53-mediated growth arrest in human cells treated with platinum nanoparticles. *Nanomedicine (Lond)* 5, 51-64.
- Ashley, J.W., Shi, Z., Zhao, H., Li, X., Kesterson, R.A., Feng, X., 2011. Genetic ablation of CD68 results in mice with increased bone and dysfunctional osteoclasts. *PLoS One* 6, e25838.
- Bachor, E., Selig, Y.K., Jahnke, K., Rettinger, G., Karmody, C.S., 2001. Vascular variations of the inner ear. *Acta Otolaryngol* 121, 35-41.
- Bagger-Sjoberg, D., Rask-Andersen, H., 1986. The permeability barrier of the endolymphatic sac. A hypothesis of fluid and electrolyte exchange based on freeze fracturing. *Am J Otol* 7, 134-140.
- Baram-Pinto, D., Shukla, S., Perkas, N., Gedanken, A., Sarid, R., 2009. Inhibition of herpes simplex virus type 1 infection by silver nanoparticles capped with mercaptoethane sulfonate. *Bioconjug Chem* 20, 1497-1502.

- Barker, C.F., Billingham, R.E., 1977. Immunologically privileged sites. *Adv Immunol* 25, 1-54.
- Beitz, E., Zenner, H.P., Schultz, J.E., 2003. Aquaporin-mediated fluid regulation in the inner ear. *Cell Mol Neurobiol* 23, 315-329.
- Bhave, S.A., Oesterle, E.C., Coltrera, M.D., 1998. Macrophage and microglia-like cells in the avian inner ear. *J Comp Neurol* 398, 241-256.
- Boraschi, D., Costantino, L., Italiani, P., 2012. Interaction of nanoparticles with immunocompetent cells: nanosafety considerations. *Nanomedicine (Lond)* 7, 121-131.
- Buckingham, R.A., Valvassori, G.E., 2001. Inner ear fluid volumes and the resolving power of magnetic resonance imaging: can it differentiate endolymphatic structures? *Ann Otol Rhinol Laryngol* 110, 113-117.
- Cai, Q., Vethanayagam, R.R., Yang, S., Bard, J., Jamison, J., Cartwright, D. et al., 2014. Molecular profile of cochlear immunity in the resident cells of the organ of Corti. *J Neuroinflammation* 11, 173.
- Cai, Q., Wang, B., Patel, M., Yang, S.M., Hu, B.H., 2013. RNAlater facilitates microdissection of sensory cell-enriched samples from the mouse cochlea for transcriptional analyses. *J Neurosci Methods* 219, 240-251.
- Cao, L., He, C., 2013. Polarization of macrophages and microglia in inflammatory demyelination. *Neurosci Bull* 29, 189-198.
- Carlson, C., Hussain, S.M., Schrand, A.M., Braydich-Stolle, L.K., Hess, K.L., Jones, R.L. et al., 2008. Unique cellular interaction of silver nanoparticles: size-dependent generation of reactive oxygen species. *J Phys Chem B* 112, 13608-13619.
- Cavaillon, J.M., 2011. The historical milestones in the understanding of leukocyte biology initiated by Elie Metchnikoff. *J Leukoc Biol* 90, 413-424.
- Cavalieri, F., Tortora, M., Stringaro, A., Colone, M., Baldassarri, L., 2014. Nanomedicines for antimicrobial interventions. *J Hosp Infect* 88, 183-190.
- Chen, G.Y., Nunez, G., 2010. Sterile inflammation: sensing and reacting to damage. *Nat Rev Immunol* 10, 826-837.
- Choi, O., Hu, Z., 2008. Size dependent and reactive oxygen species related nanosilver toxicity to nitrifying bacteria. *Environ Sci Technol* 42, 4583-4588.
- Colvin, V.L., Kulinowski, K.M., 2007. Nanoparticles as catalysts for protein fibrillation. *Proc Natl Acad Sci U S A* 104, 8679-8680.
- Cook-Mills, J.M., 2002. VCAM-1 signals during lymphocyte migration: role of reactive oxygen species. *Mol Immunol* 39, 499-508.
- Cos, P., Tote, K., Horemans, T., Maes, L., 2010. Biofilms: an extra hurdle for effective antimicrobial therapy. *Curr Pharm Des* 16, 2279-2295.
- Costa, C.S., Ronconi, J.V., Daufenbach, J.F., Goncalves, C.L., Rezin, G.T., Streck, E.L. et al., 2010. *In vitro* effects of silver nanoparticles on the mitochondrial respiratory chain. *Mol Cell Biochem* 342, 51-56.
- Couloigner, V., Teixeira, M., Sterkers, O., Rask-Andersen, H., Ferrary, E., 2004. [The endolymphatic sac: its roles in the inner ear]. *Med Sci (Paris)* 20, 304-310.
- Couloigner, V., Fay, M., Djelidi, S., Farman, N., Escoubet, B., Runembert, I. et al., 2001. Location and function of the epithelial Na channel in the cochlea. *Am J Physiol Renal Physiol* 280, F214-222.
- Counter, S.A., Zou, J., Bjelke, B., Klason, T., 2003. 3D MRI of the *in vivo* vestibulo-cochlea labyrinth during Gd-DTPA-BMA uptake. *Neuroreport* 14, 1707-1712.
- Counter, S.A., Bjelke, B., Borg, E., Klason, T., Chen, Z., Duan, M.L., 2000. Magnetic reson-

ance imaging of the membranous labyrinth during *in vivo* gadolinium (Gd-DTPA-BMA) uptake in the normal and lesioned cochlea. *Neuroreport* 11, 3979-3983.

Counter, S.A., Nikkhrou, S., Brene, S., Damberg, P., Sierakowiak, A., Klason, T. et al., 2013. MRI evidence of endolymphatic impermeability to the gadolinium molecule in the *in vivo* mouse inner ear at 9.4 tesla. *Open Neuroimag J* 7, 27-31.

Crone, C., 1965. Facilitated transfer of glucose from blood into brain tissue. *J Physiol* 181, 103-113.

Cumberland, S.A., Lead, J.R., 2009. Particle size distributions of silver nanoparticles at environmentally relevant conditions. *J Chromatogr A* 1216, 9099-9105.

da Rocha Junior, L.F., Dantas, A.T., Duarte, A.L., de Melo Rego, M.J., Pitta Ida, R., Pitta, M.G., 2013. PPARgamma Agonists in Adaptive Immunity: What Do Immune Disorders and Their Models Have to Tell Us? *PPAR Res* 2013, 519724.

Dai, M., Nuttall, A., Yang, Y., Shi, X., 2009. Visualization and contractile activity of cochlear pericytes in the capillaries of the spiral ligament. *Hear Res* 254, 100-107.

Dallos, P., 2003. Organ of Corti kinematics. *J Assoc Res Otolaryngol* 4, 416-421.

Daneman, R., Zhou, L., Kebede, A.A., Barres, B.A., 2010. Pericytes are required for blood-brain barrier integrity during embryogenesis. *Nature* 468, 562-566.

Das, A., Sinha, M., Datta, S., Abas, M., Chaffee, S., Sen, C.K. et al., 2015. Monocyte and Macrophage Plasticity in Tissue Repair and Regeneration. *Am J Pathol* 185, 2596-2606.

Davies, D., 2003. Understanding biofilm resistance to antibacterial agents. *Nat Rev Drug Discov* 2, 114-122.

Dawson, V.L., Dawson, T.M., 2004. Deadly conversations: nuclear-mitochondrial cross-talk. *J Bioenerg Biomembr* 36, 287-294.

Dobrovolskaia, M.A., McNeil, S.E., 2007. Immunological properties of engineered nanomaterials. *Nat Nanotechnol* 2, 469-478.

Doke, S.K., Dhawale, S.C., 2015. Alternatives to animal testing: A review. *Saudi Pharm J* 23, 223-229.

Egger, S., Lehmann, R.P., Height, M.J., Loessner, M.J., Schuppler, M., 2009. Antimicrobial properties of a novel silver-silica nanocomposite material. *Appl Environ Microbiol* 75, 2973-2976.

El Badawy, A.M., Silva, R.G., Morris, B., Scheckel, K.G., Suidan, M.T., Tolaymat, T.M., 2011. Surface charge-dependent toxicity of silver nanoparticles. *Environ Sci Technol* 45, 283-287.

Elsaesser, A., Howard, C.V., 2012. Toxicology of nanoparticles. *Adv Drug Deliv Rev* 64, 129-137.

Esser, P.R., Wölfle, U., Dürr, C., von Loewenich, F.D., Schempp, C.M., Freudenberg, M.A. et al., 2012. Contact sensitizers induce skin inflammation via ROS production and hyaluronic acid degradation. *PLoS One* 7, e41340.

Fatima, F., Bajpai, P., Pathak, N., Singh, S., Priya, S., Verma, S.R., 2015. Antimicrobial and immunomodulatory efficacy of extracellularly synthesized silver and gold nanoparticles by a novel phosphate solubilizing fungus *Bipolaris tetramera*. *BMC Microbiol* 15, 52.

Feng, Q.L., Wu, J., Chen, G.Q., Cui, F.Z., Kim, T.N., Kim, J.O., 2000. A mechanistic study of the antibacterial effect of silver ions on *Escherichia coli* and *Staphylococcus aureus*. *J Biomed Mater Res* 52, 662-668.

Ferrary, E., Sterkers, O., Saumon, G., Tran Ba Huy, P., Amiel, C., 1987. Facilitated transfer of glucose from blood into perilymph in the rat cochlea. *Am J Physiol* 253, F59-65.

Flemming, H.C., Wingender, J., 2010. The biofilm matrix. *Nat Rev Microbiol* 8, 623-633.

Forge, A., 1985. Outer hair cell loss and supporting cell expansion following chronic gentamicin treatment. *Hear Res* 19, 171-182.

Franci, G., Falanga, A., Galdiero, S., Palomba, L., Rai, M., Morelli, G. et al., 2015. Silver nanoparticles as potential antibacterial agents. *Molecules* 20, 8856-8874.

Frohlich, E., 2012. The role of surface charge in cellular uptake and cytotoxicity of medical nanoparticles. *Int J Nanomedicine* 7, 5577-5591.

Fujioka, M., Okano, H., Ogawa, K., 2014. Inflammatory and immune responses in the cochlea: potential therapeutic targets for sensorineural hearing loss. *Front Pharmacol* 5, 287.

Fujioka, M., Kanzaki, S., Okano, H.J., Masuda, M., Ogawa, K., Okano, H., 2006. Proinflammatory cytokines expression in noise-induced damaged cochlea. *J Neurosci Res* 83, 575-583.

Fukuda, S., Harris, J.P., Keithley, E.M., Ishikawa, K., Kucuk, B., Inuyama, Y., 1992. Spiral modiolar vein: its importance in viral load of the inner ear. *Ann Otol Rhinol Laryngol Suppl* 157, 67-71.

Gagne, F., Auclair, J., Turcotte, P., Gagnon, C., 2013. Sublethal effects of silver nanoparticles and dissolved silver in freshwater mussels. *J Toxicol Environ Health A* 76, 479-490.

Garcia-Alonso, J., Khan, F.R., Misra, S.K., Turmaine, M., Smith, B.D., Rainbow, P.S. et al., 2011. Cellular internalization of silver nanoparticles in gut epithelia of the estuarine polychaete *Nereis diversicolor*. *Environ Sci Technol* 45, 4630-4636.

Geissmann, F., Manz, M.G., Jung, S., Sieweke, M.H., Merad, M., Ley, K., 2010. Development of monocytes, macrophages, and dendritic cells. *Science* 327, 656-661.

Getz, G.S., 2005. Thematic review series: the immune system and atherogenesis. Bridging the innate and adaptive immune systems. *J Lipid Res* 46, 619-622.

Gibbs, R.A., Weinstock, G.M., Metzker, M.L., Muzny, D.M., Sodergren, E.J., Scherer, S. et al., 2004. Genome sequence of the Brown Norway rat yields insights into mammalian evolution. *Nature* 428, 493-521.

Gloddek, B., Arnold, W., 1995. Role of adhesion molecules for the immunological defense of the inner ear. *ORL J Otorhinolaryngol Relat Spec* 57, 10-14.

Gloddek, B., Arnold, W., 1998. The endolymphatic sac receives antigenetic information from the organs of the mucosa-associated lymphatic system. *Acta Otolaryngol* 118, 333-336.

Gloddek, B., Bodmer, D., Brors, D., Keithley, E.M., Ryan, A.F., 2002. Induction of MHC class II antigens on cells of the inner ear. *Audiol Neurootol* 7, 317-323.

Godbey, W.T., Wu, K.K., Mikos, A.G., 1999. Tracking the intracellular path of poly (ethyleneimine)/DNA complexes for gene delivery. *Proc Natl Acad Sci U S A* 96, 5177-5181.

Gon, Y., Asai, Y., Hashimoto, S., Mizumura, K., Jibiki, I., Machino, T. et al., 2004. A20 inhibits toll-like receptor 2- and 4-mediated interleukin-8 synthesis in airway epithelial cells. *Am J Respir Cell Mol Biol* 31, 330-336.

Gordon, S., Taylor, P.R., 2005. Monocyte and macrophage heterogeneity. *Nat Rev Immunol* 5, 953-964.

Greulich, C., Diendorf, J., Simon, T., Eggeler, G., Epple, M., Koller, M., 2011. Uptake and intracellular distribution of silver nanoparticles in human mesenchymal stem cells. *Acta Biomater* 7, 347-354.

Gross, P.M., Teasdale, G.M., Angerson, W.J., Harper, A.M., 1981. H2-Receptors mediate increases in permeability of the blood-brain barrier during arterial histamine infusion. *Brain Res* 210, 396-400.

Gu, X., Keyoumu, Y., Long, L., Zhang, H., 2014. Detection of bacterial biofilms in different types of chronic otitis media. *Eur Arch Otorhinolaryngol* 271, 2877-2883.

Guedes, R.P., Csizmadia, E., Moll, H.P., Ma, A., Ferran, C., da Silva, C.G., 2014. A20 deficiency causes spontaneous neuroinflammation in mice. *J Neuroinflammation* 11, 122.

Hall-Stoodley, L., Hu, F.Z., Gieseke, A., Nistico, L., Nguyen, D., Hayes, J. et al., 2006. Direct detection of bacterial biofilms on the middle-ear mucosa of children with chronic otitis med-

ia. JAMA 296, 202-211.

Hansell, P., Goransson, V., Odland, C., Gerdin, B., Hallgren, R., 2000. Hyaluronan content in the kidney in different states of body hydration. *Kidney Int* 58, 2061-2068.

Harris, J.P., 1983. Immunology of the inner ear: response of the inner ear to antigen challenge. *Otolaryngol Head Neck Surg* 91, 18-32.

Harris, J.P., Ryan, A.F., 1995. Fundamental immune mechanisms of the brain and inner ear. *Otolaryngol Head Neck Surg* 112, 639-653.

Harris, J.P., Fukuda, S., Keithley, E.M., 1990. Spiral modiolar vein: its importance in inner ear inflammation. *Acta Otolaryngol* 110, 357-365.

Hawkins, E., Jr., 1973. Ototoxic mechanisms. A working hypothesis. *Audiology* 12, 383-393.

Hayashi, Y., Engelmann, P., Foldbjerg, R., Szabo, M., Somogyi, I., Pollak, E. et al., 2012. Earthworms and humans *in vitro*: characterizing evolutionarily conserved stress and immune responses to silver nanoparticles. *Environ Sci Technol* 46, 4166-4173.

Hibino, H., Nin, F., Tsuzuki, C., Kurachi, Y., 2010. How is the highly positive endocochlear potential formed? The specific architecture of the stria vascularis and the roles of the ion-transport apparatus. *Pflügers Arch* 459, 521-533.

Hirose, K., Discolo, C.M., Keasler, J.R., Ransohoff, R., 2005. Mononuclear phagocytes migrate into the murine cochlea after acoustic trauma. *J Comp Neurol* 489, 180-194.

Hirose, K., Li, S.Z., Ohlemiller, K.K., Ransohoff, R.M., 2014. Systemic lipopolysaccharide induces cochlear inflammation and exacerbates the synergistic ototoxicity of kanamycin and furosemide. *J Assoc Res Otolaryngol* 15, 555-570.

Huynh, K.A., Chen, K.L., 2011. Aggregation kinetics of citrate and polyvinylpyrrolidone coated silver nanoparticles in monovalent and divalent electrolyte solutions. *Environ Sci Technol* 45, 5564-5571.

Inamura, N., Salt, A.N., 1992. Permeability changes of the blood-labyrinth barrier measured *in vivo* during experimental treatments. *Hear Res* 61, 12-18.

Iversen, P.O., Nicolaysen, A., Kvernebo, K., Benestad, H.B., Nicolaysen, G., 1999. Human cytokines modulate arterial vascular tone via endothelial receptors. *Pflügers Arch* 439, 93-100.

Jabba, S.V., Oelke, A., Singh, R., Maganti, R.J., Fleming, S., Wall, S.M. et al., 2006. Macrophage invasion contributes to degeneration of stria vascularis in Pendred syndrome mouse model. *BMC Med* 4, 37.

Jahnke, K., 1975. The fine structure of freeze-fractured intercellular junctions in the guinea pig inner ear. *Acta Otolaryngol Suppl* 336, 1-40.

Jahnke, K., 1980. The blood-perilymph barrier. *Arch Otorhinolaryngol* 228, 29-34.

Jia, S., Dallos, P., He, D.Z., 2007. Mechanoelectric transduction of adult inner hair cells. *J Neurosci* 27, 1006-1014.

Jiao, H., Zhang, Y., Yan, Z., Wang, Z.G., Liu, G., Minshall, R.D. et al., 2013. Caveolin-1 Tyr14 phosphorylation induces interaction with TLR4 in endothelial cells and mediates MyD88-dependent signaling and sepsis-induced lung inflammation. *J Immunol* 191, 6191-6199.

Johnson, T.A., Brown, C.J., 2005. Threshold prediction using the auditory steady-state response and the tone burst auditory brain stem response: a within-subject comparison. *Ear Hear* 26, 559-576.

Joshi, N., Ngwenya, B.T., French, C.E., 2012. Enhanced resistance to nanoparticle toxicity is conferred by overproduction of extracellular polymeric substances. *J Hazard Mater* 241-242, 363-370.

Juhn, S.K., 1988. Barrier systems in the inner ear. *Acta Otolaryngol Suppl* 458, 79-83.

Juhn, S.K., Rybak, L.P., 1981. Labyrinthine barriers and cochlear homeostasis. *Acta Otolaryngol* 91, 18-32.

ryngol 91, 529-534.

Juhn, S.K., Rybak, L.P., Prado, S., 1981. Nature of blood-labyrinth barrier in experimental conditions. *Ann Otol Rhinol Laryngol* 90, 135-141.

Juhn, S.K., Rybak, L.P., Fowlks, W.L., 1982. Transport characteristics of the blood-perilymph barrier. *Am J Otolaryngol* 3, 392-396.

Jung, W.K., Gattaz, G., Schon, F.J., 1989. Kinetic experiments with radionuclides concerning the perilymph-blood barrier in a guinea pig model. *Arch Otorhinolaryngol* 246, 11-19.

Kakigi, A., Nishimura, M., Takeda, T., Okada, T., Murata, Y., Ogawa, Y., 2008. Effects of gadolinium injected into the middle ear on the stria vascularis. *Acta Otolaryngol* 128, 841-845.

Kanzaki, J., 1994. Immune-mediated sensorineural hearing loss. *Acta Otolaryngol Suppl* 514, 70-72.

Kastenbauer, S., Klein, M., Koedel, U., Pfister, H.W., 2001. Reactive nitrogen species contribute to blood-labyrinth barrier disruption in suppurative labyrinthitis complicating experimental pneumococcal meningitis in the rat. *Brain Res* 904, 208-217.

Katahira, N., Tanigawa, T., Tanaka, H., Nonoyama, H., Ueda, H., 2013. Diluted gadoteridol (ProHance®) causes mild ototoxicity in cochlear outer hair cells. *Acta Otolaryngol* 133, 788-795.

Kawauchi, H., Ichimiya, I., Kaneda, N., Mogi, G., 1992. Distribution of immunocompetent cells in the endolymphatic sac. *Ann Otol Rhinol Laryngol Suppl* 157, 39-47.

Keren, I., Wu, Y., Inocencio, J., Mulcahy, L.R., Lewis, K., 2013. Killing by bactericidal antibiotics does not depend on reactive oxygen species. *Science* 339, 1213-1216.

Khan, S.S., Mukherjee, A., Chandrasekaran, N., 2011. Studies on interaction of colloidal silver nanoparticles (SNPs) with five different bacterial species. *Colloids Surf B Biointerfaces* 87, 129-138.

Kharraz, Y., Guerra, J., Mann, C.J., Serrano, A.L., Munoz-Canoves, P., 2013. Macrophage plasticity and the role of inflammation in skeletal muscle repair. *Mediators Inflamm* 2013, 491497.

Kim, J.S., Song, K.S., Sung, J.H., Ryu, H.R., Choi, B.G., Cho, H.S. et al., 2013. Genotoxicity, acute oral and dermal toxicity, eye and dermal irritation and corrosion and skin sensitisation evaluation of silver nanoparticles. *Nanotoxicology* 7, 953-960.

Kim, J.S., Kuk, E., Yu, K.N., Kim, J.H., Park, S.J., Lee, H.J. et al., 2007. Antimicrobial effects of silver nanoparticles. *Nanomedicine* 3, 95-101.

Kim, S., Choi, J.E., Choi, J., Chung, K.H., Park, K., Yi, J. et al., 2009. Oxidative stress-dependent toxicity of silver nanoparticles in human hepatoma cells. *Toxicol In Vitro* 23, 1076-1084.

Kim, S.H., Marcus, D.C., 2011. Regulation of sodium transport in the inner ear. *Hear Res* 280, 21-29.

Kim, Y.S., Song, M.Y., Park, J.D., Song, K.S., Ryu, H.R., Chung, Y.H. et al., 2010. Subchronic oral toxicity of silver nanoparticles. *Part Fibre Toxicol* 7, 20.

Klaine, S.J., Alvarez, P.J., Batley, G.E., Fernandes, T.F., Handy, R.D., Lyon, D.Y. et al., 2008. Nanomaterials in the environment: behavior, fate, bioavailability, and effects. *Environ Toxicol Chem* 27, 1825-1851.

Klein, M., Schmidt, C., Kastenbauer, S., Paul, R., Kirschning, C.J., Wagner, H. et al., 2007. MyD88-dependent immune response contributes to hearing loss in experimental pneumococcal meningitis. *J Infect Dis* 195, 1189-1193.

Koivisto, S., 1995. Is *Daphnia magna* an ecologically representative zooplankton species in toxicity tests? *Environ Pollut* 90, 263-267.

Kolpashchikov, D.M., 2010. Binary probes for nucleic acid analysis. *Chem Rev* 110, 4709-

4723.

- Korani, M., Rezayat, S.M., Gilani, K., Arbabi Bidgoli, S., Adeli, S., 2011. Acute and subchronic dermal toxicity of nanosilver in guinea pig. *Int J Nanomedicine* 6, 855-862.
- Kreuter, J., 1978. Nanoparticles and nanocapsules--new dosage forms in the nanometer size range. *Pharm Acta Helv* 53, 33-39.
- Kurz, C.L., Ewbank, J.J., 2007. Infection in a dish: high-throughput analyses of bacterial pathogenesis. *Curr Opin Microbiol* 10, 10-16.
- Kwaky-Awuah, B., Williams, C., Kenward, M.A., Radecka, I., 2008. Antimicrobial action and efficiency of silver-loaded zeolite X. *J Appl Microbiol* 104, 1516-1524.
- Ladrech, S., Wang, J., Simonneau, L., Puel, J.L., Lenoir, M., 2007. Macrophage contribution to the response of the rat organ of Corti to amikacin. *J Neurosci Res* 85, 1970-1979.
- LaFerriere, K.A., Arenberg, I.K., Hawkins, J.E., Jr., Johnsson, L.G., 1974. Melanocytes of the vestibular labyrinth and their relationship to the microvasculature. *Ann Otol Rhinol Laryngol* 83, 685-694.
- Lampikoski, H., Aarnisalo, A.A., Jero, J., Kinnari, T.J., 2012. Mastoid biofilm in chronic otitis media. *Otol Neurotol* 33, 785-788.
- Lang, H., Schulte, B.A., Goddard, J.C., Hedrick, M., Schulte, J.B., Wei, L. et al., 2008. Transplantation of mouse embryonic stem cells into the cochlea of an auditory-neuropathy animal model: effects of timing after injury. *J Assoc Res Otolaryngol* 9, 225-240.
- Lang, H., Ebihara, Y., Schmiedt, R.A., Minamiguchi, H., Zhou, D., Smythe, N. et al., 2006. Contribution of bone marrow hematopoietic stem cells to adult mouse inner ear: mesenchymal cells and fibrocytes. *J Comp Neurol* 496, 187-201.
- Lansdown, A.B., 2004. A review of the use of silver in wound care: facts and fallacies. *Br J Nurs* 13, S6-19.
- Lappas, C.M., 2015. The immunomodulatory effects of titanium dioxide and silver nanoparticles. *Food Chem Toxicol* 85, 78-83.
- Lara, H.H., Ayala-Nunez, N.V., Ixtepan-Turrent, L., Rodriguez-Padilla, C., 2010. Mode of antiviral action of silver nanoparticles against HIV-1. *J Nanobiotechnology* 8, 1.
- Lara, H.H., Ixtepan-Turrent, L., Garza, Treviño E.N., Singh, D.K., 2011. Use of silver nanoparticles increased inhibition of cell-associated HIV-1 infection by neutralizing antibodies developed against HIV-1 envelope proteins. *J Nanobiotechnology* 18, 38.
- Le Coadic, M., Simon, M., Marchetti, A., Ebert, D., Cosson, P., 2012. *Daphnia magna*, a host for evaluation of bacterial virulence. *Appl Environ Microbiol* 78, 593-595.
- Lee, Y.K., Choi, E.J., Webster, T.J., Kim, S.H., Khang, D., 2015. Effect of the protein corona on nanoparticles for modulating cytotoxicity and immunotoxicity. *Int J Nanomedicine* 10, 97-113.
- Lenaz, G., 2001. The mitochondrial production of reactive oxygen species: mechanisms and implications in human pathology. *IUBMB Life* 52, 159-164.
- Lettiero, B., Andersen, A.J., Hunter, A.C., Moghimi, S.M., 2012. Complement system and the brain: selected pathologies and avenues toward engineering of neurological nanomedicines. *J Control Release* 161, 283-289.
- Li, W.R., Xie, X.B., Shi, Q.S., Duan, S.S., Ouyang, Y.S., Chen, Y.B., 2011. Antibacterial effect of silver nanoparticles on *Staphylococcus aureus*. *Biometals* 24, 135-141.
- Li, Y., Leung, P., Yao, L., Song, Q.W., Newton, E., 2006. Antimicrobial effect of surgical masks coated with nanoparticles. *J Hosp Infect* 62, 58-63.
- Lien, K.Y., Lee, G.B., 2010. Miniaturization of molecular biological techniques for gene assay. *Analyst* 135, 1499-1518.
- Listyo, A., Brand, Y., Setz, C., Radojevic, V., Resink, T., Levano, S. et al., 2011. T-cadherin in

the mammalian cochlea. *Laryngoscope* 121, 2228-2233.

Liu, J., Hurt, R.H., 2010. Ion release kinetics and particle persistence in aqueous nano-silver colloids. *Environ Sci Technol* 44, 2169-2175.

Loesberg, C., Van Rooij, H., Nooijen, W.J., Meijer, A.J., Smets, L.A., 1990. Impaired mitochondrial respiration and stimulated glycolysis by m-iodobenzylguanidine (MIBG). *Int J Cancer* 46, 276-281.

Loeschner, K., Hadrup, N., Qvortrup, K., Larsen, A., Gao, X., Vogel, U. et al., 2011. Distribution of silver in rats following 28 days of repeated oral exposure to silver nanoparticles or silver acetate. *Part Fibre Toxicol* 8, 18.

Lu, L., Sun, R.W., Chen, R., Hui, C.K., Ho, C.M., Luk, J.M. et al., 2008. Silver nanoparticles inhibit hepatitis B virus replication. *Antivir Ther* 13, 253-262.

Lu, T.K., Zhak, S., Dallos, P., Sarpeshkar, R., 2006. Fast cochlear amplification with slow outer hair cells. *Hear Res* 214, 45-67.

Lundquist, P.G., 1976. Aspects on endolymphatic sac morphology and function. *Arch Otorhinolaryngol* 212, 231-240.

Luo, Y.H., Chang, L.W., Lin, P., 2015. Metal-Based Nanoparticles and the Immune System: Activation, Inflammation, and Potential Applications. *Biomed Res Int* 2015, 143720.

Ma, C., Billings, P., Harris, J.P., Keithley, E.M., 2000. Characterization of an experimentally induced inner ear immune response. *Laryngoscope* 110, 451-456.

Ma, W., Jing, L., Valladares, A., Mehta, S.L., Wang, Z., Li, P.A. et al., 2015. Silver Nanoparticle Exposure Induced Mitochondrial Stress, Caspase-3 Activation and Cell Death: Amelioration by Sodium Selenite. *Int J Biol Sci* 11, 860-867.

Maeda, K., Yoshida, K., Ichimiya, I., Suzuki, M., 2005. Dexamethasone inhibits tumor necrosis factor-alpha-induced cytokine secretion from spiral ligament fibrocytes. *Hear Res* 202, 154-160.

Malaczewska, J., 2014. Effect of 28-day oral administration of silver nanocolloid on the peripheral blood leukocytes in mice. *Pol J Vet Sci* 17, 263-273.

Mantovani, A., Sica, A., Sozzani, S., Allavena, P., Vecchi, A., Locati, M., 2004. The chemokine system in diverse forms of macrophage activation and polarization. *Trends Immunol* 25, 677-686.

Marcus, B.C., Hynes, K.L., Gewertz, B.L., 1997. Loss of endothelial barrier function requires neutrophil adhesion. *Surgery* 122, 420-426; discussion 426-427.

Markowska, K., Grudniak, A.M., Wolska, K.I., 2013. Silver nanoparticles as an alternative strategy against bacterial biofilms. *Acta Biochim Pol* 60, 523-530.

Marti, A.A., Jockusch, S., Stevens, N., Ju, J., Turro, N.J., 2007. Fluorescent hybridization probes for sensitive and selective DNA and RNA detection. *Acc Chem Res* 40, 402-409.

Massarsky, A., Dupuis, L., Taylor, J., Eisa-Beygi, S., Strek, L., Trudeau, V.L. et al., 2013. Assessment of nanosilver toxicity during zebrafish (*Danio rerio*) development. *Chemosphere* 92, 59-66.

Massarsky, A., Abraham, R., Nguyen, K.C., Rippstein, P., Tayabali, A.F., Trudeau, V.L. et al., 2014. Nanosilver cytotoxicity in rainbow trout (*Oncorhynchus mykiss*) erythrocytes and hepatocytes. *Comp Biochem Physiol C Toxicol Pharmacol* 159, 10-21.

Masuda, M., Yamazaki, K., Kanzaki, J., Hosoda, Y., 1997. Immunohistochemical and ultrastructural investigation of the human vestibular dark cell area: roles of subepithelial capillaries and T lymphocyte-melanophage interaction in an immune surveillance system. *Anat Rec* 249, 153-162.

Matheny, H.E., Deem, T.L., Cook-Mills, J.M., 2000. Lymphocyte migration through monolayers of endothelial cell lines involves VCAM-1 signaling via endothelial cell NADPH oxid-

ase. *J Immunol* 164, 6550-6559.

McCabe, B.F., 1979. Autoimmune sensorineural hearing loss. *Ann Otol Rhinol Laryngol* 88, 585-589.

McShan, D., Ray, P.C., Yu, H., 2014. Molecular toxicity mechanism of nanosilver. *J Food Drug Anal* 22, 116-127.

Mirzapoiiazova, T., Lennon, F.E., Mambetsariev, B., Allen, M., Riehm, J., Poroyko, V.A. et al., 2015. Extracellular Vesicles from Caveolin-Enriched Microdomains Regulate Hyaluronan-Mediated Sustained Vascular Integrity. *Int J Cell Biol* 2015, 481493.

Miyahara, N., Kokubo, T., Hara, Y., Yamada, A., Koike, T., Arai, Y., 2016. Evaluation of X-ray doses and their corresponding biological effects on experimental animals in cone-beam micro-CT scans (R-mCT2). *Radiol Phys Technol* 9, 60-68.

Mizuta, K., Iwasa, K.H., Tachibana, M., Benos, D.J., Lim, D.J., 1995. Amiloride-sensitive Na⁺ channel-like immunoreactivity in the luminal membrane of some non-sensory epithelia of the inner ear. *Hear Res* 88, 199-205.

Mogensen, T.H., 2009. Pathogen recognition and inflammatory signaling in innate immune defenses. *Clin Microbiol Rev* 22, 240-273, Table of Contents.

Mohammadzadeh, R., 2012. Hypothesis: silver nanoparticles as an adjuvant for cancertherapy. *Adv Pharm Bull* 2, 133.

Moller, M.N., Caye-Thomasen, P., Qvortrup, K., 2013. Oxygenated fixation demonstrates novel and improved ultrastructural features of the human endolymphatic sac. *Laryngoscope* 123, 1967-1975.

Moller, M.N., Brandt, C., Ostergaard, C., Caye-Thomasen, P., 2014. Bacterial invasion of the inner ear in association with pneumococcal meningitis. *Otol Neurotol* 35, e178-186.

Moller, M.N., Brandt, C., Ostergaard, C., Caye-Thomasen, P., 2015a. Endolymphatic sac involvement in bacterial meningitis. *Eur Arch Otorhinolaryngol* 272, 843-851.

Moller, M.N., Kirkeby, S., Vikesa, J., Nielsen, F.C., Caye-Thomasen, P., 2015b. Gene expression demonstrates an immunological capacity of the human endolymphatic sac. *Laryngoscope* 125, E269-275.

Monasta, L., Ronfani, L., Marchetti, F., Montico, M., Vecchi Brumatti, L., Bavcar, A. et al., 2012. Burden of disease caused by otitis media: systematic review and global estimates. *PLoS One* 7, e36226.

Moon, S.K., Woo, J.I., Lee, H.Y., Park, R., Shimada, J., Pan, H. et al., 2007. Toll-like receptor 2-dependent NF-kappaB activation is involved in nontypeable *Haemophilus influenzae*-induced monocyte chemotactic protein 1 up-regulation in the spiral ligament fibrocytes of the inner ear. *Infect Immun* 75, 3361-3372.

Morones, J.R., Elechiguerra, J.L., Camacho, A., Holt, K., Kouri, J.B., Ramirez, J.T. et al., 2005. The bactericidal effect of silver nanoparticles. *Nanotechnology* 16, 2346-2353.

Moyano, D.F., Goldsmith, M., Solfiell, D.J., Landesman-Milo, D., Miranda, O.R., Peer, D. et al., 2012. Nanoparticle hydrophobicity dictates immune response. *J Am Chem Soc* 134, 3965-3967.

Murday, J.S., Siegel, R.W., Stein, J., Wright, J.F., 2009. Translational nanomedicine: status assessment and opportunities. *Nanomedicine* 5, 251-273.

Murray, P.J., Wynn, T.A., 2011. Protective and pathogenic functions of macrophage subsets. *Nat Rev Immunol* 11, 723-737.

Naganawa, S., Nakashima, T., 2014. Visualization of endolymphatic hydrops with MR imaging in patients with Ménière's disease and related pathologies: current status of its methods and clinical significance. *Jpn J Radiol* 32, 191-204.

Naganawa, S., Yamazaki, M., Kawai, H., Bokura, K., Sone, M., Nakashima, T., 2012. Imaging

of endolymphatic and perilymphatic fluid after intravenous administration of single-dose gadodiamide. *Magn Reson Med Sci* 11, 145-150.

Neal, A.L., 2008. What can be inferred from bacterium-nanoparticle interactions about the potential consequences of environmental exposure to nanoparticles? *Ecotoxicology* 17, 362-371.

Neng, L., Zhang, F., Kachelmeier, A., Shi, X., 2013. Endothelial cell, pericyte, and perivascular resident macrophage-type melanocyte interactions regulate cochlear intrastrial fluid-blood barrier permeability. *J Assoc Res Otolaryngol* 14, 175-185.

Ngo, J.K., Pomatto, L.C., Davies, K.J., 2013. Upregulation of the mitochondrial Lon Protease allows adaptation to acute oxidative stress but dysregulation is associated with chronic stress, disease, and aging. *Redox Biol* 1, 258-264.

Nguyen, C.T., Robinson, S.R., Jung, W., Novak, M.A., Boppart, S.A., Allen, J.B., 2013. Investigation of bacterial biofilm in the human middle ear using optical coherence tomography and acoustic measurements. *Hear Res* 301, 193-200.

Niemeyer, C.M., Ceyhan, B., Hazarika, P., 2003a. Oligofunctional DNA-gold nanoparticle conjugates. *Angew Chem Int Ed Engl* 42, 5766-5770.

Niemeyer, C.M., Ceyhan, B., Noyong, M., Simon, U., 2003b. Bifunctional DNA-gold nanoparticle conjugates as building blocks for the self-assembly of cross-linked particle layers. *Biochem Biophys Res Commun* 311, 995-999.

Nieuwedorp, M., Meuwese, M.C., Mooij, H.L., van Lieshout, M.H., Hayden, A., Levi, M. et al., 2009. Tumor necrosis factor- α inhibition protects against endotoxin-induced endothelial glycocalyx perturbation. *Atherosclerosis* 202, 296-303.

Nin, F., Hibino, H., Doi, K., Suzuki, T., Hisa, Y., Kurachi, Y., 2008. The endocochlear potential depends on two K^+ diffusion potentials and an electrical barrier in the stria vascularis of the inner ear. *Proc Natl Acad Sci U S A* 105, 1751-1756.

O'Toole, G., Kaplan, H.B., Kolter, R., 2000. Biofilm formation as microbial development. *Annu Rev Microbiol* 54, 49-79.

Oh, G.S., Kim, H.J., Choi, J.H., Shen, A., Kim, C.H., Kim, S.J. et al., 2011. Activation of lipopolysaccharide-TLR4 signaling accelerates the ototoxic potential of cisplatin in mice. *J Immunol* 186, 1140-1150.

Okano, T., 2014. Immune system of the inner ear as a novel therapeutic target for sensorineural hearing loss. *Front Pharmacol* 5, 205.

Okano, T., Nakagawa, T., Kita, T., Kada, S., Yoshimoto, M., Nakahata, T. et al., 2008. Bone marrow-derived cells expressing Iba1 are constitutively present as resident tissue macrophages in the mouse cochlea. *J Neurosci Res* 86, 1758-1767.

Onodera, Y., Teramura, T., Takehara, T., Shigi, K., Fukuda, K., 2015. Reactive oxygen species induce Cox-2 expression via TAK1 activation in synovial fibroblast cells. *FEBS Open Bio* 5, 492-501.

Paino, I.M., Zucolotto, V., 2015. Poly(vinyl alcohol)-coated silver nanoparticles: activation of neutrophils and nanotoxicology effects in human hepatocarcinoma and mononuclear cells. *Environ Toxicol Pharmacol* 39, 614-621.

Pante, N., Kann, M., 2002. Nuclear pore complex is able to transport macromolecules with diameters of about 39 nm. *Mol Biol Cell* 13, 425-434.

Parfenov, A.S., Salnikov, V., Lederer, W.J., Lukyanenko, V., 2006. Aqueous diffusion pathways as a part of the ventricular cell ultrastructure. *Biophys J* 90, 1107-1119.

Park, M., Lee, H.S., Kim, H., Oh, S.H., Lee, J.H., Suh, M.W., 2016. Differences in perilymphatic space enhancement and adverse inflammatory reaction after intratympanic injection of two different gadolinium agents: A 9.4-T magnetic resonance imaging study. *Hear Res*

333, 118-126.

Park, M.V., Neigh, A.M., Vermeulen, J.P., de la Fonteyne, L.J., Verharen, H.W., Briede, J.J. et al., 2011. The effect of particle size on the cytotoxicity, inflammation, developmental toxicity and genotoxicity of silver nanoparticles. *Biomaterials* 32, 9810-9817.

Patel, M., Hu, Z., Bard, J., Jamison, J., Cai, Q., Hu, B.H., 2013. Transcriptome characterization by RNA-Seq reveals the involvement of the complement components in noise-traumatized rat cochleae. *Neuroscience* 248, 1-16.

Pawankar, R., Tomiyama, S., Jinnouchi, K., Ikezono, T., Nonaka, M., Yagi, T., 1998. Intercellular adhesion molecule-1 expression in the inner ear of rats following secondary immune reaction in the endolymphatic sac. *Acta Otolaryngol Suppl* 539, 5-14.

Penha, R., Escada, P., 2003. Interrelations between the middle and inner ear in otitis media. *Int Tinnitus J* 9, 87-91.

Piao, M.J., Kim, K.C., Choi, J.Y., Choi, J., Hyun, J.W., 2011a. Silver nanoparticles down-regulate Nrf2-mediated 8-oxoguanine DNA glycosylase 1 through inactivation of extracellular regulated kinase and protein kinase B in human Chang liver cells. *Toxicol Lett* 207, 143-148.

Piao, M.J., Kang, K.A., Lee, I.K., Kim, H.S., Kim, S., Choi, J.Y. et al., 2011b. Silver nanoparticles induce oxidative cell damage in human liver cells through inhibition of reduced glutathione and induction of mitochondria-involved apoptosis. *Toxicol Lett* 201, 92-100.

Pondugula, S.R., Sanneman, J.D., Wangemann, P., Milhaud, P.G., Marcus, D.C., 2004. Glucocorticoids stimulate cation absorption by semicircular canal duct epithelium via epithelial sodium channel. *Am J Physiol Renal Physiol* 286, F1127-1135.

Posgai, R., Cipolla-McCulloch, C.B., Murphy, K.R., Hussain, S.M., Rowe, J.J., Nielsen, M.G., 2011. Differential toxicity of silver and titanium dioxide nanoparticles on *Drosophila melanogaster* development, reproductive effort, and viability: size, coatings and antioxidants matter. *Chemosphere* 85, 34-42.

Pyykkö, I., Zou, J., Poe, D., Nakashima, T., Naganawa, S., 2010. Magnetic resonance imaging of the inner ear in Meniere's disease. *Otolaryngol Clin North Am* 43, 1059-1080.

Rai, M., Yadav, A., Gade, A., 2009. Silver nanoparticles as a new generation of antimicrobials. *Biotechnol Adv* 27, 76-83.

Rask-Andersen, H., Stahle, J., 1980. Immunodefence of the inner ear? Lymphocyte-macrophage interaction in the endolymphatic sac. *Acta Otolaryngol* 89, 283-294.

Rask-Andersen, H., Bagger-Sjoberg, D., Lundquist, P.G., 1983. The fenestrated blood vessels of the endolymphatic sac. A freeze-fracture and transmission electron microscopic study. *Am J Otol* 4, 214-221.

Rees, A.J., 2010. Monocyte and macrophage biology: an overview. *Semin Nephrol* 30, 216-233.

Reese, T.S., Karnovsky, M.J., 1967. Fine structural localization of a blood-brain barrier to exogenous peroxidase. *J Cell Biol* 34, 207-217.

Repetto, G., del Peso, A., Zurita, J.L., 2008. Neutral red uptake assay for the estimation of cell viability/cytotoxicity. *Nat Protoc* 3, 1125-1131.

Rio, C., Dikkes, P., Liberman, M.C., Corfas, G., 2002. Glial fibrillary acidic protein expression and promoter activity in the inner ear of developing and adult mice. *J Comp Neurol* 442, 156-162.

Rom, S., Fan, S., Reichenbach, N., Dykstra, H., Ramirez, S.H., Persidsky, Y., 2012. Glycogen synthase kinase 3beta inhibition prevents monocyte migration across brain endothelial cells via Rac1-GTPase suppression and down-regulation of active integrin conformation. *Am J Pathol* 181, 1414-1425.

Rosner, W., Tempel, K., 1966. [Quantitative determination of the permeability of the so-

called blood-brain barrier of Evans blue (T 1824)]. *Med Pharmacol Exp Int J Exp Med* 14, 169-182.

Ruebhausen, M.R., Brozoski, T.J., Bauer, C.A., 2012. A comparison of the effects of isoflurane and ketamine anesthesia on auditory brainstem response (ABR) thresholds in rats. *Hear Res* 287, 25-29.

Ryan, A.F., Wickham, M.G., Bone, R.C., 1979. Element content of intracochlear fluids, outer hair cells, and stria vascularis as determined by energy-dispersive roentgen ray analysis. *Otolaryngol Head Neck Surg* 87, 659-665.

Rybak, L.P., Green, T.P., Juhn, S.K., Morizono, T., 1984. Probenecid reduces cochlear effects and perilymph penetration of furosemide in chinchilla. *J Pharmacol Exp Ther* 230, 706-709.

Sabanayagam, C.R., Lakowicz, J.R., 2007. Increasing the sensitivity of DNA microarrays by metal-enhanced fluorescence using surface-bound silver nanoparticles. *Nucleic Acids Res* 35, e13.

Sahu, P.K., Iyer, P.S., Barage, S.H., Sonawane, K.D., Chopade, B.A., 2014. Characterization of the *algC* gene expression pattern in the multidrug resistant *Acinetobacter baumannii* AIIMS 7 and correlation with biofilm development on abiotic surface. *Scientific World Journal* 2014, 593546.

Saito, T., Zhang, Z.J., Tokuriki, M., Ohtsubo, T., Noda, I., Shibamori, Y. et al., 2001. Expression of p-glycoprotein is associated with that of multidrug resistance protein 1 (MRP1) in the vestibular labyrinth and endolymphatic sac of the guinea pig. *Neurosci Lett* 303, 189-192.

Sakagami, M., Matsunaga, T., Hashimoto, P.H., 1982. Fine structure and permeability of capillaries in the stria vascularis and spiral ligament of the inner ear of the guinea pig. *Cell Tissue Res* 226, 511-522.

Salt, A.N., Henson, M.M., Gewalt, S.L., Keating, A.W., DeMott, J.E., Henson, O.W., Jr., 1995. Detection and quantification of endolymphatic hydrops in the guinea pig cochlea by magnetic resonance microscopy. *Hear Res* 88, 79-86.

Saptarshi, S.R., Duschl, A., Lopata, A.L., 2013. Interaction of nanoparticles with proteins: relation to bio-reactivity of the nanoparticle. *J Nanobiotechnology* 11, 26.

Sassolas, A., Leca-Bouvier, B.D., Blum, L.J., 2008. DNA biosensors and microarrays. *Chem Rev* 108, 109-139.

Sato, E., Shick, H.E., Ransohoff, R.M., Hirose, K., 2008. Repopulation of cochlear macrophages in murine hematopoietic progenitor cell chimeras: the role of CX3CR1. *J Comp Neurol* 506, 930-942.

Sato, E., Shick, H.E., Ransohoff, R.M., Hirose, K., 2010. Expression of fractalkine receptor CX3CR1 on cochlear macrophages influences survival of hair cells following ototoxic injury. *J Assoc Res Otolaryngol* 11, 223-234.

Satoh, H., Firestein, G.S., Billings, P.B., Harris, J.P., Keithley, E.M., 2003. Proinflammatory cytokine expression in the endolymphatic sac during inner ear inflammation. *J Assoc Res Otolaryngol* 4, 139-147.

Schmidley, J.W., Dadson, J., Iyer, R.S., Salomon, R.G., 1992. Brain tissue injury and blood-brain barrier opening induced by injection of LGE2 or PGE2. *Prostaglandins Leukot Essent Fatty Acids* 47, 105-110.

Schultz, T.W., Freeman, S.R., Dumont, J.N., 1980. Uptake, depuration, and distribution of selenium in *Daphnia* and its effects on survival and ultrastructure. *Arch Environ Contam Toxicol* 9, 23-40.

Scott, C.L., Henri, S., Guillems, M., 2014. Mononuclear phagocytes of the intestine, the skin, and the lung. *Immunol Rev* 262, 9-24.

Sharma, H.S., Hussain, S., Schlager, J., Ali, S.F., Sharma, A., 2010. Influence of nanoparticles

on blood-brain barrier permeability and brain edema formation in rats. *Acta Neurochir Suppl* 106, 359-364.

Shavandi, Z., Ghazanfari, T., Moghaddam, K.N., 2011. *In vitro* toxicity of silver nanoparticles on murine peritoneal macrophages. *Immunopharmacol Immunotoxicol* 33, 135-140.

Shi, H., Li, Y., Yin, S., Zou, J., 2014. The predominant vestibular uptake of gadolinium through the oval window pathway is compromised by endolymphatic hydrops in Ménière's disease. *Otol Neurotol* 35, 315-322.

Shi, X., 2009. Cochlear pericyte responses to acoustic trauma and the involvement of hypoxia-inducible factor-1alpha and vascular endothelial growth factor. *Am J Pathol* 174, 1692-1704.

Shi, X., 2010. Resident macrophages in the cochlear blood-labyrinth barrier and their renewal via migration of bone-marrow-derived cells. *Cell Tissue Res* 342, 21-30.

Shi, X., 2011. Physiopathology of the cochlear microcirculation. *Hear Res* 282, 10-24.

Shi, X., Nuttall, A.L., 2007. Expression of adhesion molecular proteins in the cochlear lateral wall of normal and PARP-1 mutant mice. *Hear Res* 224, 1-14.

Shimazaki, T., Ichimiya, I., Suzuki, M., Mogi, G., 2002. Localization of glucocorticoid receptors in the murine inner ear. *Ann Otol Rhinol Laryngol* 111, 1133-1138.

Shinomori, Y., Spack, D.S., Jones, D.D., Kimura, R.S., 2001. Volumetric and dimensional analysis of the guinea pig inner ear. *Ann Otol Rhinol Laryngol* 110, 91-98.

Singh, R.P., Ramarao, P., 2012. Cellular uptake, intracellular trafficking and cytotoxicity of silver nanoparticles. *Toxicol Lett* 213, 249-259.

Sintubin, L., Verstraete, W., Boon, N., 2012. Biologically produced nanosilver: current state and future perspectives. *Biotechnol Bioeng* 109, 2422-2436.

So, H., Kim, H., Lee, J.H., Park, C., Kim, Y., Kim, E. et al., 2007. Cisplatin cytotoxicity of auditory cells requires secretions of proinflammatory cytokines via activation of ERK and NF-kappaB. *J Assoc Res Otolaryngol* 8, 338-355.

Soliman, A.M., 1992. Immune-mediated inner ear disease. *Am J Otol* 13, 575-579.

Sondi, I., Salopek-Sondi, B., 2004. Silver nanoparticles as antimicrobial agent: a case study on *E. coli* as a model for Gram-negative bacteria. *J Colloid Interface Sci* 275, 177-182.

Spicer, S.S., Schulte, B.A., 2005a. Pathologic changes of presbycusis begin in secondary processes and spread to primary processes of strial marginal cells. *Hear Res* 205, 225-240.

Spicer, S.S., Schulte, B.A., 2005b. Novel structures in marginal and intermediate cells presumably relate to functions of apical versus basal strial strata. *Hear Res* 200, 87-101.

Stearns, G.S., Keithley, E.M., Harris, J.P., 1993. Development of high endothelial venule-like characteristics in the spiral modiolar vein induced by viral labyrinthitis. *Laryngoscope* 103, 890-898.

Stensberg, M.C., Wei, Q., McLamore, E.S., Porterfield, D.M., Wei, A., Sepulveda, M.S., 2011. Toxicological studies on silver nanoparticles: challenges and opportunities in assessment, monitoring and imaging. *Nanomedicine (Lond)* 6, 879-898.

Sterkers, O., Saumon, G., Tran Ba Huy, P., Amiel, C., 1982. K, Cl, and H₂O entry in endolymph, perilymph, and cerebrospinal fluid of the rat. *Am J Physiol* 243, F173-180.

Sterkers, O., Ferrary, E., Saumon, G., Amiel, C., 1987. Na and nonelectrolyte entry into inner ear fluids of the rat. *Am J Physiol* 253, F50-58.

Sterkers, O., Saumon, G., Tran Ba Huy, P., Ferrary, E., Amiel, C., 1984. Electrochemical heterogeneity of the cochlear endolymph: effect of acetazolamide. *Am J Physiol* 246, F47-53.

Sulić, S., Panić, L., Dikić, I., Volarević, S., 2005. Deregulation of cell growth and malignant transformation. *Croat Med J* 46, 622-638.

Sun, C., Wu, M.H., Yuan, S.Y., 2011. Nonmuscle myosin light-chain kinase deficiency attenu-

ates atherosclerosis in apolipoprotein E-deficient mice via reduced endothelial barrier dysfunction and monocyte migration. *Circulation* 124, 48-57.

Sun, S., Yu, H., Yu, H., Honglin, M., Ni, W., Zhang, Y. et al., 2015. Inhibition of the activation and recruitment of microglia-like cells protects against neomycin-induced ototoxicity. *Mol Neurobiol* 51, 252-267.

Sung, J.H., Ji, J.H., Park, J.D., Yoon, J.U., Kim, D.S., Jeon, K.S. et al., 2009. Subchronic inhalation toxicity of silver nanoparticles. *Toxicol Sci* 108, 452-461.

Swan, E.E., Mescher, M.J., Sewell, W.F., Tao, S.L., Borenstein, J.T., 2008. Inner ear drug delivery for auditory applications. *Adv Drug Deliv Rev* 60, 1583-1599.

Tachibana, M., Sankar, R., Domer, F., 1981. Effects of acute hypertension on the extravasation of macromolecule in the temporal bone--the possible involvement of the blood-inner ear barrier. *Arch Otorhinolaryngol* 232, 11-19.

Tagaya, M., Yamazaki, M., Teranishi, M., Naganawa, S., Yoshida, T., Otake, H. et al., 2011. Endolymphatic hydrops and blood-labyrinth barrier in Ménière's disease. *Acta Otolaryngol* 131, 474-479.

Takahashi, M., Harris, J.P., 1988a. Anatomic distribution and localization of immunocompetent cells in normal mouse endolymphatic sac. *Acta Otolaryngol* 106, 409-416.

Takahashi, M., Harris, J.P., 1988b. Analysis of immunocompetent cells following inner ear immunostimulation. *Laryngoscope* 98, 1133-1138.

Takemura, K., Komeda, M., Yagi, M., Himeno, C., Izumikawa, M., Doi, T. et al., 2004. Direct inner ear infusion of dexamethasone attenuates noise-induced trauma in guinea pig. *Hear Res* 196, 58-68.

Tan, B.T., Lee, M.M., Ruan, R., 2008. Bone-marrow-derived cells that home to acoustic deafened cochlea preserved their hematopoietic identity. *J Comp Neurol* 509, 167-179.

Taylor, K.R., Gallo, R.L., 2006. Glycosaminoglycans and their proteoglycans: host-associated molecular patterns for initiation and modulation of inflammation. *FASEB J* 20, 9-22.

Tenzer, S., Docter, D., Kuharev, J., Musyanovych, A., Fetz, V., Hecht, R. et al., 2013. Rapid formation of plasma protein corona critically affects nanoparticle pathophysiology. *Nat Nanotechnol* 8, 772-781.

Teodoro, J.S., Simoes, A.M., Duarte, F.V., Rolo, A.P., Murdoch, R.C., Hussain, S.M. et al., 2011. Assessment of the toxicity of silver nanoparticles *in vitro*: a mitochondrial perspective. *Toxicol In Vitro* 25, 664-670.

Todaro, G.J., Green, H., 1963. Quantitative studies of the growth of mouse embryo cells in culture and their development into established lines. *J Cell Biol* 17, 299-313.

Tomankova, K., Horakova, J., Harvanova, M., Malina, L., Soukupova, J., Hradilova, S. et al., 2015. Cytotoxicity, cell uptake and microscopic analysis of titanium dioxide and silver nanoparticles *in vitro*. *Food Chem Toxicol* 82, 106-115.

Tomiyaama, S., 1992. Development of endolymphatic hydrops following immune response in the endolymphatic sac of the guinea pig. *Acta Otolaryngol* 112, 470-478.

Tomiyaama, S., Harris, J.P., 1986. The endolymphatic sac: its importance in inner ear immune responses. *Laryngoscope* 96, 685-691.

Tomiyaama, S., Harris, J.P., 1987. The role of the endolymphatic sac in inner ear immunity. *Acta Otolaryngol* 103, 182-188.

Tomiyaama, S., Harris, J.P., 1989. Elevation of inner ear antibody levels following direct antigen challenge of the endolymphatic sac. *Acta Otolaryngol* 107, 202-209.

Tomiyaama, S., Kinoshita, T., Jinnouchi, K., Ikezono, T., Gotoh, Y., Pawanker, R. et al., 1995. Fluctuating hearing loss following immune reaction in the endolymphatic sac of guinea pigs. *ORL J Otorhinolaryngol Relat Spec* 57, 122-128.

Tornabene, S.V., Sato, K., Pham, L., Billings, P., Keithley, E.M., 2006. Immune cell recruitment following acoustic trauma. *Hear Res* 222, 115-124.

Trune, D.R., 1997. Cochlear immunoglobulin in the C3H/lpr mouse model for autoimmune hearing loss. *Otolaryngol Head Neck Surg* 117, 504-508.

Trune, D.R., Nguyen-Huynh, A., 2012. Vascular Pathophysiology in Hearing Disorders. *Semin Hear* 33, 242-250.

Turrens, J.F., 2003. Mitochondrial formation of reactive oxygen species. *J Physiol* 552, 335-344.

Viberg, A., Canlon, B., 2004. The guide to plotting a cochleogram. *Hear Res* 197, 1-10.

Vogh, B.P., Maren, T.H., 1975. Sodium, chloride, and bicarbonate movement from plasma to cerebrospinal fluid in cats. *Am J Physiol* 228, 673-683.

Vorbrodt, A.W., Lossinsky, A.S., Dobrogowska, D.H., Wisniewski, H.M., 1986. Distribution of anionic sites and glycoconjugates on the endothelial surfaces of the developing blood-brain barrier. *Brain Res* 394, 69-79.

Wackym, P.A., Friberg, U., Bagger-Sjoberg, D., Linthicum, F.H., Jr., Friedmann, I., Rask-Andersen, H., 1987a. Human endolymphatic sac: possible mechanisms of pressure regulation. *J Laryngol Otol* 101, 768-779.

Wackym, P.A., Friberg, U., Linthicum, F.H., Jr., Bagger-Sjoberg, D., Bui, H.T., Hofman, F. et al., 1987b. Human endolymphatic sac: morphologic evidence of immunologic function. *Ann Otol Rhinol Laryngol* 96, 276-281.

Wagner, S.C., Roskamp, M., Pallerla, M., Araghi, R.R., Schlecht, S., Kokschi, B., 2010. Nanoparticle-induced folding and fibril formation of coiled-coil-based model peptides. *Small* 6, 1321-1328.

Wang, H., Wu, L., Reinhard, B.M., 2012. Scavenger receptor mediated endocytosis of silver nanoparticles into J774A.1 macrophages is heterogeneous. *ACS Nano* 6, 7122-7132.

Warchol, M.E., 1997. Macrophage activity in organ cultures of the avian cochlea: demonstration of a resident population and recruitment to sites of hair cell lesions. *J Neurobiol* 33, 724-734.

Warchol, M.E., Schwendener, R.A., Hirose, K., 2012. Depletion of resident macrophages does not alter sensory regeneration in the avian cochlea. *PLoS One* 7, e51574.

Warchol, M.E., Matsui, J.I., Simkus, E.L., Ogilvie, J.M., 2001. Ongoing cell death and immune influences on regeneration in the vestibular sensory organs. *Ann N Y Acad Sci* 942, 34-45.

Wenzel, G.I., Anvari, B., Mazhar, A., Pikkula, B., Oghalai, J.S., 2007. Laser-induced collagen remodeling and deposition within the basilar membrane of the mouse cochlea. *J Biomed Opt* 12, 021007.

Wessman, M., Bjarnsholt, T., Eickhardt-Sorensen, S.R., Johansen, H.K., Homoe, P., 2015. Mucosal biofilm detection in chronic otitis media: a study of middle ear biopsies from Greenlandic patients. *Eur Arch Otorhinolaryngol* 272, 1079-1085.

Wigginton, N.S., de Titta, A., Piccapietra, F., Dobias, J., Nesatyy, V.J., Suter, M.J. et al., 2010. Binding of silver nanoparticles to bacterial proteins depends on surface modifications and inhibits enzymatic activity. *Environ Sci Technol* 44, 2163-2168.

Williams, Y., Sukhanova, A., Nowostawska, M., Davies, A.M., Mitchell, S., Oleinikov, V. et al., 2009. Probing cell-type-specific intracellular nanoscale barriers using size-tuned quantum dots. *Small* 5, 2581-2588.

Wise, J.P., Sr., Goodale, B.C., Wise, S.S., Craig, G.A., Pongan, A.F., Walter, R.B. et al., 2010. Silver nanospheres are cytotoxic and genotoxic to fish cells. *Aquat Toxicol* 97, 34-41.

Wispelwey, B., Lesse, A.J., Hansen, E.J., Scheld, W.M., 1988. *Haemophilus influenzae* lipopolysaccharide-induced blood brain barrier permeability during experimental meningitis in the

rat. *J Clin Invest* 82, 1339-1346.

Woo, J.I., Pan, H., Oh, S., Lim, D.J., Moon, S.K., 2010. Spiral ligament fibrocyte-derived MCP-1/CCL2 contributes to inner ear inflammation secondary to nontypeable *H. influenzae*-induced otitis media. *BMC Infect Dis* 10, 314.

Wu, W.H., Sun, X., Yu, Y.P., Hu, J., Zhao, L., Liu, Q. et al., 2008. TiO₂ nanoparticles promote beta-amyloid fibrillation *in vitro*. *Biochem Biophys Res Commun* 373, 315-318.

Xu, Y., Tang, H., Wang, H., Liu, Y., 2015. Blockade of oral tolerance to ovalbumin in mice by silver nanoparticles. *Nanomedicine (Lond)* 10, 419-431.

Xu, Y., Tang, H., Liu, J.H., Wang, H., Liu, Y., 2013. Evaluation of the adjuvant effect of silver nanoparticles both *in vitro* and *in vivo*. *Toxicol Lett* 219, 42-48.

Yan, J.K., Ma, H.L., Cai, P.F., Wu, J.Y., 2015. Highly selective and sensitive nucleic acid detection based on polysaccharide-functionalized silver nanoparticles. *Spectrochim Acta A Mol Biomol Spectrosc* 134, 17-21.

Yang, E.J., Kim, S., Kim, J.S., Choi, I.H., 2012. Inflammasome formation and IL-1 β release by human blood monocytes in response to silver nanoparticles. *Biomaterials* 33, 6858-6867.

Yang, W., Vethanayagam, R.R., Dong, Y., Cai, Q., Hu, B.H., 2015. Activation of the antigen presentation function of mononuclear phagocyte populations associated with the basilar membrane of the cochlea after acoustic overstimulation. *Neuroscience* 303, 1-15.

Yang, Y., Dai, M., Wilson, T.M., Omelchenko, I., Klimek, J.E., Wilmarth, P.A. et al., 2011. Na⁺/K⁺-ATPase α 1 identified as an abundant protein in the blood-labyrinth barrier that plays an essential role in the barrier integrity. *PLoS One* 6, e16547.

Yeo, S.W., Gottschlich, S., Harris, J.P., Keithley, E.M., 1995. Antigen diffusion from the perilymphatic space of the cochlea. *Laryngoscope* 105, 623-628.

Yimtae, K., Song, H., Billings, P., Harris, J.P., Keithley, E.M., 2001. Connection between the inner ear and the lymphatic system. *Laryngoscope* 111, 1631-1635.

Yuan, S.Y., Shen, Q., Rigor, R.R., Wu, M.H., 2012. Neutrophil transmigration, focal adhesion kinase and endothelial barrier function. *Microvasc Res* 83, 82-88.

Zhang, F., Zhang, J., Neng, L., Shi, X., 2013a. Characterization and inflammatory response of perivascular-resident macrophage-like melanocytes in the vestibular system. *J Assoc Res Otolaryngol* 14, 635-643.

Zhang, F., Dai, M., Neng, L., Zhang, J.H., Zhi, Z., Fridberger, A. et al., 2013b. Perivascular macrophage-like melanocyte responsiveness to acoustic trauma--a salient feature of strial barrier associated hearing loss. *FASEB J* 27, 3730-3740.

Zhang, R., Piao, M.J., Kim, K.C., Kim, A.D., Choi, J.Y., Choi, J. et al., 2012a. Endoplasmic reticulum stress signaling is involved in silver nanoparticles-induced apoptosis. *Int J Biochem Cell Biol* 44, 224-232.

Zhang, T., Wang, L., Chen, Q., Chen, C., 2014. Cytotoxic potential of silver nanoparticles. *Yonsei Med J* 55, 283-291.

Zhang, W., Dai, M., Fridberger, A., Hassan, A., Degagne, J., Neng, L. et al., 2012b. Perivascular-resident macrophage-like melanocytes in the inner ear are essential for the integrity of the intrastrial fluid-blood barrier. *Proc Natl Acad Sci U S A* 109, 10388-10393.

Zhang, X.F., Choi, Y.J., Han, J.W., Kim, E., Park, J.H., Gurunathan, S. et al., 2015. Differential nanoreprotoxicity of silver nanoparticles in male somatic cells and spermatogonial stem cells. *Int J Nanomedicine* 10, 1335-1357.

Zhang, Z., Wen, Y., Ma, Y., Luo, J., Jiang, L., Song, Y., 2011. Mixed DNA-functionalized nanoparticle probes for surface-enhanced Raman scattering-based multiplex DNA detection. *Chem Commun (Camb)* 47, 7407-7409.

Zheng, Z., Yin, W., Zara, J.N., Li, W., Kwak, J., Mamidi, R. et al., 2010. The use of BMP-2 coupled - Nanosilver-PLGA composite grafts to induce bone repair in grossly infected segmental defects. *Biomaterials* 31, 9293-9300.

Zhou, Y., Kong, Y., Kundu, S., Cirillo, J.D., Liang, H., 2012. Antibacterial activities of gold and silver nanoparticles against *Escherichia coli* and bacillus Calmette-Guérin. *J Nanobiotechnology* 10, 19.

Zolnik, B.S., Gonzalez-Fernandez, A., Sadrieh, N., Dobrovolskaia, M.A., 2010. Nanoparticles and the immune system. *Endocrinology* 151, 458-465.

Zou, J., 2012. Transport augmentation through the blood-inner ear barriers of guinea pigs treated with 3-nitropropionic acid and patients with acute hearing loss, visualized with 3.0 T MRI: figure labeling clarification. *Otol Neurotol* 33, 691.

Zou, J., Pyykko, I., Bjelke, B., Toppila, E., 2007. *In vivo* MRI visualization of endolymphatic hydrops induced by keyhole limpet hemocyanin round window immunization. *Audiol Med* 5, 182-187.

Zou, J., Jiang, S., Gu, R., 1996. An observation on otoacoustic emission and ultrastructure of cochlea in experimental autoimmune inner ear disease. *Chin Med J (Engl)* 109, 639-644.

Zou, J., Ramadan, U.A., Pyykkö, I., 2010a. Gadolinium uptake in the rat inner ear perilymph evaluated with 4.7 T MRI: a comparison between transtympanic injection and gelatin sponge-based diffusion through the round window membrane. *Otol Neurotol* 31, 637-641.

Zou, J., Poe, D., Bjelke, B., Pyykko, I., 2009a. Visualization of inner ear disorders with MRI *in vivo*: from animal models to human application. *Acta Otolaryngol Suppl* 560, 22-31.

Zou, J., Poe, D., Ramadan, U.A., Pyykkö, I., 2012a. Oval window transport of Gd-DOTA from rat middle ear to vestibulum and scala vestibuli visualized by *in vivo* magnetic resonance imaging. *Ann Otol Rhinol Laryngol* 121, 119-128.

Zou, J., Zhang, Y., Yin, S., Wu, H., Pyykkö, I., 2009b. Mitochondrial dysfunction disrupts trafficking of Kir4.1 in spiral ganglion satellite cells. *J Neurosci Res* 87, 141-149.

Zou, J., Pyykkö, I., Counter, S.A., Klason, T., Bretlau, P., Bjelke, B., 2003. *In vivo* observation of dynamic perilymph formation using 4.7 T MRI with gadolinium as a tracer. *Acta Otolaryngol* 123, 910-915.

Zou, J., Zhang, W., Poe, D., Zhang, Y., Ramadan, U.A., Pyykkö, I., 2010b. Differential passage of gadolinium through the mouse inner ear barriers evaluated with 4.7T MRI. *Hear Res* 259, 36-43.

Zou, J., Sood, R., Ranjan, S., Poe, D., Ramadan, U.A., Kinnunen, P.K. et al., 2010c. Manufacturing and *in vivo* inner ear visualization of MRI traceable liposome nanoparticles encapsulating gadolinium. *J Nanobiotechnology* 8, 32.

Zou, J., Li, M., Zhang, Y., Zheng, G., Chen, D., Chen, S. et al., 2011. Transport augmentation through the blood-inner ear barriers of guinea pigs treated with 3-nitropropionic acid and patients with acute hearing loss, visualized with 3.0 T MRI. *Otol Neurotol* 32, 204-212.

Zou, J., Sood, R., Ranjan, S., Poe, D., Ramadan, U.A., Pyykkö, I. et al., 2012b. Size-dependent passage of liposome nanocarriers with preserved posttransport integrity across the middle-inner ear barriers in rats. *Otol Neurotol* 33, 666-673.

Zou, J., Zhang, Y., Zhang, W., Poe, D., Zhai, S., Yang, S. et al., 2013. Mitochondria toxin-induced acute cochlear cell death indicates cellular activity-correlated energy consumption. *Eur Arch Otorhinolaryngol* 270, 2403-2415.

Zuo, J., Curtis, L.M., Yao, X., ten Cate, W.J., Bagger-Sjoberg, D., Hultcrantz, M. et al., 1995. Glucocorticoid receptor expression in the postnatal rat cochlea. *Hear Res* 87, 220-227.

Full texts for original publications

The author appreciates that the following copyright holders grant the permission of reproducing the original publications:

I and II Springer

III and IV BioMed Central

RESEARCH

Open Access

Toxicity of silver nanoparticle in rat ear and BALB/c 3T3 cell line

Jing Zou^{1,3*}, Hao Feng¹, Marika Mannerström², Tuula Heinonen² and Ilmari Pyykkö¹

Abstract

Background: Silver nanoparticles (AgNPs) displayed strong activities in anti-bacterial, anti-viral, and anti-fungal studies and was reportedly efficient in treating otitis media. The potential impact of AgNPs on the inner ear was missing.

Objective: Attempted to evaluate the potential toxicity of AgNPs in the inner ear, middle ear, and external ear canal after transtympanic injection in rats.

Results: In in vitro studies, the IC₅₀ for AgNPs in neutral red uptake assay was lower than that in NAD(P)H-dependent cellular oxidoreductase enzyme assay (WST-1) and higher than that in total cellular ATP and nuclear membrane integrity (propidium iodide) assessments. In in vivo experiments, magnetic resonance imaging (MRI) showed that significant changes in the permeability of biological barriers occurred in the middle ear mucosa, the skin of the external ear canal, and the inner ear at 5 h post-transtympanic injection of AgNPs at concentrations ranging from 20 µg/ml to 4000 µg/ml. The alterations in permeability showed a dosage-response relationship, and were reversible. The auditory brainstem response showed that 4000 µg/ml AgNPs induced hearing loss with partial recovery at 7 d, whereas 20 µg/ml caused reversible hearing loss. The functional change in auditory system was in line with the histology results. In general, the BALB/c 3T3 cell line is more than 1000 times more sensitive than the in vivo studies. Impairment of the mitochondrial function was indicated to be the mechanism of toxicity of AgNPs.

Conclusion: These results suggest that AgNPs caused significant, dose-dependent changes in the permeability of biological barriers in the middle ear mucosa, the skin of the external ear canal, and the inner ear. In general, the BALB/c 3T3 cell line is more than 1000 times more sensitive than the in vivo studies. The rat ear model might be expended to other engineered nanomaterials in nanotoxicology study.

Keywords: Animal model, Biological barrier, Ear, Imaging, Nanomaterial

Background

Chronic otitis media, characterized by recurrent infections causing pain and purulent otorrhea, is still a significant public health problem affecting 0.5–30% of any given population in developing and developed countries. However, antibiotic is not always efficient because of the appearance of multidrug resistant strains of bacteria. Formation of biofilm was recently reported in the middle ear of patients with chronic otitis media all over

the world [1-4]. Silver nanoparticles (AgNPs) displayed strong activities in anti-bacterial, anti-viral, and anti-fungal studies attributed to the mechanisms of inhibiting the formation of biofilm and destroying viral structures and boosting innate immune response among others [5-9]. The medical applications of AgNPs include surgical fields, such as urology, dentistry, general surgery and orthopedics, and wound dressing to take advantage of good antibacterial activity [10]. Therefore, AgNPs will potentially be selected as an alternative strategy to treat diseases in the ear by combating biofilm formation and any potential multidrug resistant strains of bacteria that is big challenge for conventional antibiotics. A clinical study on treatment of relapses of chronic suppurative otitis media showed that a preparation containing silver

* Correspondence: Jing.Zou@uta.fi

¹Hearing and Balance Research Unit, Field of Oto-laryngology, School of Medicine, University of Tampere, Tampere, Finland

³Department of Otolaryngology-Head and Neck Surgery, Center for Otolaryngology-Head & Neck Surgery of Chinese PLA, Changhai Hospital, Second Military Medical University, Shanghai, China

Full list of author information is available at the end of the article

nanoparticles eliminated clinical symptoms and positive dynamics of the objective signs of the disease, such as reduction or termination of pathological exudation and stimulation of the epidermization processes, which was stable during the observation time of 6 months [11]. However, before formal application in the clinic practice, sophisticated toxicological study on AgNPs in the inner ear to evaluate any potential risk of the new agent is necessary.

In vivo rodent studies have shown that AgNPs induce liver and neural toxicity after intravenous injection [12]. The neural toxicity in the brain is suspected to be the result of the passage of AgNPs across and breaking down the blood–brain barrier [13]. Biological barriers are defined as a membrane, tissue, or mechanisms that selectively transport certain substances into the tissue and block others. Previous work showed that a rat's inner ear has also a sophisticated barrier system isolating different compartments as well as the engineered nanomaterials distributed in the inner ear after middle ear administration [14-17]. This membranous barrier system in the inner ear is similar to that in the brain and the functional changes in the barriers resulting from hazardous exposure can be evaluated using MRI with high accuracy [18,19]. The auditory function alteration caused by toxic substances can also be measured accurately, which is otherwise inconvenient in the brain or cranial nerves [15,20]. The blood-endolymph and blood-perilymph barriers control the interaction between the inner ear and blood. The blood-perilymph barrier is permeable to certain small molecules and is similar to that of cerebrospinal fluid, with minor variations [21-23]. The blood-endolymph barrier is as tight as the blood–brain barrier and does not allow the MRI contrast agent, gadolinium chelate, to pass through under physiological conditions [24,25]. AgNPs may pass through and impair these barriers in the inner ear. In addition, the skin in the external ear canal and mucosa in the middle ear cavity are also exposed to AgNPs when the agent is delivered to the external ear canal to treat otitis media. Transtympanic injection of AgNPs in rats can mimic the clinical application and the animal suffering is minor. This multifunctional rat ear model can also be utilized for evaluating potential toxicity of other types of engineered nanomaterials with a focus on the impacts on the biological barriers in the skin (external ear canal), mucosa (middle ear cavity), nerve system (inner ear).

In the work presented here, *in vitro* study was performed in the BALB/c 3T3 cell line that were exposed to AgNPs for 24 h, a longer exposure time than the literature report in order ensure adequate toxicity [26]. Using the neutral red uptake (NRU) assay which is an *in vitro* evaluation of acute mammalian toxicity accepted by Organization for Economic Cooperation and Development (OECD

GD 129, 2010) [27] (<http://www.alttox.org/ttrc/validation-ra/validated-ra-methods.html>). The NRU study was further compared with three other cytotoxicity assays with different end points: NAD(P)H-dependent cellular oxidoreductase enzyme assay (WST-1) for evaluating the mitochondrial function (which produces a water-soluble formazan, reacts with the mitochondrial respiratory Complex II, and is more stable than conventional MTT assay) [28], the total cellular ATP measurement as a general indicator of mitochondrial activity, and the propidium iodide staining for assessing the nuclear membrane integrity that are alternative methods. Cytotoxicity of AgNPs was compared with AgCl (in the case of Ag⁺ release, AgCl is the major product in the body), as well as AgNO₃ as a material control that was reported in the literature [29]. *In vivo* experiments were carried out in rats after transtympanic injection of either AgNPs, or solution of AgNO₃ or AgCl. Functional changes in the blood-inner ear barriers, as well as in the capillary barriers in the skin of the external ear canal and mucosa of the middle ear cavity, were evaluated using gadolinium-enhanced magnetic resonance imaging (MRI). Auditory function was monitored by the auditory brainstem response (ABR) measurement. The potential cell death of different cellular populations in the cochlea was analyzed.

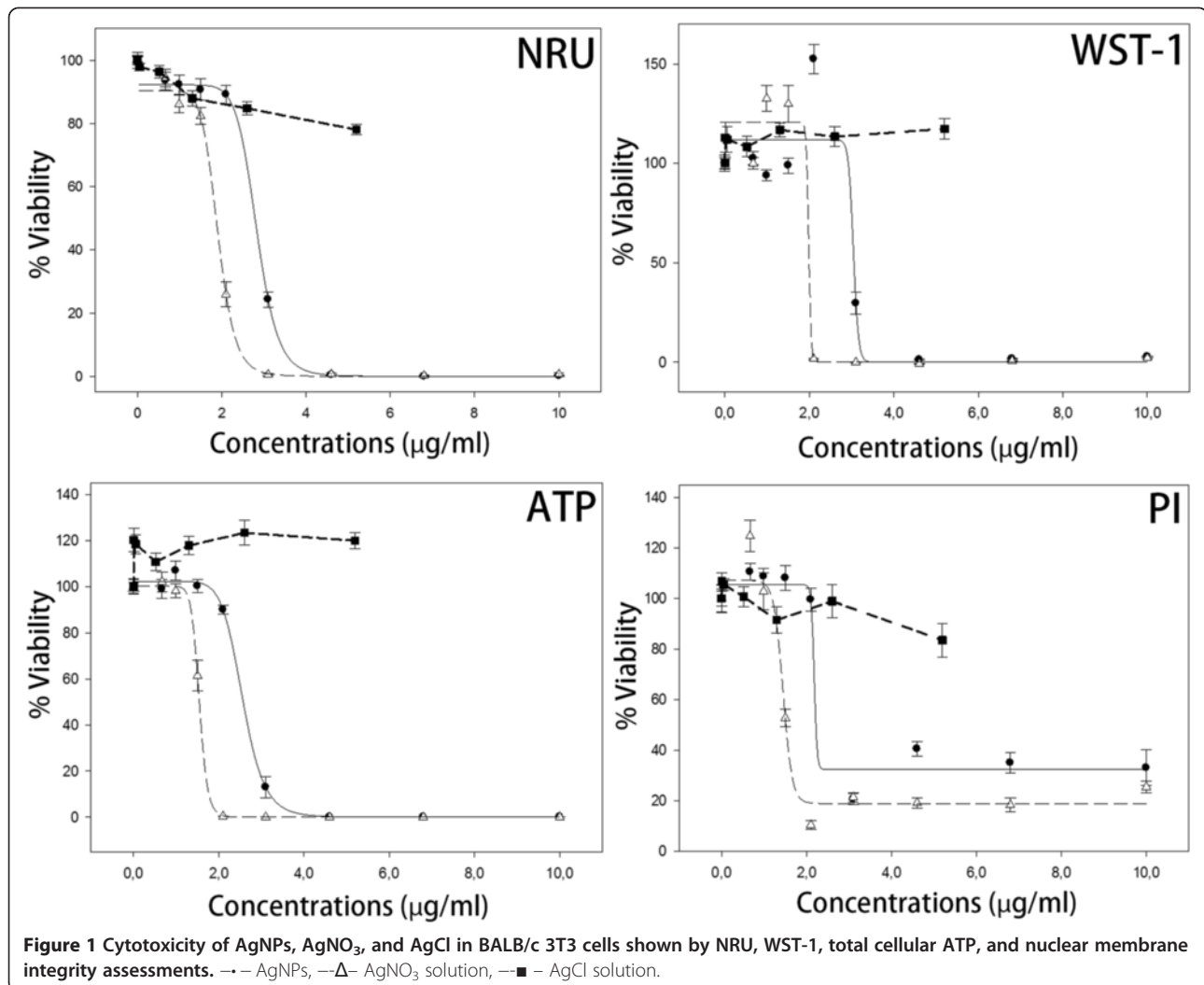
Results

Comparison of AgNP toxicity in BALB/c 3T3 cells between NRU and other end points

The IC₅₀ for AgNPs was 2.8 µg/ml in NRU assay, which was lower than that in WST-1 and higher than that in total cellular ATP and nuclear membrane integrity (propidium iodide) assessments (Figure 1, Table 1). There was a significant ($P < 0.001$) ~50% increase in mitochondrial activity of BALB/c 3T3 cells at AgNP concentration 2.1 µg/ml (shown by WST-1). Thereafter the viability dropped steeply. Other cytotoxicity assays showed no such increase in viability compared to control value (untreated cells). The IC₅₀ for AgNO₃ was lower than that for the AgNPs in all the measurement methods. However, AgCl up to saturated concentration was insignificantly toxic.

Permeability change of the biological barriers in rat ear after AgNP exposure

Significant changes in the permeability of the biological barriers occurred in the middle ear mucosa, skin of the external ear canal, and the inner ear at 5 h post-transtympanic injection at concentrations ranging from 20 µg/ml to 4000 µg/ml. The induced permeability alteration showed a dosage-response relationship and recovered to base line in barriers in the middle ear mucosa, external ear canal skin, and the inner ear except vestibule, that only



partially recovered at 7 d post-exposure to concentrations lower than 4000 µg/ml of Ag NPs (Figures 2 and 3).

The impact of AgNP exposure on the auditory function of rats

ABR is an auditory evoked potential extracted from ongoing electrical activity in the brain and recorded with

Table 1 IC₅₀ of AgNPs and AgNO₃ evaluated in BALB/c 3T3 cells using NRU, WST-1, ATP, and PI methods

| Assay | IC ₅₀ (µg/ml) and coefficient of determination (R ²) | | | |
|-------|---|----------------|-------------------|----------------|
| | AgNPs | | AgNO ₃ | |
| | IC ₅₀ | R ² | IC ₅₀ | R ² |
| NRU | 2.8 | 0.97 | 1.9 | 0.97 |
| WST-1 | 3.0 | 0.86 | 2.0 | 0.93 |
| ATP | 2.6 | 0.96 | 1.5 | 0.95 |
| PI | 2.2 | 0.80 | 1.4 | 0.78 |

ATP, total ATP measurement; NRU, neutral red uptake assay; PI, propidium iodide penetration assay; WST-1, NAD(P)H-dependent cellular oxidoreductase enzyme assay.

subcutaneous platinum needle electrodes placed in the scalp. The resulting recording is a series of vertex positive waves of which I through V are evaluated. The wave II is the most evident and stable response in rats and utilized to identify the threshold which is the minimum visible and repeatable response. The hearing loss level was presented as threshold shift in the ABR measurement, which is that the larger the threshold shift the more severe the hearing loss. The increase in this parameter indicates the degree of hearing loss that is expressed by decibel (dB). Figure 4 showed the induced hearing loss in rats. At 2 d post-transtympanic injection, the AgNPs at a concentration of 4000 µg/ml caused significant threshold shifts of 29 dB upon click stimuli and from 18 dB to 32 dB with tone burst stimuli at frequencies of 2 kHz, 4 kHz, 8 kHz, 16 kHz, and 32 kHz ($p < 0.01$, independent sample t-test); however, AgNPs at a concentration of 200 µg/ml caused only a significant threshold shift of 16 dB at 32 kHz ($p < 0.01$, independent sample t-test). On 4 d post-transtympanic injection,

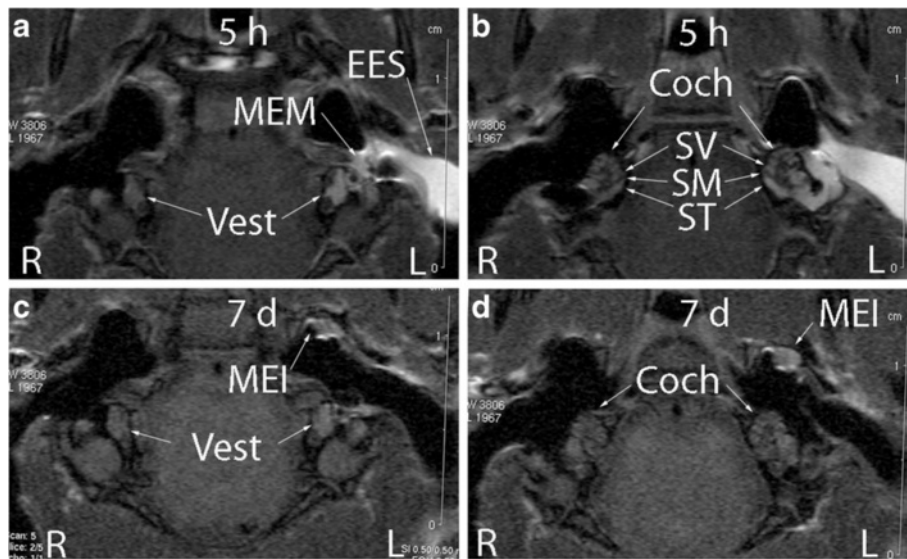


Figure 2 Gd-contrasted MRI showed that dynamic changes in the permeability of the biological barriers occurred in the middle ear mucosa, skin of the external ear canal, and the inner ear after exposure to 400 µg/ml AgNPs. Figures a and b are measured 5 h after exposure and figures c and d 7 d after exposure. Quantification data was shown in Figure 3. Coch: cochlea; MEI: middle ear infiltration; MEM: middle ear mucosa; SM: scala media; ST: scala tympani; SV: scala vestibuli; Vest: vestibulum.

AgNPs at a concentration of 4000 µg/ml caused significant threshold shifts of 19 dB upon click stimuli and from 14 dB to 35 dB on tone burst stimuli at frequencies of 2 kHz, 4 kHz, 8 kHz, 16 kHz, and 32 kHz ($p < 0.01$, independent sample t-test). The threshold shift induced by AgNPs at a concentration of 200 µg/ml reduced to 4 dB at 32 kHz but remained significant ($p < 0.01$, independent sample t-test). At 7 d post-transtympanic injection, AgNPs at a concentration of 4000 µg/ml caused no significant threshold shifts upon click stimuli and tone

burst stimuli at a frequency of 2 kHz, but significant threshold shifts from 5 dB to 33 dB at frequencies of 4 kHz through 32 kHz were observed ($p < 0.01$, independent sample t-test). No significant threshold shift was detected in rats exposed to AgNPs at a concentration of 200 µg/ml. There was a significant positive linear correlation between the threshold shift and frequency in rats exposed to AgNPs at a concentration of 4000 µg/ml at the observation time points of 2 d, 4 d, and 7 d ($p < 0.01$, 2-tailed Pearson correlation).

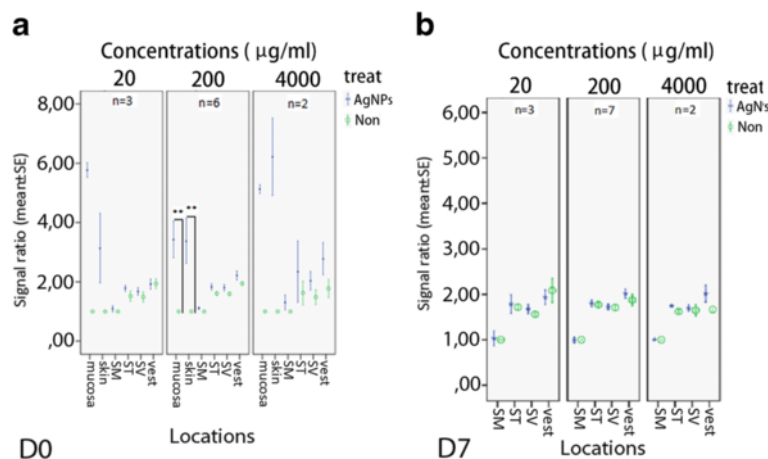
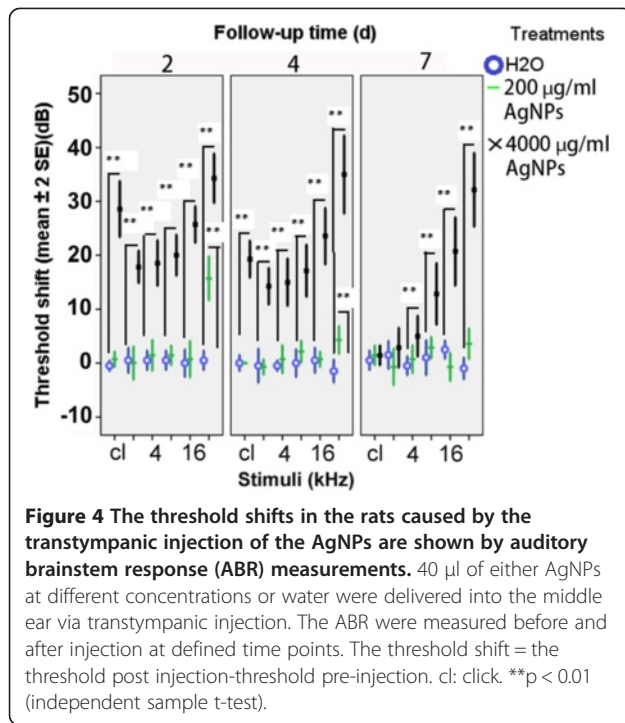
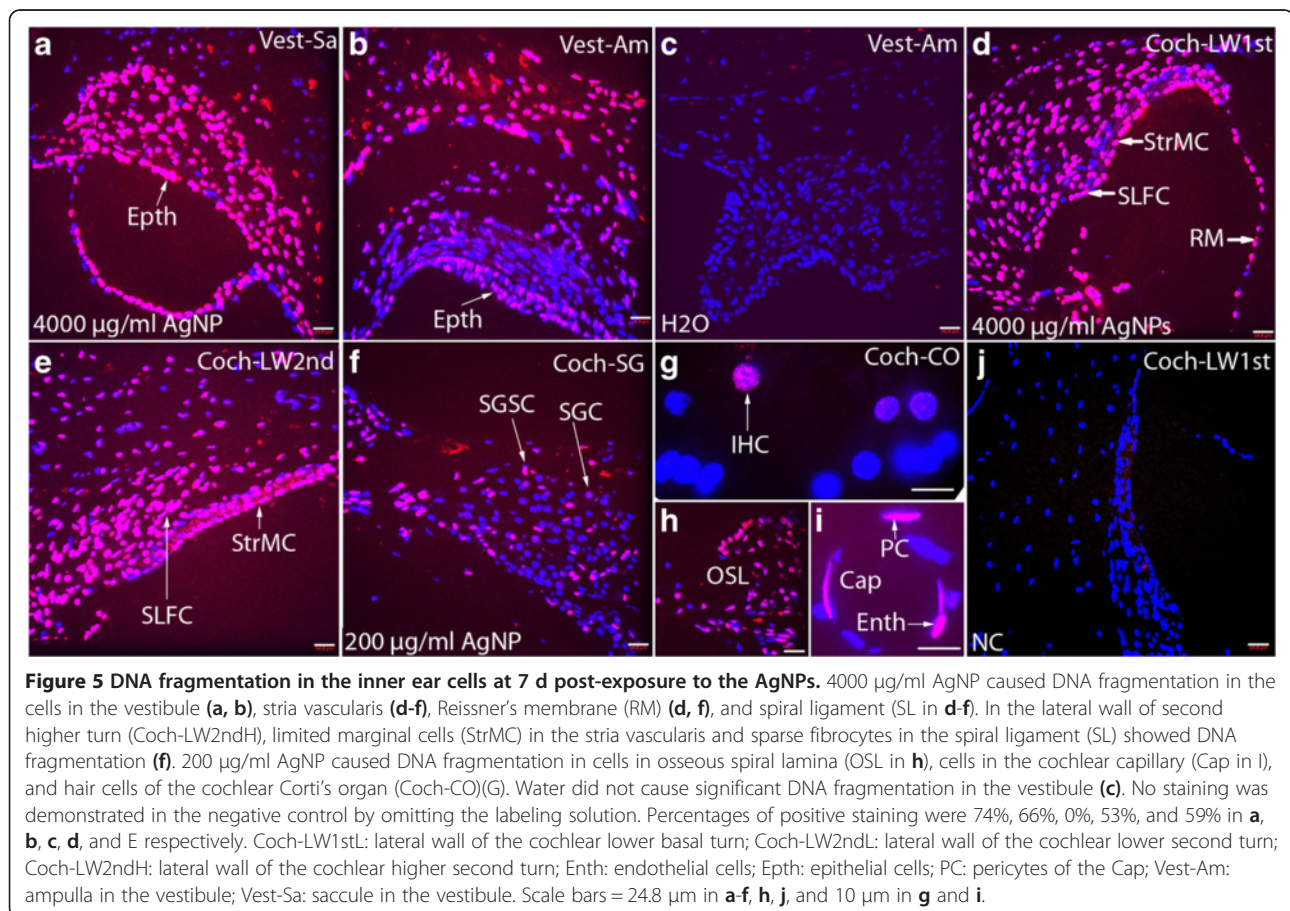


Figure 3 Quantifications on AgNP induced permeability changes in the biological barriers in the skin, mucosa, and inner ear shown by Gd-DOTA-enhanced MRI. a. Results on d 0. b. Results on d 7. * $p < 0.05$; ** $p < 0.01$ (independent t-test). SM: scala media; ST: scala tympani; SV: scala vestibule; vest: vestibule.



Cell death in the rat inner ear after AgNP exposure

Inner ear cell death (apoptosis) was detected in the inner ear exposed to AgNPs at concentrations of both 200 µg/ml and 4000 µg/ml, as indicated by DNA fragmentation. In general, greater cell death occurred in the vestibule than in the cochlea. This was more obvious at the lower concentration of AgNPs. In the cochlea, the stria marginal cells were among the most sensitive cells to develop apoptosis after AgNP exposure, and were followed by the osteocytes in the cochlear shell, the osseous spiral limbus, epithelial cells of the Reissner's membrane, the spiral ligament fibrocytes, the spiral ganglion satellite cells, endothelial cells and pericytes of the cochlea capillaries, and cochlear hair cells. At 4000 µg/ml of AgNPs, there was universal cell death in the vestibule end organ and cochlea, between the hook region and the second lower turn, as well as the Reissner's membrane, part of the spiral ganglion, sparse stria vascularis, spiral ligament, capillary, and osseous spiral limbus from the second higher turn to the apex. At 200 µg/ml AgNPs, there was cell death in most the vestibular end organ cells, and cochlear cell populations, which was similar to that caused by 4000 µg/ml AgNPs in the higher turns (Figure 5).



Discussion

MRI results showed that the biological barriers in the skin, mucosa, and inner ear of rats were opened by the AgNPs in a dose-dependent manner, which was supported by histology. Changes in the biological barrier function of the ear were reversible in rats exposed to AgNPs at tested concentrations. The biological barriers impede the passage of substances as nanoparticles into the tissue and protect the organ so that it can function properly. Hence, they constrain the bioavailability of AgNPs. As the direct contact site, the barrier in the middle ear mucosa is the most accessible structure observed in the MRI study. The middle ear mucosa is a direct continuation of the mucosa of the upper respiratory tract; data acquired in the middle ear mucosa is relevant to explaining the impact of AgNPs on the respiratory mucosa, including the nasal mucosa.

After passing through the barriers of the round and oval windows, AgNPs entered the inner ear and disrupted the blood-perilymph and blood-endolymph barriers, causing hearing loss. Greater cell death in the vestibule than that in the cochlea indicated that the oval window is more permeable to AgNPs than the round window which is in accordance with the phenomenon observed in gadolinium transport from the middle ear to the inner ear [30]. However, no balance problem was observed in the animals exposed to any of these concentrations of AgNPs (data will be reported separately). Although AgNPs may directly damage the sensorineural cells in the inner ear, complete recovery of hearing loss induced by 200 µg/ml AgNPs suggested that most of the inner and outer hair cells and spiral ganglion cells are preserved, and hearing loss is mainly due to destabilized ion homeostasis [18,31,32]. The blood-endolymph barrier was rather resistant to AgNPs, suggesting that the blood-endolymph barrier integrity is critical to maintaining hearing function.

The present study showed that individual cells *in vitro* are more sensitive to AgNPs than the inner ear cells *in vivo*. It is in accordance with a previous study showing that individual primary cochlear cells are more sensitive to the mitochondrial toxin, 3-nitropropionic acid (3NP), than the cells in the cochlea of living guinea pigs [33]. In the present study, AgNP caused BALB/c 3T3 cell death with IC₅₀ values ranging from 2.2 to 3.0 µg/ml, as determined by measuring the NAD(P)H-dependent cellular oxidoreductase enzyme activity (WST-1), total cellular ATP, nuclear membrane permeability (propidium iodide), and NRU. The observed significant increase in mitochondrial activity of BALB/c 3T3 cells at AgNP concentration 2.1 µg/ml without alteration in ATP levels indicated that the net ATP level might be affected by several activities. We suspect that an augmented cellular activity accompany an increased mitochondrial activity and the cells consume

more ATP giving rise to a stable cellular ATP level as presented in the data. This indicates that WST-1 assay is a more sensitive and reliable parameter of cellular viability than measuring the ATP level. Therefore, WST-1 assay was selected for inter-laboratory validation in nanotoxicology of European Commission FP7 large-scale integrating project NanoValid (internal data) [34]. The IC₅₀ for AgNO₃ was lower than that for AgNPs. It has been reported that both AgNPs and ionic Ag⁺ (using AgNO₃ as material control) are toxic to the cells [29]. This is actually doubtful because no AgNO₃ remains in either the animal or human body after administration because AgNO₃ reacts with saline and is converted to AgCl and NO₃⁻ in plasma (and medium in the cell culture). It is well known that NO₃⁻ ion is extremely toxic to any cells. If Ag⁺ is released from the AgNPs, the major product is AgCl, which has low water solubility. In the present study AgCl was, indeed, insignificantly toxic to the BALB/c 3T3 cells tested up to the saturated concentration. To correlate with *in vitro* studies, 200 µg/ml AgNPs induced reversible changes in the biological barrier and auditory functions. The dose of 4000 µg/ml AgNPs caused hearing loss (with partial recovery). In general, the IC₅₀ in the present *in vitro* tests are more than 1000 times more sensitive than the *in vivo* studies, which is most likely attributed to the protective function of the highly regulated double layer of the biological barriers (the oval and round windows, and the endolymph barrier in the inner ear) and the extracellular matrix.

The hearing measurement was in line with the cell death observed in histology. At a dose of 200 µg/ml, AgNPs caused a reversible hearing loss at 32 kHz, correlating with the lower basal turn of the cochlea. This is in accordance with the cell death map (Figure 5). A dose of 4000 µg/ml AgNPs caused irreversible hearing loss above 8 kHz, matching the broadly distributed cell death up to the second lower turn (Figure 5) [35]. However, only partial hearing loss occurred at the frequencies of 16 kHz and 32 kHz instead of total loss on day 7. Our explanation for this disparity is that spatial information on Corti's organ dysfunction provided by tone burst ABR is much less accurate than the histology. It is known that the tone burst, which has relatively broad spectra, also elicits a response from a region of intact Corti's organ that is distant from the nominal stimulus frequency and causes a false positive result [36]. Therefore, the 16 kHz and 32 kHz stimuli elicited nerve fibers that are responsible for higher tone hearing where the Corti's organs did not show any impairment at the higher turns when the Corti's organs at their specific frequency were damaged.

The vestibular cells demonstrated greater impairment than the cochlear cells after exposure to AgNPs at a low concentration, indicating that the passage of AgNPs into the vestibule through the oval window might be more efficient than the passage into the

cochlea through the round window because AgNP induced cellular toxicity is concentration-dependent, as shown in the in vitro study. However, this hypothesis needs to be tested in future studies.

Our results suggest that the AgNPs impaired mitochondrial function through inhibition of the mitochondrial succinate-tetrazolium reductase activity (shown by WST-1) and ATP production. The notable ~50% increase in mitochondrial activity (as shown by WST-1) at 2.1 µg/ml prior to its ~50% reduction at 3.0 µg/ml indicated the onset of defense process upon AgNP stimuli, i.e., hormesis (other cytotoxicity assays did not show any increase at this concentration) and further supported the occurrence of oxidative stress within the mitochondria [37]. These results also support the previously reported findings that showed that mitochondrial dysfunction is involved in hearing loss by causing energy shortage. The sensitivity of different cell populations to mitochondrial toxins is determined by the cellular activity-related energy consumption [18,33]. The cells that are impaired in the blood-perilymph and blood-endolymph barriers after the delivery of AgNPs are among the sensitive populations. A comprehensive gene sequencing study in zebrafish embryos demonstrated that the most notably affected gene pathway by silver in the nano-, bulk-, and ionic forms is associated with oxidative phosphorylation and protein synthesis [38]. The mitochondria is the site of oxidative phosphorylation, and AgNPs disrupt mitochondrial membrane permeability as well as decrease the activity of the mitochondrial respiratory chain complexes I, II, III, and IV in cells from the brain, skeletal muscle, heart, and liver of rats [39,40]. Specifically, AgNPs induced apoptosis in NIH3T3 cells was reportedly associated with the generation of reactive oxygen species (ROS) and Jun amino-terminal kinases (JNK) activation, leading to the release of cytochrome C into the cytosol and translocation Bax to mitochondria [26]. Consequently, the cell death of BALB/c 3T3 cells induced by AgNPs in the present study was associated with the disrupted integrity of the nuclear membrane, which was visible by propidium iodide staining.

In conclusion, AgNPs caused significant, dose-dependent changes in the permeability of biological barriers in the middle ear mucosa, the skin of the external ear canal, and the inner ear. The functional change in the auditory system

was in line with the histology results. In general, the BALB/c 3T3 cell line is more than 1000 times more sensitive than the in vivo studies. Impairment of the mitochondrial function was indicated to be the toxic mechanism caused by the AgNP exposure. These results suggest that the concentration of AgNPs should be tightly controlled in clinic application in treating otitis media. The rat ear model might be expended to other engineered nanomaterials in nanotoxicology study.

Materials and methods

The polyvinylpyrrolidone stabilized AgNPs was supplied by Colorobbia (Firenze, Italy). The AgNPs were dispersed in deionized water (40 mg/ml) and scanning electron microscopy showed that the AgNPs are spheroids in morphology with a particle size of around 100 nm. Dynamic light scattering (DLS) showed a mean hydrodynamic size of 117 ± 24 nm and a mean zeta potential of -20 ± 9 mV. The selected AgNPs is stable in artificial perilymph which is the main solution in the inner ear that AgNPs would interact (data including the full characterization data will be published separately).

The murine fibroblast cell line BALB/c 3T3 clone 31 was purchased from ATCC (American Type Culture Collection, LGC Promochem AB, Boras, Sweden). Dulbecco's Modification of Eagle's Medium (DMEM), L-glutamine, and newborn calf serum (NBCS) were purchased from Gibco Invitrogen (Carlsbad, USA). Stability of the AgNPs in the DMEM is still under investigation between several laboratory in Europe within the European Union 7th frame programme (EU FP7) large-scale integrating project NanoValid [34] (http://cordis.europa.eu/result/rcn/140307_en.html). An ATP Determination Kit was purchased from Life Technologies (California, USA). WST-1 and an In Situ Cell Death Detection Kit (TMR red) were purchased from Roche (Basel, Switzerland). Propidium iodide, paraformaldehyde (PFA), 4,6-diamidino-2-phenylindole (DAPI), and Fluoromoun™ were purchased from Sigma-Aldrich (St. Louis, USA).

Fourteen male Sprague Dawley rats for the MRI study, weighing between 287 g and 524 g, were maintained in the Biomedicum Helsinki, Laboratory Animal Centre, University of Helsinki. Fourteen male Sprague Dawley rats for ABR measurements weighing between 330 g and 410 g, were maintained in the Experimental Animal Unit, School of Medicine, University of Tampere, Finland (Table 2). All

Table 2 Assignments of rats in MRI and ABR measurements post-intratympanic administration of AgNPs

| Measures | Number of rats exposed to varied concentration of AgNPs for different time | | | | | | | | | |
|----------|--|-----|-----|-----|------------|-----|-----|-----|------------|-----|
| | 4000 µg/ml | | | | 200 µg/ml* | | | | 2000 µg/ml | |
| | 5 h | 2 d | 4 d | 7 d | 5 h | 2 d | 4 d | 7 d | 5 h | 7 d |
| MRI | 2 | - | - | 2 | 7 | - | - | - | 5 | 5 |
| ABR | - | 7 | 7 | 7 | - | 7 | 7 | 7 | - | - |

*Three rats receiving 400 µg/ml AgNP injection were pooled in the 200 µg/ml group in MRI study. ABR: auditory brainstem response. -: no exposure.

animal experiments were approved by the Ethical Committee of University of Tampere (permission: ESAVI/3033/04.10.03/2011). Animal care and experimental procedures were conducted in accordance with European legislation. Animals for the MRI study were anesthetized with isoflurane with a 5% isoflurane–oxygen mixture (flow-rate 1.0 L/min) for induction and 3% for maintenance via a facemask. The ABR measurements were performed under general anesthesia after the intraperitoneal injection of a mixture of 0.8 mg/kg of medetomidine hydrochloride (Domitor, Orion, Espoo, Finland) and 80 mg/kg of ketamine hydrochloride (Ketalar; Pfizer, Helsinki, Finland). During the experiments, Viscotears® (Novartis Healthcare A/S, Denmark) were used to protect the animals' eyes.

BALB/c 3T3 cells were cultured in DMEM containing 4 mM L-glutamine and supplemented with 10% NBCS at 37°C with 5% CO₂, they were then seeded to 96-well plates at a density of ~3000 cells/well and allowed to form a 50–70% confluent monolayer after 24 ± 2 h. For the propidium iodide assays, 96-well black plates with clear bottoms were used. After replacing the medium with 90 µl DMEM containing 4 mM L-glutamine and 5% NBCS, 10 µl AgNP dilutions (prepared immediately prior to use in deionized water) were added to the wells to reach eight different AgNP and AgNO₃ (final concentrations 0.67–10.0 µg/ml) and six different AgCl (final concentrations 0.0052–5.2 µg/ml) concentrations with 6 replicates. The plates were then incubated for 24 h. The exposure time was defined according the results showing that AgNPs remained in rat cochlear for at least 24 h after transtympanic injection (unpublished data acquired using micro computed tomography). The medium containing 10% deionized water was used as a vehicle control. Four different assays were used to study the viability of BALB/c 3T3 cells after AgNP exposure, which are NRU, WST-1, the total cellular ATP, and propidium iodide staining. Each assay was performed twice (Additional file 1: Support material 1).

Under general anesthesia, 40–50 µl of AgNPs at defined concentrations were injected into the left middle ear cavity through the tympanic membrane penetration under an operating microscope (Table 2). After injection, the animals were kept in the lateral position with the injected ear oriented upward for 15 min before further measurements.

A 4.7 T MR scanner with a bore diameter of 155 mm (PharmaScan, Bruker BioSpin, Germany) was used in the MR measurements for evaluation of the biological barrier function in the ear. The maximum gradient strength was 300 mT/m with an 80-µs rise time. A gadolinium-tetraazacyclo-dodecane-tetra-acetic acid (Gd-DOTA, 500 mM, DOTAREM, Guerbet, Cedex, France) solution was injected into the tail vein at a dosage of 0.725 mM/kg 2 h before the MRI measurements. MRI scanning commenced at several

time points after the transtympanic injection. The first MRI time of 5 h was determined by taking the penetration time of liposome nanoparticles from the middle ear to the inner ear as a reference [16]. The final imaging time of 7 d was selected according to the course of acute inflammation. For imaging protocols, refer to the Additional file 1: Support material 2.

BioSig32 (Tucker Davis Technologies, Florida, USA) was used for the ABR threshold recording in rats in a custom made, soundproof chamber. Both click and tone burst stimuli were used for the ABR measurements at a certain time point post-administration of AgNPs. The first ABR measurement was followed on 2 d post-administration of AgNPs allowing the animals to recover from the general anesthesia during the injection and ensure the injected solution to be entirely cleared from the middle ear cavity. The second follow-up time of 4 d post-injection was chosen because it is close to the peak time of mitochondrial toxin-induced cell death in the cochlea [33]. The third follow-up time of 7 d is the period of acute inflammation. For details on the ABR recording, refer to the Additional file 1: Support material 3.

For nuclear DNA fragmentation analysis in rat cochlea, animals were perfused with 4% PFA in 0.1 M PBS (pH 7.4) following cardiac perfusion and the removal of the blood with 50 mL physiological saline containing 0.3 mL heparin (100 IE). The bullae were collected and fixed with 4% PFA overnight and processed for nuclear DNA fragmentation investigation using terminal transferase (TdT) to label the free 3'OH breaks in the DNA strands of apoptotic cells with TMR-dUTP. For details on the analysis, refer to the Additional file 1: Support material 4.

Additional file

Additional file 1: Support materials 1-4.

Abbreviations

ABR: Auditory brainstem response; AgNPs: Silver nanoparticles; DAPI: 4,6-diamidino-2-phenylindole; DMEM: Dulbecco's Modification of Eagle's Medium; Gd-DOTA: Gadolinium-tetra-azacyclo-dodecane-tetra-acetic acid; JNK: Jun amino-terminal kinases; MRI: Magnetic resonance imaging; NBCS: Newborn calf serum; NRU: Neutral red uptake; OECD: Organization for Economic Cooperation and Development; PFA: Paraformaldehyde; ROS: Reactive oxygen species; TdT: Terminal transferase.

Competing interests

The authors declare that they have no competing interests.

Authors' contributions

Conceived and designed the experiments: JZ MM TH IP. Performed the experiments: JZ HF MM. Analyzed the data: JZ HF MM. Wrote the paper: JZ MM. All authors read and approved the final manuscript.

Acknowledgements

The authors gratefully acknowledge financial support from European Community FP7 large-scale integrating project NanoValid (contract: 263147).

The authors also want to thank Lesley Tobin de Fuentes (Institute of Nanotechnology, UK) for proofreading the manuscript.

Author details

¹Hearing and Balance Research Unit, Field of Oto-laryngology, School of Medicine, University of Tampere, Tampere, Finland. ²The Finnish Centre for Alternative Methods, School of Medicine, University of Tampere, Tampere, Finland. ³Department of Otolaryngology-Head and Neck Surgery, Center for Otolaryngology-Head & Neck Surgery of Chinese PLA, Changhai Hospital, Second Military Medical University, Shanghai, China.

Received: 17 August 2014 Accepted: 12 November 2014

Published online: 03 December 2014

References

- Hall-Stoodley L, Hu FZ, Gieseke A, Nistico L, Nguyen D, Hayes J, Forbes M, Greenberg DP, Dice B, Burrows A, Wackym PA, Stoodley P, Post JC, Ehrlich GD, Kerschner JE: **Direct detection of bacterial biofilms on the middle-ear mucosa of children with chronic otitis media.** *JAMA* 2006, **296**(2):202–211.
- Wessman M, Bjarnsholt T, Eickhardt-Sorensen SR, Johansen HK, Homoe P: **Mucosal biofilm detection in chronic otitis media: a study of middle ear biopsies from Greenlandic patients.** *Eur Arch Otorhinolaryngol* 2014.
- Gu X, Keyoumu Y, Long L, Zhang H: **Detection of bacterial biofilms in different types of chronic otitis media.** *Eur Arch Otorhinolaryngol* 2013.
- Nguyen CT, Robinson SR, Jung W, Novak MA, Boppart SA, Allen JB: **Investigation of bacterial biofilm in the human middle ear using optical coherence tomography and acoustic measurements.** *Hear Res* 2013, **301**:193–200.
- Sawada I, Fachrul R, Ito T, Ohmukai Y, Maruyama T, Matsuyama H: **Development of a hydrophilic polymer membrane containing silver nanoparticles with both organic antifouling and antibacterial properties.** *J Membr Sci* 2012, **387**–388:1–6.
- Doudi M, Naghsh N, Setorki M: **Comparison of the effects of silver nanoparticles on pathogenic bacteria resistant to beta-lactam antibiotics (ESBLs) as a prokaryote model and Wistar rats as a eukaryote model.** *Med Sci Monit Basic Res* 2013, **19**:103–110.
- Lu Z, Rong K, Li J, Yang H, Chen R: **Size-dependent antibacterial activities of silver nanoparticles against oral anaerobic pathogenic bacteria.** *J Mater Sci Mater Med* 2013, **24**(6):1465–1471.
- Pinto RJ, Almeida A, Fernandes SC, Freire CS, Silvestre AJ, Neto CP, Trindade T: **Antifungal activity of transparent nanocomposite thin films of pullulan and silver against *Aspergillus niger*.** *Colloids Surf B Biointerfaces* 2013, **103**:143–148.
- Xiang D, Zheng Y, Duan W, Li X, Yin J, Shigdar S, O'Connor ML, Marappan M, Zhao X, Miao Y, Xiang B, Zheng C: **Inhibition of A/Human/Hubei/3/2005 (H3N2) influenza virus infection by silver nanoparticles in vitro and in vivo.** *Int J Nanomedicine* 2013, **8**:4103–4113.
- You C, Han C, Wang X, Zheng Y, Li Q, Hu X, Sun H: **The progress of silver nanoparticles in the antibacterial mechanism, clinical application and cytotoxicity.** *Mol Biol Rep* 2012, **39**:9193–9201.
- Semenov FV, Fidarova KM: **The treatment of the patients presenting with chronic inflammation of the trepanation cavity with a preparation containing silver nanoparticles following sanitation surgery of the open type.** *Vestn Otorinolaringol* 2012, **6**:117–119.
- Kim YS, Song MY, Park JD, Song KS, Ryu HR, Chung YH, Chang HK, Lee JH, Oh KH, Kelman BJ, Hwang IK, Yu JJ: **Subchronic oral toxicity of silver nanoparticles.** *Part Fibre Toxicol* 2010, **7**:20.
- Sharma HS, Hussain S, Schlager J, Ali SF, Sharma A: **Influence of nanoparticles on blood-brain barrier permeability and brain edema formation in rats.** *Acta Neurochir Suppl* 2010, **106**:359–364.
- Zou J, Saulnier P, Perrier T, Zhang Y, Manninen T, Toppila E, Pyykko I: **Distribution of lipid nanocapsules in different cochlear cell populations after round window membrane permeation.** *J Biomed Mater Res B Appl Biomater* 2008, **87**(1):10–18.
- Zhang Y, Zhang W, Lobler M, Schmitz KP, Saulnier P, Perrier T, Pyykko I, Zou J: **Inner ear biocompatibility of lipid nanocapsules after round window membrane application.** *Int J Pharm* 2011, **404**(1–2):211–219.
- Zou J, Sood R, Ranjan S, Poe D, Ramadan UA, Kinnunen PK, Pyykko I: **Manufacturing and in vivo inner ear visualization of MRI traceable liposome nanoparticles encapsulating gadolinium.** *J Nanobiotechnology* 2010, **8**:32.
- Zou J, Sood R, Ranjan S, Poe D, Ramadan UA, Pyykko I, Kinnunen PK: **Size-dependent passage of liposome nanocarriers with preserved posttransport integrity across the middle-inner ear barriers in rats.** *Otol Neurotol* 2012, **33**(4):666–673.
- Zou J, Li M, Zhang Y, Zheng G, Chen D, Chen S, Zheng H: **Transport augmentation through the blood-inner ear barriers of guinea pigs treated with 3-nitropropionic acid and patients with acute hearing loss, visualized with 3.0 T MRI.** *Otol Neurotol* 2011, **32**(2):204–212.
- Counter SA, Bjelke B, Borg E, Klason T, Chen Z, Duan ML: **Magnetic resonance imaging of the membranous labyrinth during in vivo gadolinium (Gd-DTPA-BMA) uptake in the normal and lesioned cochlea.** *Neuroreport* 2000, **11**(18):3979–3983.
- Powers BE, Widholm JJ, Lasky RE, Schantz SL: **Auditory deficits in rats exposed to an environmental PCB mixture during development.** *Toxicol Sci* 2006, **89**(2):415–422.
- Ferrary E, Sterkers O, Saumon G, Tran Ba Huy P, Amiel C: **Facilitated transfer of glucose from blood into perilymph in the rat cochlea.** *Am J Physiol* 1987, **253**(1 Pt 2):F59–F65.
- Sterkers O, Ferrary E, Saumon G, Amiel C: **Na and nonelectrolyte entry into inner ear fluids of the rat.** *Am J Physiol* 1987, **253**(1 Pt 2):F50–F58.
- Zou J, Pyykko I, Counter SA, Klason T, Bretlau P, Bjelke B: **In vivo observation of dynamic perilymph formation using 4.7 T MRI with gadolinium as a tracer.** *Acta Otolaryngol* 2003, **123**(8):910–915.
- Counter SA, Bjelke B, Klason T, Chen Z, Borg E: **Magnetic resonance imaging of the cochlea, spiral ganglia and eighth nerve of the guinea pig.** *Neuroreport* 1999, **10**(3):473–479.
- Zou J, Zhang W, Poe D, Zhang Y, Ramadan UA, Pyykko I: **Differential passage of gadolinium through the mouse inner ear barriers evaluated with 4.7 T MRI.** *Hear Res* 2010, **259**(1–2):36–43.
- Hsin YH, Chen CF, Huang S, Shih TS, Lai PS, Chueh PJ: **The apoptotic effect of nanosilver is mediated by a ROS- and JNK-dependent mechanism involving the mitochondrial pathway in NIH3T3 cells.** *Toxicol Lett* 2008, **179**(3):130–139.
- Organisation for Economic Co-operation and Development: **Guidance document on using cytotoxicity tests to estimate starting doses for acute oral systemic toxicity tests.** *ENV/JM/MONO* 2010, **20**(No. 129):1–54.
- Ngamwongsatit P, Banada PP, Panbangred W, Bhunia AK: **WST-1-based cell cytotoxicity assay as a substitute for MTT-based assay for rapid detection of toxigenic *Bacillus* species using CHO cell line.** *J Microbiol Methods* 2008, **73**(3):211–215.
- Gagne F, Auclair J, Turcotte P, Gagnon C: **Sublethal effects of silver nanoparticles and dissolved silver in freshwater mussels.** *J Toxicol Environ Health A* 2013, **76**(8):479–490.
- Zou J, Poe D, Ramadan UA, Pyykko I: **Oval window transport of Gd-DOTA from rat middle ear to vestibulum and scala vestibuli visualized by in vivo magnetic resonance imaging.** *Ann Otol Rhinol Laryngol* 2012, **121**(2):119–128.
- Zou J, Zhang Y, Yin S, Wu H, Pyykko I: **Mitochondrial dysfunction disrupts trafficking of Kir4.1 in spiral ganglion satellite cells.** *J Neurosci Res* 2009, **87**(1):141–149.
- Zou J: **Transport augmentation through the blood-inner ear barriers of guinea pigs treated with 3-nitropropionic acid and patients with acute hearing loss, visualized with 3.0 T MRI: figure labeling clarification.** *Otol Neurotol* 2012, **33**(5):691.
- Zou J, Zhang Y, Zhang W, Poe D, Zhai S, Yang S, Pyykko I: **Mitochondria toxin-induced acute cochlear cell death indicates cellular activity-correlated energy consumption.** *Eur Arch Otorhinolaryngol* 2013, **270**(9):2403–2415.
- Reuther R: **NANOVALID Report Summary.** 2013. http://cordis.europa.eu/result/rcn/140307_en.html
- Viberg A, Canlon B: **The guide to plotting a cochleogram.** *Hear Res* 2004, **197**(1–2):1–10.
- Johnson TA, Brown CJ: **Threshold prediction using the auditory steady-state response and the tone burst auditory brain stem response: a within-subject comparison.** *Ear Hear* 2005, **26**(6):559–576.
- Ngo JK, Pomatto LC, Davies KJ: **Upregulation of the mitochondrial Lon Protease allows adaptation to acute oxidative stress but dysregulation is associated with chronic stress, disease, and aging.** *Redox Biol* 2013, **1**(1):258–264.
- van Aerle R, Lange A, Moorhouse A, Paszkiewicz KH, Ball K, Johnston BD, de-Bastos E, Booth T, Tyler CR, Santos EM: **Molecular Mechanisms of Toxicity of Silver Nanoparticles in Zebrafish Embryos.** *Environ Sci Technol* 2013

39. Teodoro JS, Simoes AM, Duarte FV, Rolo AP, Murdoch RC, Hussain SM, Palmeira CM: **Assessment of the toxicity of silver nanoparticles in vitro: a mitochondrial perspective.** *Toxicol In Vitro* 2011, **25**(3):664–670.
40. Costa CS, Ronconi JV, Daufenbach JF, Goncalves CL, Rezin GT, Streck EL, Paula MM: **In vitro effects of silver nanoparticles on the mitochondrial respiratory chain.** *Mol Cell Biochem* 2010, **342**(1–2):51–56.

doi:10.1186/s12951-014-0052-6

Cite this article as: Zou et al.: Toxicity of silver nanoparticle in rat ear and BALB/c 3T3 cell line. *Journal of Nanobiotechnology* 2014 **12**:52.

**Submit your next manuscript to BioMed Central
and take full advantage of:**

- Convenient online submission
- Thorough peer review
- No space constraints or color figure charges
- Immediate publication on acceptance
- Inclusion in PubMed, CAS, Scopus and Google Scholar
- Research which is freely available for redistribution

Submit your manuscript at
www.biomedcentral.com/submit



RESEARCH

Open Access

Micro CT visualization of silver nanoparticles in the middle and inner ear of rat and transportation pathway after transtympanic injection

Jing Zou^{1,5*}, Markus Hannula^{2†}, Superb Misra^{3,7†}, Hao Feng^{1†}, Roberto Hanoi Labrador⁴, Antti S Aula^{2,6}, Jari Hyttinen² and Ilmari Pyykkö¹

Abstract

Background: Silver nanoparticles (Ag NPs) displayed strong activities in anti-bacterial, anti-viral, and anti-fungal studies and were reportedly efficient in treating otitis media. Information on distribution of AgNPs in different compartments of the ear is lacking.

Objective: To detect distribution of Ag NPs in the middle and inner ear and transportation pathways after transtympanic injection.

Methods: Contrast effect of Ag NPs in the micro CT imaging was assessed in a phantom. AgNPs at various concentrations (1.85 mM, 37.1 mM, and 370.7 mM) were administered to rat middle ear using transtympanic injection and cadaver heads were imaged using micro CT at several time points.

Results: The lowest concentration of Ag NPs that could be visualized using micro CT was 37.1 mM. No difference was observed between the solvents, deionized H₂O and saline. Ag NPs at 37.1 mM were visible in the middle ear on 7 d post-administration. Ag NPs at 370.7 mM generated signals in the middle ear, ossicular chain, round window membrane, oval window, scala tympani, and Eustachian tube for both 4 h and 24 h time points. A gradient distribution of Ag NPs from the middle ear to the inner ear was detected. The pathways for Ag NPs to be transported from the middle ear into the inner ear are round and oval windows.

Conclusion: This study provided the imaging evidence that Ag NPs are able to access the inner ear in a dose-dependent manner after intratympanic administration, which is relevant to design the delivery concentration in the future clinic application in order to avoid adverse inner ear effect.

Keywords: Silver nanoparticles, Micro CT, Ear, Animal, Pathway

Introduction

Silver nanoparticles (Ag NPs) displayed strong activities in anti-bacterial, anti-viral, and anti-fungal studies attributed to the mechanisms of inhibiting the formation of biofilm and destroying viral structures and boosting innate immune response among others [1-5]. Study performed by Radzig et al. supports the hypothesis that Ag

NPs exert the antibacterial action through inducing generation of reactive oxygen species and causing DNA damage by oxidative stress, which can be also involved in the mechanisms of antiviral and antifungal activities [6]. Ag NPs also showed excellent behavior in surface-enhanced Raman scattering for the advanced Raman spectroscopy, which has potential for broad range of applications in clinical molecular imaging [7].

Potentially, Ag NPs will be used to treat otitis media and the consequential sensorineural hearing loss through intratympanic administration. Chronic otitis media, characterized by recurrent infections causing pain and purulent otorrhea, is still a significant public health problem affecting 0.5–30% of any given population in developing

* Correspondence: Jing.Zou@uta.fi

†Equal contributors

¹Hearing and Balance Research Unit, Field of Oto-laryngology, School of Medicine, University of Tampere, Medisiinarinkatu 3, 33520 Tampere, Finland

⁵Department of Otolaryngology-Head and Neck Surgery, Center for Otolaryngology-Head & Neck Surgery of Chinese PLA, Changhai Hospital, Second Military Medical University, Shanghai, China

Full list of author information is available at the end of the article

and developed countries. Complications with sensorineural hearing loss and vestibular impairment were repeatedly reported in the literatures [8-12]. Endolymphatic hydrops secondary to the middle ear infection was demonstrated in both animal model and patient with Meniere's disease using gadolinium enhancement magnetic resonance imaging (MRI) [13,14]. However, antibiotic is not always efficient because of the appearance of multidrug resistant strains of bacteria. Formation of biofilm was recently reported in the middle ear of patients with chronic otitis media all over the world [15-18]. Through a completely different mechanism, Ag NPs may overcome all the disadvantages of any antibiotics and eliminate the microorganisms with high efficacy in the ear therapy. This therapeutic strategy was encouraged by a clinical study on treatment of relapses of chronic suppurative otitis media using a preparation containing Ag NPs. The study showed that Ag NPs eliminated clinical symptoms and positive dynamics of the objective signs of the disease, such as reduction or termination of pathological exudation and stimulation of the epidermization processes, which was stable during the observation time of 6 months [19]. In order to persuade this novel therapy with sophisticated design, detailed information on distribution and pathway of Ag NPs

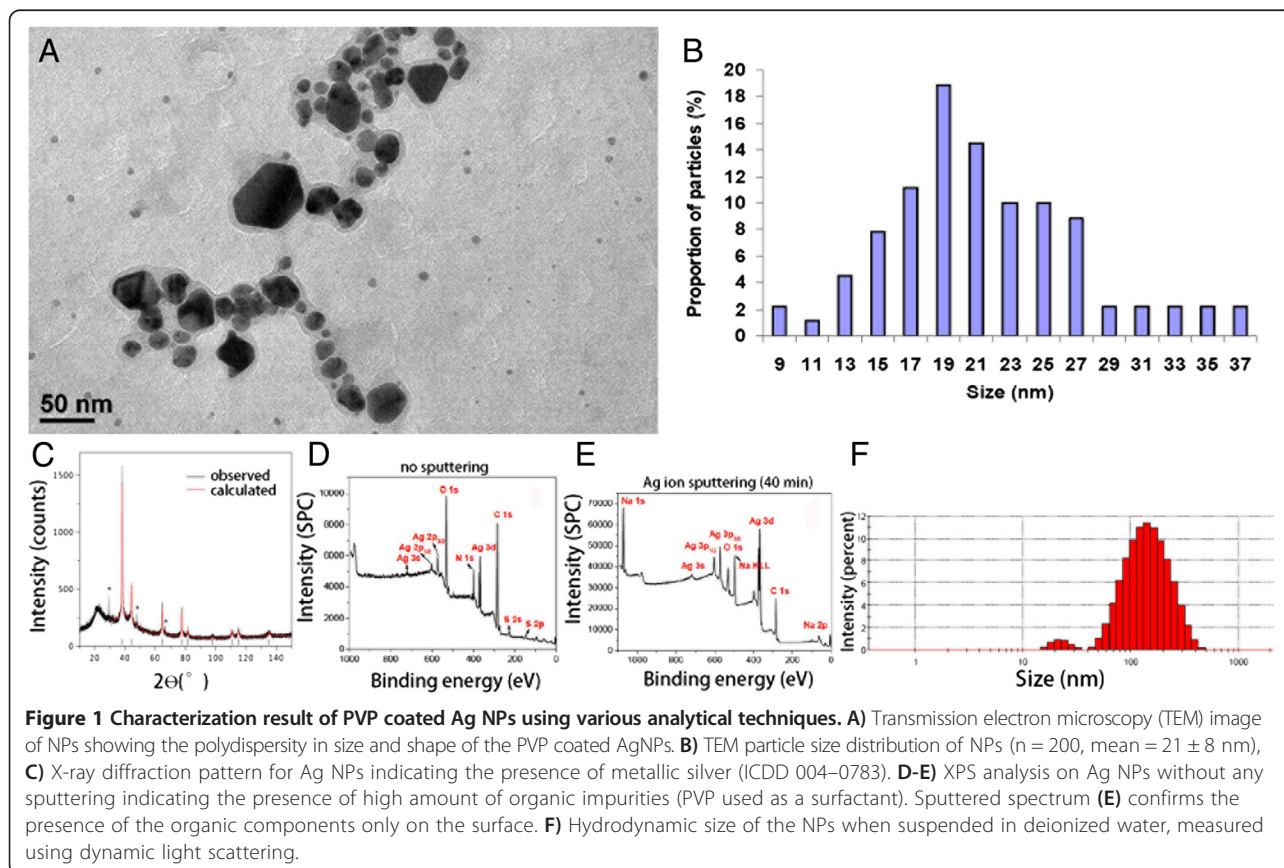
in the middle and inner ear is necessary but currently lacking in the literature.

Micro computed tomography (CT) has been engaged in middle and inner ear imaging of animals and implicated to be a useful tool to trace kinetics of drugs in the inner ear [20,21]. The gray levels in a CT slice image correspond to X-ray attenuation, which reflects the proportion of X-rays scattered or absorbed as they pass through each voxel, and is affected by the density and composition of the material being imaged. Hence, Ag NPs are speculated to attenuate the X-rays and be visible in micro CT images. In the present work, first a phantom study was performed to check the dose response of the imaging system. Next, an *in vivo* experiment was carried out in rats by injecting Ag NP suspensions with different concentrations into the middle ear cavity and following the kinetics of Ag NPs in the middle and inner ear up to 7 d.

Results

Characterization of Ag NPs and potential interaction with artificial perilymph

The Ag NPs used in this study were highly faceted with a mean size of 21 ± 8 nm. The particles were polydispersed in size and shape, as shown in Figure 1. The transmission electron microscope (TEM) images and



size distribution of the particles are shown in Figure 1a. X-ray diffraction (XRD) analysis confirmed the crystalline nature of the particles (ICDD: 004–0783). The mean hydrodynamic size of the particles when suspended in deionized water was 117 ± 24 nm, and the zeta potential was measured to be -20 ± 9 mV. Inductively coupled plasma measurements on the particles showed a very low level of species other than silver, which were mostly cations (Figure 2). Because the nanoparticles were stabilized in the suspension using polyvinylpyrrolidone (PVP), XPS analysis was performed to characterize the surface of the particles. The un-sputtered spectrum of the particles showed a high presence of organic carbon, which was evidently due to the presence of PVP used as the capping agent/surfactant. However, after increasing the sputtering time, the Ag 3d peak started to appear stronger, suggesting a core shell structure wherein the core was metallic silver and the shell was composed of an organic coating with PVP. Incubation with artificial perilymph for 4 h did not significantly affect the size distribution of the Ag NPs (Table 1).

Sensitivity of micro CT imaging of Ag NPs

The current setup of micro CT showed a detection limit for Ag NPs at a concentration of 37 mM. Good linearity between the signal intensity and Ag NPs concentration was obtained in the range of 37–370.7 mM that were dissolved in H₂O (Figure 3). Significant correlation was observed between signal intensities of Ag NPs generated in H₂O and NaCl solutions, but the H₂O provided significantly higher signal intensities than the NaCl with normalized value of 1.04 ($p < 0.001$, paired samples t-test).

Distribution of AgNPs in the middle and inner ear and pathways

The heterogeneous fine structures of rat cochlea were demonstrated by iodine-contrast micro CT in Figure 4.

The optimized protocol for rat ear micro CT imaging had a resolution of 21.9 μ m, which can utilize both the middle ear and inner ear for detecting the distribution of the Ag NPs in both compartments. At 4 h after transtympanic injection of 370.7 mM Ag NPs, the nanoparticles distributed along the middle ear mucosa, diffused to the Eustachian tube, and the extra Ag NPs flowed out into the external ear canal. Abundant Ag NP accumulation on the surface of ossicular chain and stapes artery was detected. The Ag NPs significantly distributed in the round window membrane and continuously moved to the mesothelium of the scala tympani and the annular ligament across the stapediostibular joint, which is the junctional site between the middle ear and vestibule (Figure 5). At 24 h, Ag NPs showed abundant distribution on in the round window membrane and oval window, and became more visible within the cochlea (Figure 5). Ag NPs was detected in the middle ear mucosa at 4 h post-transtympanic injection at 37 mM in one rat. Aggregated Ag NPs were visualized in both middle ear and cochlea on 7 d after injection at 37 mM (Figure 5). Higher estimated concentrations of Ag NPs in various locations of the ear than the applied concentrations supported the aggregation or accumulation of Ag NPs in the corresponding area (Table 2). However, transtympanic injection of Ag NPs at 1.85 mM did not produce any signal of Ag NP at the time points of 4 h, 24 h, and 7 d post-administration. There was not any fluid detected in the middle ear cavity at these time points indicating that there was no infiltration.

Discussion

The present work demonstrated that the PVP-coated Ag NPs were visible in the ear by micro CT after transtympanic injection and entered in the inner ear through the round and oval windows. The detected bright signals in the ear by micro CT could be either aggregated Ag NPs or silver compound formed upon contacting the

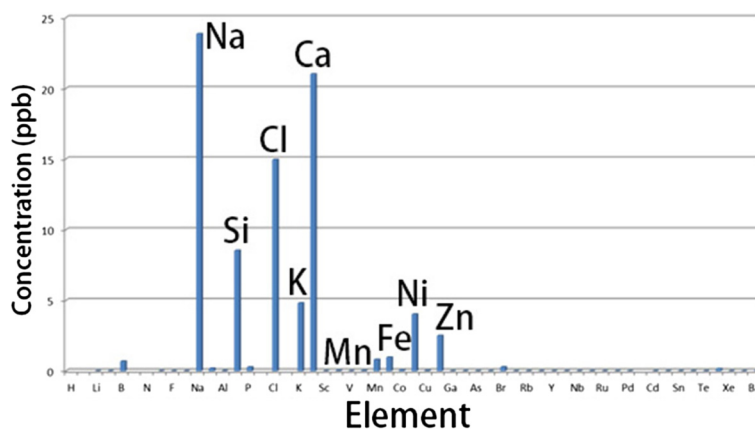


Figure 2 Level of impurities found in the Ag NPs shown by inductively couple plasma-mass spectrometry.

Table 1 Size distribution of AgNPs in artificial perilymph for 4 h at different dilutions

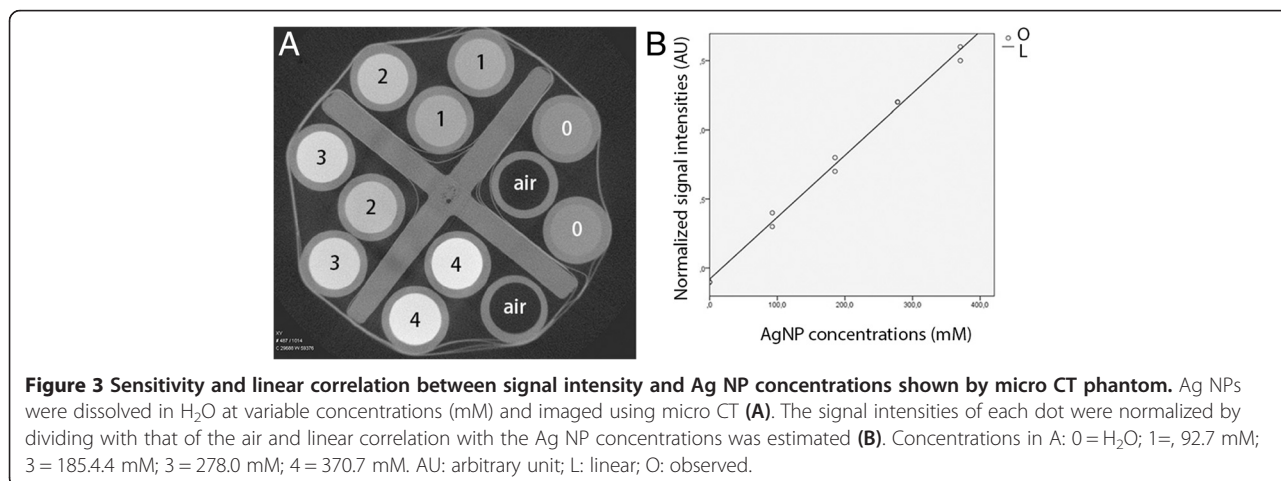
| Concentration (dilution) | Z _{mean} (nm) |
|--------------------------|------------------------|
| x10 | 106.9 ± 0.3 |
| X100 | 102.9 ± 0.7 |
| X1000 | 100.2 ± 1.0 |
| X10000 | 100.7 ± 1.2 |

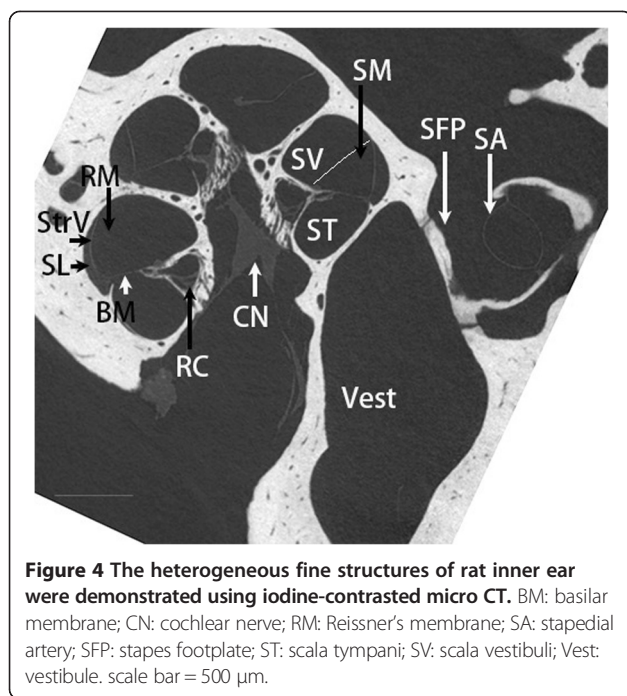
extracellular or cellular fluids. Ag NPs encounter different extracellular environments in the external ear canal, middle ear, and inner ear. The plentiful perilymph in the inner ear may interact with Ag NPs and form a compound immediately after the entry. However, the incubation of Ag NPs with artificial perilymph did not change the size distribution over a period of 25 h, suggesting that the bright signals in the ear represent the Ag NPs. It was reported that silver might be developed as a radiographic contrast agent in dual-energy breast X-ray imaging [22]. However, the detection sensitivity of Ag NPs by micro CT is rather low and the detection limit is 37 mM, a concentration that demonstrated toxicity in the rat ear [23]. These results did not support that the current form of Ag NPs will be used as a contrast agent for CT imaging. Clinical feasibility, however, warrants further studies.

The oval window pathway was recently proved to be more efficient than the round window to transport chelated-gadolinium from the middle ear to the inner ear in animals and human shown by MRI [24,25]. The pathways for the Ag NPs to enter the inner ear were clearly shown to be the round and oval windows. This indicates that the oval window potentially has a broad spectrum of substance transportation in addition to chelated-gadolinium. At 24 h post-administration to the middle ear at a concentration of 370.7 mM, Ag NPs accumulated in the round window membrane and oval

window, and concentrated in the scala tympani, which indicates that the entry of Ag NPs into the inner ear is a dynamic process. This conclusion was further supported by the quantification of Ag NPs in various regions of the ear (Table 2). Obvious Ag NP signal was detected in the middle ear after administration at a concentration of 37.1 mM that was the lowest detection limit of the present setup, which may result from accumulation or aggregation of Ag NPs in the middle ear as supported by the quantification result (Table 2). No signal was detected in the inner ear when Ag NPs were administered at a concentration of 37 mM. This might be caused by the low sensitivity of micro CT visualization. Our explanation is that the layer of Ag NPs formed on tissue surfaces of the inner ear is too thin to raise the value of the voxel as a result of the partial volume effect (the grayscale value of a voxel is the volume fraction weighted sum of all the materials present in the voxel). A previous study demonstrated that hearing loss occurred in rats after middle ear administration of 37.1 mM Ag NPs, which suggests that certain amount of Ag NPs (below the detection threshold of the micro CT) should have entered the inner ear [23].

The long term remaining of Ag NPs in the middle ear cavity for 7 d post-transtympanic injection supports that Ag NP is a potential candidate to combat otitis media. Although no signal was detected in the inner ear on 7 d post-administration of 37.1 mM Ag NP, it did not rule out the penetration of Ag NPs into the inner ear because hearing loss and pathological changes were detected in rats exposed to Ag NPs at this concentration [23]. 1.85 mM Ag NPs did not generate either micro CT signal of AgNPs or infiltration in the middle ear cavity. No infiltration indicates that 1.85 mM of Ag NPs is a safe level for the ear, which is in accordance with our observation that neither hearing loss nor cytokine up-regulation in the inner ear was induced by Ag NPs at this concentration (unpublished data). Importantly, 1.85 mM of Ag NPs





is sufficient to inhibit biofilm formation during bacterial infection which only demands 0.1-2 mM Ag NPs [26].

In addition, the extra Ag NPs were secreted to the nasal pharynx through the Eustachian tube and flowed to the external ear canal through the tympanic membrane penetration. Dysfunction of the Eustachian tube is a common complication of otitis media. The distribution of Ag NPs in the Eustachian tube suggest that Ag NPs may have direct effect on the extension of otitis media. The dendrimer-stabilized silver nanoparticles, that have similar sizes as the Ag NPs utilized in the present study, were reportedly effective in X-ray computed tomography (CT) imaging and stable in water, PBS buffer, fetal bovine serum, and resistant to changes in pH and temperature [27]. There is a possibility that the dendrimer-stabilized silver nanoparticles may be used as a contrast agent in the CT imaging of the external, middle, and inner ears and the Eustachian tube in the future based on the present results.

Conclusions

The distribution of Ag NPs in the middle and inner ear is visible by micro CT and a gradient concentration from the middle ear to the inner ear was detected. The pathways for Ag NPs to be transported from the middle ear into the inner ear are round and oval windows. This study provided the imaging evidence that Ag NPs are able to access various regions of the ear after intratympanic administration in a dosage-dependent manner, which is relevant to design the delivery concentration in

the future clinic application in order to avoid adverse inner ear effect.

Materials and methods

Materials

The Ag NPs was supplied by Colorobbia (Firenze, Italy). Ten male Sprague Dawley rats, weighing between 330 g and 410 g, were maintained in the Experimental Animal Unit, School of Medicine, University of Tampere, Finland. All animal experiments were approved by the Ethical Committee of University of Tampere (permission: ESAVI/3033/04.10.03/2011). Animal care and experimental procedures were conducted in accordance with European legislation. Two rats were assigned into each group with respect to concentrations of AgNPs and imaging time (Table 3). Animal care and experimental procedures were conducted in accordance with European legislation. All experiments were performed under general anesthesia with intraperitoneal injection of a mixture of 0.8 mg/kg of medetomidine hydrochloride (Domitor, Orion, Espoo, Finland) and 80 mg/kg of ketamine hydrochloride (Ketalar; Pfizer, Helsinki, Finland) followed by intramuscular injection of Enrofloxacin (Baytril[®]vet, Orion, Turku, Finland) at a dose of 10 mg/kg to prevent potential infection. During experiments, the animal's eyes were protected by Visco-tears[®] (Novartis Healthcare A/S, Denmark).

Characterization of Ag NPs

The Ag NPs were dispersed in water (370.7 mM) and characterized using a range of analytical techniques, to assess various physicochemical properties (eg. size, shape, zeta potential, surface properties etc.). For TEM measurements, a diluted suspension of Ag NPs was deposited on a copper grid for TEM imaging (Hitachi 7100, 100 kV). XRD was performed on the NPs using an Enraf-Nonius diffractometer coupled to INEL CPS 120 position-sensitive detector with Co-K α radiation, and the phase identification was performed using STOE software. The hydrodynamic size and zeta potential of the nanoparticles were measured using a Malvern Zetasizer (Malvern Instruments, Malvern, UK). ICP-AES (Varian Instruments) analysis was performed to determine the initial concentration of silver in the aqueous nanoparticulate suspension and to measure the level of any impurities present in the matrix. X-ray photoelectron spectroscopy (XPS, Omicron Nanotechnology) was used to study the chemical composition and chemical state of the Ag NPs. The XPS analyses were performed in an ultra-high vacuum medium (pressure of 10⁻¹⁰ mbar) using an Al, K α (h ν = 1486.7 eV) X-ray source, with power given by the emission of 16 mA at a voltage of 12.5 kV. For the silver element, the high-resolution spectra were obtained with analyzer pass energy of 50 eV and a step size of 0.01 eV. The argon ion flux was employed to sputter the

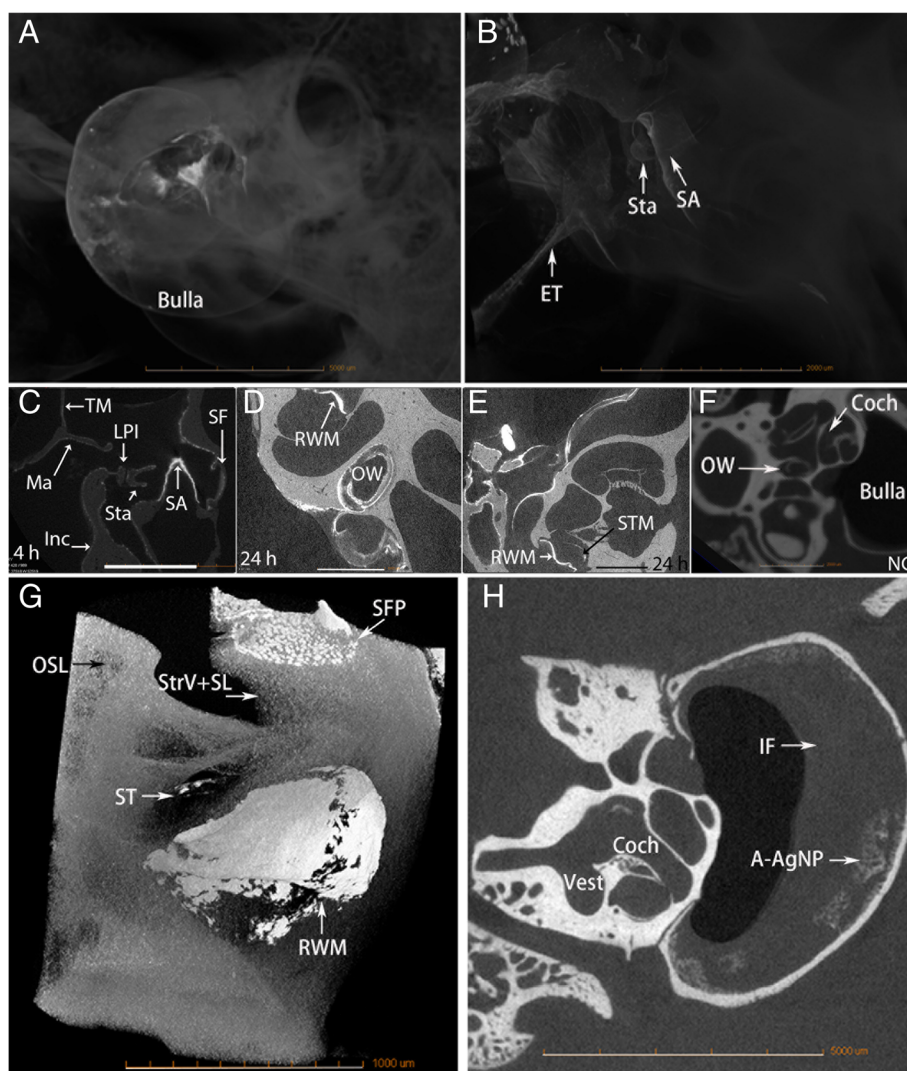


Figure 5 Distribution of Ag NPs in the ear after transtympanic injection shown by micro CT. Either 370.7 mM (A-E, G) or 37.1 mM (H) of Ag NPs were injected at a volume of 50 μ l. At 4 h post-administration (370.7 mM), AgNPs generated bright signal that appeared in the bulla, tympanic membrane (TM) Eustachian tube (ET), and the ossicular chain including malleus (Ma), incus (Inc) and stapes (Sta) (A-C). Abundant Ag NPs were found in the stapedial artery (SA) (C). At 24 h (370.7 mM), abundant distribution of AgNPs was detected in the round window membrane (RWM), oval window (OW), and scala tympani medial wall (STM) of the cochlea (D, E, G). On 7 d (37 mM), middle ear infiltration (IF) and AgNP aggregation (A-AgNPs) were observed (H). No Ag NPs were detected in the ear of non-treatment control (NC) (F). Coch: cochlea; LPI: lenticular process of incus; SF: stapes footplate; ST: scala tympani. Scale bars = 5 mm (A), 2 mm (B, F), 1 mm (C-E). A-F, H: 4x, Pixel size 21.8498; G: 10x, pixel size 1.7 μ m.

surface and remove the adsorbed species, with an energy of 3.5 kV, emission of 20 mA, and incidence angle of 45° over a period of 20 and 40 min. The binding energies were referred to the carbon 1 s level, which was set as 284.6 eV.

Potential impact of perilymph on Ag NPs

Since the Ag NPs will interact with perilymph once enter the inner ear, the potential impact of perilymph on Ag NPs was evaluated. The artificial perilymph containing 145.5 mM NaCl, 2.7 mM KCl, 2.0 mM MgSO₄, 1.2 mM CaCl₂, and 5.0 mM HEPES, with the pH adjusted to 7.4,

was prepared as previously reported [28]. Ag NPs were diluted with artificial perilymph at 10, 100, 1000 and 10000-fold and stored at room temperature for 4 h before the size distribution was measured using DLS (Malvern Zeta Sizer Nano ZS, UK). For the change in the DLS over 25 h, the dilutions were 10-fold.

Micro CT studies

Phantom study

The first round experiment was designed to check the sensitivity of the imaging system using solutions of Ag

Table 2 Concentrations (mM) of AgNPs distributes in various locations of rat ear after transtympanic injection measured by μ CT

| AgNP con delivered | Time | ME | ME-flu | Mall | Inc | Stap | StapArt | StapFoot | OW | RWM | Coc | EEC |
|--------------------|------|------|--------|------|-----|------|---------|----------|------|------|-----|------|
| 371 | 5 h | 1270 | | 547 | 677 | 500 | 769 | | 1038 | | 639 | 1177 |
| 371 | 4 h | 1084 | | 232 | 269 | 408 | 677 | | 232 | | | |
| 371 | 24 h | | | 816 | 639 | 769 | | 639 | 1177 | | | |
| 371 | 24 h | | | 677 | 593 | 723 | 1084 | 769 | 955 | 1177 | 593 | |
| 37 | 4 h | 139 | | | | | | | | | | |
| 37 | 1 w | 232 | 93 | | | | | | | | | |
| 37 | 1 w | 185 | | | | | | | | | | |

Intensities in various locations of rat ear after transtympanic injection of AgNPs were normalized by the intensities of the cochlear perilymph imaged by μ CT. The concentrations of AgNPs were estimated using the formula of $y = 4.88x - 4.86$ obtained in a phantom study, where "y" is the concentration and "x" is the normalized intensity. AgNP con: AgNP concentration; Coc: cochlea; EEC: external ear canal; Inc: incus; ME: middle ear mocusa; ME-flu: middle ear fluid; Mall: malleus; OW: oval window; RWM: round window membrane; Stap: stapes; StapArt: stapedial artery.

NPs with broad concentration range (370.7 mM, 37.1 mM, 3.7 mM, 0.37 mM, and 0.037 mM) that were prepared with either deionized H₂O or saline and placed into plastic phantom tubes arranged concentrically on the modified piston rod of a 50 ml syringe. Negative controls were prepared using saline. Each sample was prepared in duplicate. The phantom was firmly installed on the specimen stage of the MicroXCT-400 (Carl Zeiss X-ray Microscopy, Inc, Jena, Germany) and imaged using the following parameters: Voltage 120 kV, current 83 μ A, pixel size 33.95 μ m, exposure time 0.5 s. The detection limit of the imaging system with the defined parameters was shown to be 37.1 mM based on the first round experiment. The second round experiment was performed using solutions of Ag NPs with smaller concentration range (370.7 mM, 278.0 mM, 185.4 mM, 92.7 mM) suspended in H₂O according to the above protocol to determine the accurate correlation between the concentration and signal intensity.

Animal study

Under general anesthesia, 50 μ l of Ag NPs at defined concentrations were injected into the left middle ear cavity through the tympanic membrane penetration under an operating microscope according to a previously reported procedure [29]. After injection, the animals were kept in the lateral position with the injected ear oriented upward for 15 min to ensure the sufficient amount of Ag NPs to remain in the middle ear cavity

before intraperitoneal injection of Antisendan (atipamezole hydrochloride, Orion Pharma, Finland) (2 mg/kg) to accelerate recovery from anesthesia. At certain observation time points post-administration (Table 3), animals were injected intraperitoneally with pentobarbital sodium at a dosage of 100 mg/kg. The temporal bones were fixed through cardiac perfusion with 0.01 M PBS containing 0.6% (v/v) heparin (pH 7.4) and then 4% paraformaldehyde (Merck, Espoo, Finland). After decapitation, the animal head was further fixed with 4% paraformaldehyde for 2 h, covered with parafilm, and placed on the specimen stage of the micro CT. During imaging, three objectives were used, 1X for the large field of view images, 4X for the images that were focused onto the cochlea, 10x for imaging the oval and round windows. The voltage varied from 60 to 120 kV, the source distance was adjusted to 60–100 mm, and the detector distance was 38–40 mm. The pixel size ranged from 1.7 to 35.4 μ m according to different setup parameters. Afterwards, one bulla was processed for iodine-contrast micro CT imaging in order to demonstrate the soft tissue in the inner ear. The stapes was displaced and about 5 μ l iodixanol (VisipaqueTM, 320 g I/ml, GE Healthcare, Helsinki, Finland) was infused into the inner ear using a high-performance polyimide tubing (MicroLumen, Tampa, FL, USA) that was connected to polyethylene tubing (PE10, Becton, Dickinson and Company, Franklin Lakes, NJ, USA) [28]. The images were acquired with a 4x-objective, source voltage of 40 kV and current 200 μ A, pixel size of 5.6 μ m. Images were

Table 3 Assignments of rats in micro CT measurements and distribution of AgNPs in the ear post-intratympanic administration

| AgNPs conc | 370.7 mM | 37.1 mM | 1.85 mM | | |
|-------------------------------|-----------------------------|-----------------------------|---------|-------|------|
| Time points | 4 h* | 24 h* | 4 h* | 7 d2* | 7 d* |
| Locations of AgNPs in the ear | ME, OC, SA, RWM, OW, ET, ST | ME, OC, SA, RWM, OW, ET, ST | ND | ME | ND |

*Two rats were assigned into each group. conc: concentration; ET: Eustachian tube; ME: middle ear; ND: not detected; OC: ossicular chain; OW: oval window; RWM: round window membrane; SA: stapes artery; ST: scala tympani.

collected using the Xradia TXMController software and reconstructed using the Xradia TXMR reconstructor software.

Image analysis and statistics

Signal intensities in the region of interest were evaluated using Image J 1.46r software (National Institutes of Health, Bethesda, MD). Linear equation was used for the curve estimation between Ag NP concentration and signal intensity obtained using micro CT in phantom. Paired samples T-test (IBM SPSS statistics 20) was used to compare the signal intensity generated by Ag NPs in deionized H₂O and NaCl solutions. Intensities in various locations of rat ear after transtympanic injection of Ag NPs were normalized by the intensities of the cochlear perilymph imaged by μ CT. The concentrations of Ag NPs were estimated according to the linear curve obtained in the phantom study.

Abbreviations

AgNPs: Silver nanoparticles; CT: Computed tomography; MRI: Magnetic resonance imaging; PVP: Polyvinylpyrrolidone; TEM: Transmission electron microscope; XRD: X-ray diffraction.

Competing interests

The authors declare that they have no competing interests.

Authors' contributions

Conceived and designed the experiments: JZ. Performed the experiments: JZ, MH, SM, HF, RHL, ASA. Analyzed the data: JZ, SM, MH. Wrote the paper: JZ, SM. Edited the paper: JH, IP. All authors read and approved the final manuscript.

Acknowledgements

This study was supported by the EU FP7 large-scale integrating project NanoValid (contract: 263147). The authors acknowledge the support of Dr. Joyce Rodrigues de Araujo (Inmetro, Brazil) for performing the XPS analysis on the Ag NPs.

Author details

¹Hearing and Balance Research Unit, Field of Oto-laryngology, School of Medicine, University of Tampere, Medisiininkatu 3, 33520 Tampere, Finland. ²BioMediTech and Department of Electronics and Communications Engineering, Tampere University of Technology, Tampere, Finland. ³School of Geography, Earth and Environmental Sciences, University of Birmingham, Birmingham, UK. ⁴Nanologica AB, Stockholm, Sweden. ⁵Department of Otolaryngology-Head and Neck Surgery, Center for Otolaryngology-Head & Neck Surgery of Chinese PLA, Changhai Hospital, Second Military Medical University, Shanghai, China. ⁶Department of Medical Physics, Imaging Centre, Tampere University Hospital, Tampere, Finland. ⁷Materials Science and Engineering, Indian Institute of Technology-Gandhinagar, Ahmedabad, India.

Received: 17 October 2014 Accepted: 7 January 2015

Published online: 27 January 2015

References

- Martinez-Gutierrez F, Boegli L, Agostinho A, Sanchez EM, Bach H, Ruiz F, et al. Anti-biofilm activity of silver nanoparticles against different microorganisms. *Biofouling*. 2013;29(6):651–60.
- Doudi M, Naghsh N, Setorki M. Comparison of the effects of silver nanoparticles on pathogenic bacteria resistant to beta-lactam antibiotics (ESBLs) as a prokaryote model and Wistar rats as a eukaryote model. *Med Sci Monit Basic Res*. 2013;19:103–10.
- Lu Z, Rong K, Li J, Yang H, Chen R. Size-dependent antibacterial activities of silver nanoparticles against oral anaerobic pathogenic bacteria. *J Mater Sci Mater Med*. 2013;24(6):1465–71.
- Pinto RJ, Almeida A, Fernandes SC, Freire CS, Silvestre AJ, Neto CP, et al. Antifungal activity of transparent nanocomposite thin films of pullulan and silver against *Aspergillus niger*. *Colloids Surf B: Biointerfaces*. 2013;103:143–8.
- Xiang D, Zheng Y, Duan W, Li X, Yin J, Shigdar S, et al. Inhibition of A/Human/Hubei/3/2005 (H3N2) influenza virus infection by silver nanoparticles in vitro and in vivo. *Int J Nanomedicine*. 2013;8:4103–13.
- Radzig MA, Nadochenko VA, Koksharova OA, Kiwi J, Lipasova VA, Khmel IA. Antibacterial effects of silver nanoparticles on gram-negative bacteria: influence on the growth and biofilms formation, mechanisms of action. *Colloids Surf B: Biointerfaces*. 2013;102:300–6.
- Zhang C, Wang K, Han D, Pang Q. Surface enhanced Raman scattering (SERS) spectra of trinitrotoluene in silver colloids prepared by microwave heating method. *Spectrochim Acta A Mol Biomol Spectrosc*. 2014;122:387–91.
- Margolis RH, Hunter LL, Rykken JR, Giebink GS. Effects of otitis media on extended high-frequency hearing in children. *Ann Otol Rhinol Laryngol*. 1993;102(1 Pt 1):1–5.
- Papp Z, Rezes S, Jokay I, Sziklai I. Sensorineural hearing loss in chronic otitis media. *Otol Neurotol*. 2003;24(2):141–4.
- Luntz M, Yehudai N, Haifler M, Sigal G, Most T. Risk factors for sensorineural hearing loss in chronic otitis media. *Acta Otolaryngol*. 2013;133(11):1173–80.
- Mostafa BE, Shafik AG, El Makhzangy AM, Taha H, Abdel Mageed HM. Evaluation of vestibular function in patients with chronic suppurative otitis media. *ORL J Otorhinolaryngol Relat Spec*. 2013;75(6):357–60.
- Chang CW, Cheng PW, Young YH. Inner ear deficits after chronic otitis media. *Eur Arch Otorhinolaryngol*. 2014;271(8):2165–70.
- Zou J, Pyykkö I, Börje B, Toppila E. In vivo MRI visualization of endolymphatic hydrops induced by keyhole limpet hemocyanin round window immunization. *Audiol Med*. 2007;5:182–7.
- Zou J, Pyykkö I. Endolymphatic hydrops in Meniere's disease secondary to otitis media and visualized by gadolinium-enhanced magnetic resonance imaging. *World J Otorhinolaryngol*. 2013;3(1):22–5.
- Hall-Stoodley L, Hu FZ, Gieseke A, Nistico L, Nguyen D, Hayes J, et al. Direct detection of bacterial biofilms on the middle-ear mucosa of children with chronic otitis media. *Jama*. 2006;296(2):202–11.
- Wessman M, Bjarnsholt T, Eickhardt-Sorensen SR, Johansen HK, Homoe P. Mucosal biofilm detection in chronic otitis media: a study of middle ear biopsies from Greenlandic patients. *Eur Arch Otorhinolaryngol*. 2014; Jan 30. [Epub ahead of print].
- Gu X, Keyoumu Y, Long L, Zhang H. Detection of bacterial biofilms in different types of chronic otitis media. *Eur Arch Otorhinolaryngol*. 2014;271(11):2877–83.
- Nguyen CT, Robinson SR, Jung W, Novak MA, Boppart SA, Allen JB. Investigation of bacterial biofilm in the human middle ear using optical coherence tomography and acoustic measurements. *Hear Res*. 2013;301:193–200.
- Semenov FV, Fidarova KM. The treatment of the patients presenting with chronic inflammation of the trepanation cavity with a preparation containing silver nanoparticles following sanitation surgery of the open type. *Vestn Otorinolaringol*. 2012;6:117–9.
- Seifert H, Roher U, Staszky C, Angrisani N, Dziuba D, Meyer-Lindenberg A. Optimising μ CT imaging of the middle and inner ear. *Anat Histol Embryol*. 2012;41(2):113–21.
- Haghpahani M, Gladstone MB, Zhu X, Frisina RD, Borkholder DA. Noninvasive technique for monitoring drug transport through the murine cochlea using micro-computed tomography. *Ann Biomed Eng*. 2013;41(10):2130–42.
- Karunamuni R, Tsourkas A, Maidment AD. Exploring silver as a contrast agent for contrast-enhanced dual-energy X-ray breast imaging. *British J Radiol*. 2014;87(1041):20140081.
- Zou J, Feng H, Mannerström M, Heinonen T, Pyykkö I. Toxicity of silver nanoparticle in rat ear and BALB/c 3T3 cell line. *J Nanobiotechnol*. 2014;12(1):52 [Epub ahead of print].
- Zou J, Poe D, Ramadan UA, Pyykkö I. Oval window transport of Gd-DOTA from rat middle ear to vestibulum and scala vestibuli visualized by in vivo magnetic resonance imaging. *Ann Otol Rhinol Laryngol*. 2012;121(2):119–28.
- Shi H, Li Y, Yin S, Zou J. The predominant vestibular uptake of gadolinium through the oval window pathway is compromised by endolymphatic hydrops in Meniere's disease. *Otol Neurotol*. 2014;35(2):315–22.
- Markowska K, Grudniak AM, Wolska KI. Silver nanoparticles as an alternative strategy against bacterial biofilms. *Acta Biochim Pol*. 2013;60(4):523–30.

27. Liu H, Wang H, Guo R, Cao X, Zhao J, Luo Y, et al. Size-controlled synthesis of dendrimer-stabilized silver nanoparticles for X-ray computed tomography imaging applications. *Polym Chem.* 2010;1(10):1677–83.
28. Takemura K, Komeda M, Yagi M, Himeno C, Izumikawa M, Doi T, et al. Direct inner ear infusion of dexamethasone attenuates noise-induced trauma in guinea pig. *Hear Res.* 2004;196(1-2):58–68.
29. Zou J, Ramadan UA, Pyykko I. Gadolinium uptake in the rat inner ear perilymph evaluated with 4.7 T MRI: a comparison between transtympanic injection and gelatin sponge-based diffusion through the round window membrane. *Otol Neurotol.* 2010;31(4):637–41.

**Submit your next manuscript to BioMed Central
and take full advantage of:**

- Convenient online submission
- Thorough peer review
- No space constraints or color figure charges
- Immediate publication on acceptance
- Inclusion in PubMed, CAS, Scopus and Google Scholar
- Research which is freely available for redistribution

Submit your manuscript at
www.biomedcentral.com/submit



NANO EXPRESS

Open Access



Involvement of Ubiquitin-Editing Protein A20 in Modulating Inflammation in Rat Cochlea Associated with Silver Nanoparticle-Induced CD68 Upregulation and TLR4 Activation

Hao Feng¹, Ilmari Pyykkö¹ and Jing Zou^{1,2*}

Abstract

Silver nanoparticles (AgNPs) were shown to temporarily impair the biological barriers in the skin of the external ear canal, mucosa of the middle ear, and inner ear, causing partially reversible hearing loss after delivery into the middle ear. The current study aimed to elucidate the molecular mechanism, emphasizing the TLR signaling pathways in association with the potential recruitment of macrophages in the cochlea and the modulation of inflammation by ubiquitin-editing protein A20. Molecules potentially involved in these signaling pathways were thoroughly analysed using immunohistochemistry in the rat cochlea exposed to AgNPs at various concentrations through intratympanic injection. The results showed that 0.4 % AgNPs but not 0.02 % AgNPs upregulated the expressions of CD68, TLR4, MCP1, A20, and RNF11 in the stria basilar cells, spiral ligament fibrocytes, and non-sensory supporting cells of Corti's organ. 0.4 % AgNPs had no effect on CD44, TLR2, MCP2, Rac1, myosin light chain, VCAM1, Erk1/2, JNK, p38, IL-1 β , TNF- α , TNFR1, TNFR2, IL-10, or TGF- β . This study suggested that AgNPs might confer macrophage-like functions on the stria basilar cells and spiral ligament fibrocytes and enhance the immune activities of non-sensory supporting cells of Corti's organ through the upregulation of CD68, which might be involved in TLR4 activation. A20 and RNF11 played roles in maintaining cochlear homeostasis via negative regulation of the expressions of inflammatory cytokines.

Background

With the rapid development of nanotechnology and increasing applications of engineered nanomaterials in our daily lives, their potential safety issues have become a serious concern in public health. The rat ear model has been applied to investigate the impact of silver nanoparticles (AgNPs) on the permeability of biological barriers in the skin, mucosa, and inner ear that is analogous to the nervous system (e.g. the brain and spinal cord) [1]. Previous research showed that AgNPs led to hyaluronan accumulation in the cochlea,

impaired biological barriers in the skin of the external ear canal, mucosa of the middle ear, and inner ear, and consequently caused hearing loss after delivery into the middle ear [1–3]. Hyaluronan acts as an endogenous pathogen-associated molecular pattern (PAMP) in response to hazardous signals through binding hyaluronan-binding proteins (hyaladherins) including toll-like receptors 2/4 (TLR2/4), CD44, receptor for hyaluronan-mediated motility, and tumour necrosis factor- α (TNF- α)-stimulated glycoprotein-6 [4–7]. Among them, TLR2/4 is a category of mammalian homologues of *Drosophila* Toll proteins that are of great importance for innate host defence. They belong to the pattern recognition receptors (PRRs) that specifically recognize and respond to an expansive variety of PAMPs [8]. Moreover, TLR4 is responsible for sensing danger/damage-associated molecular patterns

* Correspondence: Jing.Zou@staff.uta.fi

¹Hearing and Balance Research Unit, Field of Oto-laryngology, School of Medicine, University of Tampere, Medisiininkatu 3, 33520 Tampere, Finland

²Department of Otolaryngology-Head and Neck Surgery, Center for Otolaryngology-Head and Neck Surgery of Chinese PLA, Changhai Hospital, Second Military Medical University, Shanghai, China

(DAMPs) and conferring immunostimulatory activity [9]. The activation of TLRs initiates the upregulation of transcription factors (e.g. nuclear factor- κ B (NF- κ B) and activator protein-1) that play pivotal roles in producing inflammatory molecules (e.g. interleukin-1 β (IL-1 β), interleukin-6 (IL-6), and TNF- α together with its receptors TNFRs), chemokines (e.g. monocyte chemoattractant proteins (MCPs)), and reactive oxygen/nitrogen species, leading to inflammatory diseases [10–12].

Several proteins that are implicated in mediating TLR signaling attenuation have been identified such as the ubiquitin-editing protein A20 [13–15]. A20 acts as a negative effector in regulating TLR-mediated inflammatory response, and its overexpression inhibits TLR2- and TLR4-mediated IL-8 syntheses in airway epithelial cells [16]. A20 loss elevates the levels of NF- κ B-regulated inflammatory cytokines and causes spontaneous cerebral inflammation [17]. RING finger protein 11 (RNF11), a critical component of A20, is indicated as one of the key negative regulators in controlling the NF- κ B signaling pathway. RNF11 was shown to protect microglia irritated by lipopolysaccharide through manipulating the NF- κ B signaling pathway [18]. RNF11 knockdown in the monocytes led to persistent TNF- and lipopolysaccharide-mediated NF- κ B signaling activation and upregulated NF- κ B-associated inflammatory gene transcripts [18, 19].

As another important hyaladherin, CD44 is capable of recruiting monocytes from the peripheral blood upon hyaluronan binding [20]. Further study has revealed that weakened interaction between CD44 and hyaluronan decreases the production of MCPs and consequently undermines the recruitment of mononuclear cells [21]. MCPs are a family of small heparin-binding, positively charged chemokines that play an indispensable role in controlling cell behaviour in response to exogenous stimulation. They are crucial in triggering the mobilization and migration of immunocompetent cells such as monocytes, neutrophils, lymphocytes, and dendritic cells along the bone marrow sinusoids that frequently anastomose with capillaries and in directing them into the inflamed tissues [22]. In the inner ear, spiral ligament fibrocytes act as the primary immune sensors in response to lipopolysaccharide, involving TLR2-dependent NF- κ B signaling activation and MCP1 upregulation and resulting in monocyte migration and consequential infiltration [23, 24].

Adhesion molecules play a critical role in mediating leukocyte immobilization as a result of anchoring [25]. Among them, vascular cell adhesion molecule 1 (VCAM1) enables rolling monocytes along the microvascular wall at a far slower velocity to adhere to the endothelial cells [26]. Rac1, a member of Rho-like small GTPase, mediated by the phosphorylation of myosin light chain protein, facilitates actin cytoskeletal remodelling and modulates tight junctional proteins (e.g. occludin and claudin).

The breakdown of tight junction in the microvascular wall enables the leukocytes to infiltrate into the targeting site [27–29]. The extracellular signal-regulated kinases 1/2 (Erk1/2), c-Jun N-terminal kinases 1/2/3 (JNK1/2/3) (also known as stress-activated protein kinases), and p38 isoforms (α , β , γ , and δ) that belong to the MAPKs family are considered to be the elementary components of cellular signaling transduction underlying leukocyte locomotion and endothelial cell activities [30, 31].

Migrated monocytes can differentiate into macrophages. Plasticity and flexibility are the key features of macrophages and reflect their activation states [32]. Activated macrophages have distinctive functional phenotypes that are similar to the Th1/Th2 polarization paradigm of T lymphocytes and can be defined as M1 and M2. M1 induced by Th1 signature cytokines (e.g. interferon- γ (IFN- γ) and TNF- α), which are associated with the TLR-dependent signaling pathway, has the ability of upregulating genes involved in cell-biased immunity, enhancing antigen presentation, and producing a distinctive array of inflammatory cytokines (e.g. IL-1 β , IL-6, and TNF- α). M2 induced by Th2 signature cytokines (e.g. IL-4 and IL-13) plays an important role in immune suppression, anti-inflammation (e.g. interleukin-10 (IL-10)), tissue regeneration, and wound healing (e.g. transforming growth factor- β (TGF- β) and vascular endothelial growth factor (VEGF)) [33, 34].

The current study aimed to elucidate the exact mechanism of AgNP-induced biological barrier functional changes in the inner ear. We exposed the rat inner ear to AgNPs and hypothesized that TLR signaling pathways were involved in AgNP-induced hearing loss in association with the potential recruitment of macrophages in the rat cochlea. A20 might play a role in regulating the downstream signaling of TLR pathways. Molecules potentially involved in these signaling pathways were thoroughly analysed using immunohistochemistry in the rat cochlea after AgNP exposure.

Methods

Animal and AgNPs

Ten albino male Sprague-Dawley rats weighing between 250 and 300 g were kept at an ambient temperature of 20–22 °C with a relative humidity of 50 \pm 5 % under a 12/12-h light/dark cycle in the experimental animal unit, University of Tampere. The experiments were performed under general anaesthesia with a mixture of 0.5 mg/kg medetomidine hydrochloride (Domitor[®], Orion, Espoo, Finland) and 75 mg/kg ketamine hydrochloride (Ketalar[®], Pfizer, Helsinki, Finland) administered via intraperitoneal injection, followed by intramuscular injection of enrofloxacin (Baytril[®]vet, Orion, Turku, Finland) at a dose of 10 mg/kg to prevent potential infection. The animals' eyes were protected by carbomer (Viscotears[®], Novartis Healthcare A/S, Denmark). All procedures in the study

complied with the local ethics committee standards (permission number: ESAVI/3033/04.10.03/2011) and were conducted in accordance with European Legislation. The AgNPs (Colorobbia, Firenze, Italy) used in this study were highly faceted with a mean size of 21 ± 8 nm using transmission electron microscope. The mean hydrodynamic size of the particles was 117 ± 24 nm when suspended in deionized water (dH_2O) using dynamic light scattering, and the zeta potential was measured to be -20 ± 9 mV [2]. More results for the characterization could be referred to our previous study [2].

AgNP Administration

After anaesthetization, 40 μl of either 0.4 ($n = 5$) or 0.02 % ($n = 5$) AgNPs were injected into the middle ear cavity under an operating microscope (OPMI1-F, Carl Zeiss, Jena, Germany) according to a previously reported procedure [1–3]. The tested concentrations were selected according to the auditory brainstem response results showing that 0.4 % AgNPs caused reversible hearing loss that partially recovered at the seventh day, while 0.02 % AgNPs only induced hearing loss at 32 kHz that returned to the baseline at the seventh day. Moreover, micro-CT scanning displayed that 0.4 % AgNPs caused an obvious middle ear infiltration that was absent in the rats exposed to 0.02 % AgNPs [1–3]. The contralateral ear ($n = 10$) received dH_2O under the same circumstances and was used as a negative control.

Sample Preparation

On the seventh day post-injection, the anaesthetized rats were perfused with 0.01 M pH 7.4 phosphate-buffered saline (PBS) containing 0.6 % (v/v) heparin (LEO Pharma A/S, Ballerup, Denmark) via a cardiac approach followed by 4 % paraformaldehyde (Merck, Espoo, Finland) to fix the head. The bullae were isolated after decapitation and decalcified using 10 % EDTA (Sigma-Aldrich, Steinheim, Germany) in the following 4 weeks with weekly solution changes. A standard procedure for paraffin embedding and tissue block was conducted in accordance with the protocol in a previous study [3].

Immunofluorescence Staining

The procedure for immunofluorescence staining was in accordance with the protocol in a previous study [3]. The primary antibodies used in the assay were hosted in rabbit and were anti-CD68 (1:200, Abcam, UK), anti-CD44 (1:400, Abcam, UK), anti-TLR2 (1:250, Novus Biologicals, UK), anti-TLR4 (1:200, Novus Biologicals, UK), anti-MCP1 (1:4000, Novus Biologicals, UK), anti-MCP2 (1:200, GeneTex, USA), anti-Rac1 (1:800, Abcam, UK), anti-myosin light chain (1:100, Cell Signaling Technology, USA), anti-VCAM1 (1:50, Proteintech, USA), anti-Erk1/2 (1:400, Abcam, UK), anti-JNK (1:100, Cell

Signaling Technology, USA), anti-p38 (1:100, Cell Signaling Technology, USA), anti-TNF- α (1:800, Abcam, UK), anti-TNFR1 (1:500, Abcam, UK), anti-TNFR2 (1:50, Abcam, UK), anti-IL-1 β (1:400, Novus Biologicals, UK), anti-IL-10 (1:400, Abbotec, USA), anti-TGF- β (1:500, Abcam, UK), anti-A20 (1:200, Sigma-Aldrich, USA), and anti-RNF11 (1:100, Abcam, UK). Briefly, the slices were incubated with the primary antibodies listed above at 4 °C overnight followed by Alexa Fluor® 488 Goat Anti-Rabbit IgG (1:200, diluted with 0.1 % BSA, Life Technologies™, New York, USA) as a secondary antibody at room temperature for 1 h in a dark environment. The nuclei were counterstained with 10 $\mu\text{g}/\text{ml}$ DAPI (Life Technologies™, New York, USA) at room temperature for 10 min, and the slides were mounted for confocal microscopy with anti-quenching fluoromount (Sigma-Aldrich, St. Louis, USA). In the negative control slices, the primary antibodies were replaced with 0.1 % BSA (dissolved in 0.01 M PBS pH 7.4; Sigma-Aldrich, St. Louis, USA).

Immunostaining Visualized by 3,3'-Diaminobenzidine

After deparaffinization and hydration, the slices were immersed in 3 % H_2O_2 -methanol at room temperature for 30 min. After rinsing with PBS for 2×2 min, the slices were digested with 0.1 % trypsin (dissolved in 0.01 M PBS pH 7.4; Sigma-Aldrich, St. Louis, USA) at 37 °C for 30 min. After rinsing with 0.1 % PBS-Tween® 20 (diluted in 0.01 M PBS pH 7.4; Sigma-Aldrich, St. Louis, USA) for 3×2 min, the slices were incubated with 10 % normal goat serum (Invitrogen, Paisley, UK) at room temperature for 30 min followed by the primary antibodies listed above at 4 °C overnight. After rinsing with 0.1 % PBS-Tween® 20 for 3×2 min, the slices were incubated with biotinylated goat anti-rabbit IgG at a dilution of 1:100 (Vector Laboratories Ltd., Peterborough, UK) at room temperature for 1 h. After rinsing with 0.1 % PBS-Tween® 20 for 3×2 min, the slices were incubated with the streptavidin-biotin-peroxidase complex (Vector Laboratories Ltd., Peterborough, UK) at 37 °C for 1 h. After rinsing with 0.1 % PBS-Tween® 20 for 3×5 min, antibody binding was visualized by 3,3'-diaminobenzidine using the DAB Peroxidase Substrate Kit (Vector Laboratories Ltd., Peterborough, UK) at room temperature for 5 min. Alternatively, the nuclei were counterstained using Harris's solution (Merck, Darmstadt, Germany). Dehydration and vitrification were completed by a standard protocol (70 % alcohol 10 s, 94 % alcohol 2×10 s, absolute alcohol 2×1 min, and xylene 3×3 min). The slides were mounted for light microscopy with Clarion™ Mounting Medium (Sigma-Aldrich, St. Louis, USA). Slices for negative controls were prepared after the replacement of primary antibodies with 0.1 % BSA (dissolved in 0.01 M PBS pH 7.4; Sigma-Aldrich, St. Louis, USA). The staining intensities (shown by the greyscale

value that was inversely correlated with the staining intensity) in the strial basal cells, spiral ligament fibrocytes, and spiral ganglion cells were measured and semi-quantified using ImageJ 1.45S software (NIH, Bethesda, USA).

Confocal and Light Microscopies

The samples from immunofluorescence staining were observed and images obtained under a Nikon microscope (ECLIPSE Ti) combined with an Andor confocal system installed with Andor iQ 2.8 software (Andor Technology, Belfast, UK). The excitation lasers were 405 (blue excitation) and 488 nm (green excitation) from an Andor Laser Combiner system, and the corresponding emission filters were 450–465 (DAPI) and 525/50 nm (FITC), respectively. The immunostained samples visualized by 3,3'-diaminobenzidine were observed under a light microscope (LEICA DM 2000, Espoo, Finland), and images were digitally photographed using a camera video (Olympus DP 25, Tokyo, Japan) with the cellSens Dimension 1.6 Olympus software (Olympus Corporation, Tokyo, Japan) installed.

Analysis and Statistics

Statistical analyses were performed using the IBM® SPSS® Statistics Version 20 software package (SPSS Inc., Chicago, USA). One-way ANOVA was used to compare the staining intensities for CD68, TLR2, TLR4, MCP1, MCP2, A20, and RNF11 in the designated structures of different cochlear turns among the cochleae exposed to 0.4 % AgNPs, 0.02 % AgNPs, and dH₂O. The LSD post hoc test was used to evaluate the pairwise difference. The independent sample *t* test was used to compare the staining intensities for CD44, Rac1, Erk1/2, IL-1 β , IL-10, and TGF- β in the designated structures of different cochlear turns between the cochleae exposed to 0.4 % AgNPs and dH₂O. A value of $p < 0.05$ indicated that the difference was statistically significant.

Results

AgNPs Augment the Sensitivity and Chemotactic Proteins of Cochlear Cells

In the cochleae exposed to dH₂O, the inner hair cells and pillar cells of Corti's organ showed moderate staining for CD68, while the outer hair cells and Deiters' cells demonstrated extremely weak staining for CD68 (Fig. 1h). The strial basal cells, spiral ligament fibrocytes, and spiral ganglion cells exhibited mild staining for CD68 (Fig. 1d, f). In the cochlear lateral wall, 0.4 % AgNPs intensified CD68 staining remarkably in the strial basal cells ($p < 0.01$, post hoc test) and spiral ligament fibrocytes (mainly type III) ($p < 0.01$, post hoc test) in the first turn (Fig. 1a). However, no enhanced staining was observed in cells in the second and third turns (Fig. 1b, c) ($p > 0.05$, post hoc test).

In the CD68⁺ cell population, sparse ramified cells and mononuclear cells were identified in the spiral ligament and the modiolus, respectively (Fig. 1c, i). In Corti's organ, 0.4 % AgNPs increased CD68 staining in the inner hair cells and pillar cells but not in the outer hair cells and Deiters' cells (Fig. 1g). In the spiral ganglion cells and capillary endothelial cells, 0.4 % AgNPs did not alter CD68 staining in all turns (Fig. 1e) ($p > 0.05$, post hoc test). The 0.02 % AgNPs had no influence on CD68 staining in the aforementioned cells in all turns (images not shown) ($p > 0.05$, post hoc test).

In the cochleae exposed to dH₂O, the strial intermediate cells, strial basal cells, spiral ligament fibrocytes, spiral ganglion cells, and outer hair cells, pillar cells, and Deiters' cells of Corti's organ showed intensive staining for CD44 (Additional file 1: Figure S1B, S1D, and S1F), while the inner hair cells demonstrated mild staining for CD44 (Additional file 1: Figure S1F). 0.4 % AgNPs had no influence on the staining in the aforementioned cells in all turns (Additional file 1: Figure S1A, S1C, and S1E) ($p > 0.05$, independent sample *t* test).

In the cochleae exposed to dH₂O, the strial basal cells, spiral ligament fibrocytes (mainly type II), spiral ganglion cells, and inner hair cells and pillar cells of Corti's organ showed intensive staining for TLR2 (Additional file 2: Figure S2B, S2D, and S2F), while the outer hair cells and Deiters' cells displayed extremely weak staining for TLR2 (Additional file 2: Figure S2F). The strial basal cells and spiral ligament fibrocytes demonstrated mild staining for TLR4 (Fig. 2d), while the spiral ganglion cells and hair cells, pillar cells, and Deiters' cells of Corti's organ exhibited extremely weak staining for TLR4 (Fig. 2f, h). In the cochleae exposed to 0.4 % AgNPs, the outer hair cells and Deiters' cells of Corti's organ showed more intensive staining for TLR2 (Additional file 2: Figure S2E). However, the strial basal cells, spiral ligament fibrocytes, and spiral ganglion cells did not show any changes in the staining of TLR2 in all turns (Additional file 2: Figure S2A and S2C) ($p > 0.05$, one-way ANOVA) nor in the inner hair cells and pillar cells (Additional file 2: Figure S2E). The strial basal cells ($p < 0.05$ in the first and second turns and $p < 0.01$ in the third turn, one-way ANOVA) and spiral ligament fibrocytes (Fig. 2a–c) ($p < 0.05$ in the first, second, and third turns, one-way ANOVA) demonstrated more intensive staining for TLR4 that was independent of the cochlear turn ($p > 0.05$, one-way ANOVA). The inner hair cells, pillar cells, and Deiters' cells displayed more intensive staining for TLR4, but the outer hair cells did not (Fig. 2g). However, the spiral ganglion cells did not show any changes (Fig. 2e). The 0.02 % AgNPs had no influence on the staining of TLR2 and TLR4 in the aforementioned cells in all turns (images not shown) ($p > 0.05$, one-way ANOVA).

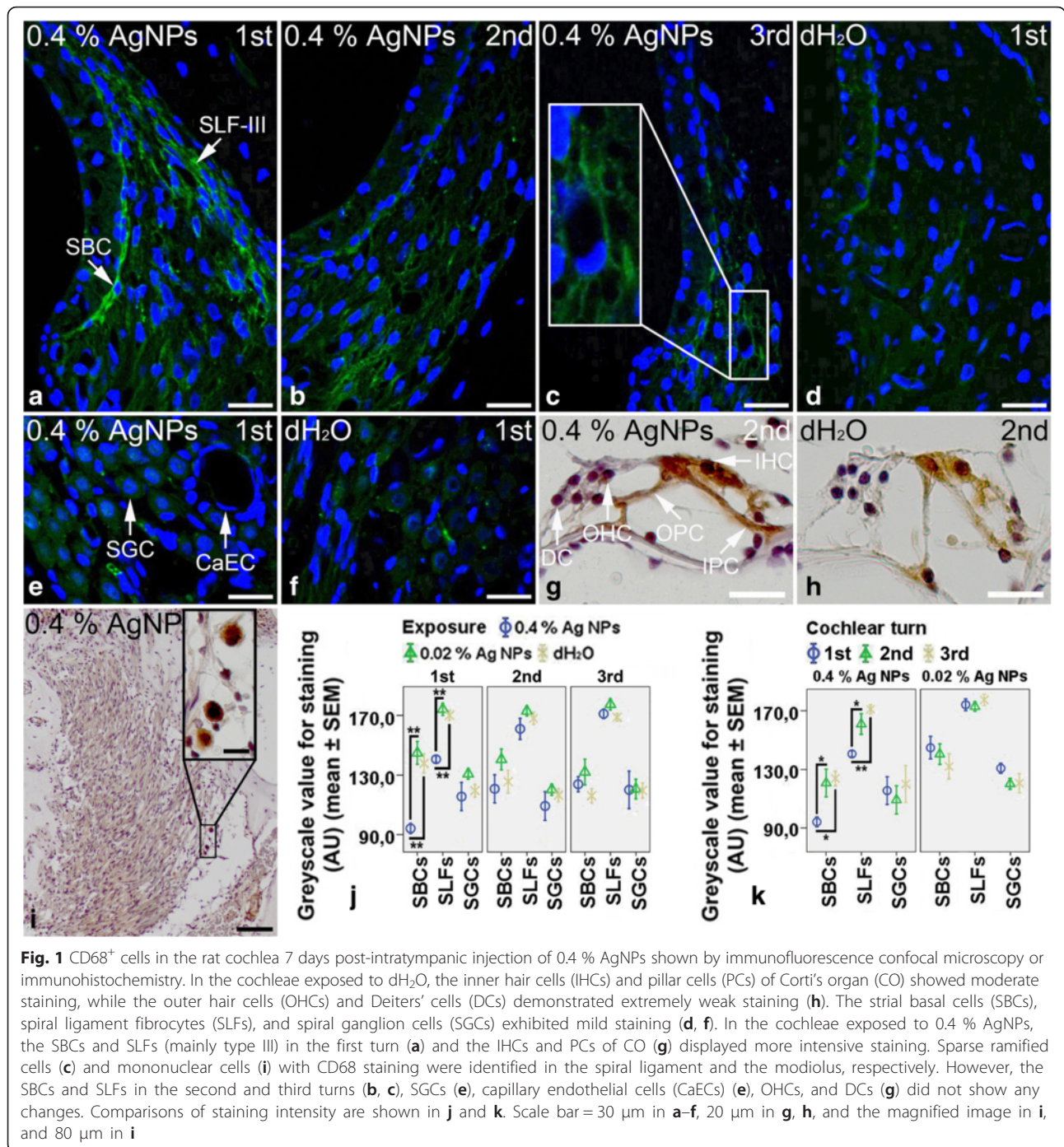


Fig. 1 CD68⁺ cells in the rat cochlea 7 days post-intratympanic injection of 0.4 % AgNPs shown by immunofluorescence confocal microscopy or immunohistochemistry. In the cochleae exposed to dH₂O, the inner hair cells (IHCs) and pillar cells (PCs) of Corti's organ (CO) showed moderate staining, while the outer hair cells (OHCs) and Deiters' cells (DCs) demonstrated extremely weak staining (h). The strial basal cells (SBCs), spiral ligament fibrocytes (SLFs), and spiral ganglion cells (SGCs) exhibited mild staining (d, f). In the cochleae exposed to 0.4 % AgNPs, the SBCs and SLFs (mainly type III) in the first turn (a) and the IHCs and PCs of CO (g) displayed more intensive staining. Sparse ramified cells (c) and mononuclear cells (i) with CD68 staining were identified in the spiral ligament and the modiolus, respectively. However, the SBCs and SLFs in the second and third turns (b, c), SGCs (e), capillary endothelial cells (CaECs) (e), OHCs, and DCs (g) did not show any changes. Comparisons of staining intensity are shown in j and k. Scale bar = 30 μm in a–f, 20 μm in g, h, and the magnified image in i, and 80 μm in i

In the cochleae exposed to dH₂O, the Deiters' cells of Corti's organ showed intensive staining for MCP1, while the inner hair cells and inner pillar cells exhibited moderate staining for MCP1 (Fig. 3h). The strial intermediate cells, strial basal cells, spiral ganglion cells, outer hair cells, and outer pillar cells demonstrated mild staining for MCP1 (Fig. 3d, f, h), while the spiral ligament fibrocytes displayed extremely weak

staining for MCP1 (Fig. 3d). Unexpectedly, the strial basal cells, spiral ligament fibrocytes, spiral ganglion cells, and the hair cells, pillar cells, and Deiters' cells of Corti's organ showed intensive staining for MCP2 (Additional file 3: Figure S3B, S3D, and S3F). In the cochleae exposed to 0.4 % (Fig. 3a) and 0.02 % AgNPs (image not shown), the strial intermediate cells, capillary endothelial cells, and strial basal cells ($p < 0.01$, one-way ANOVA) in the first

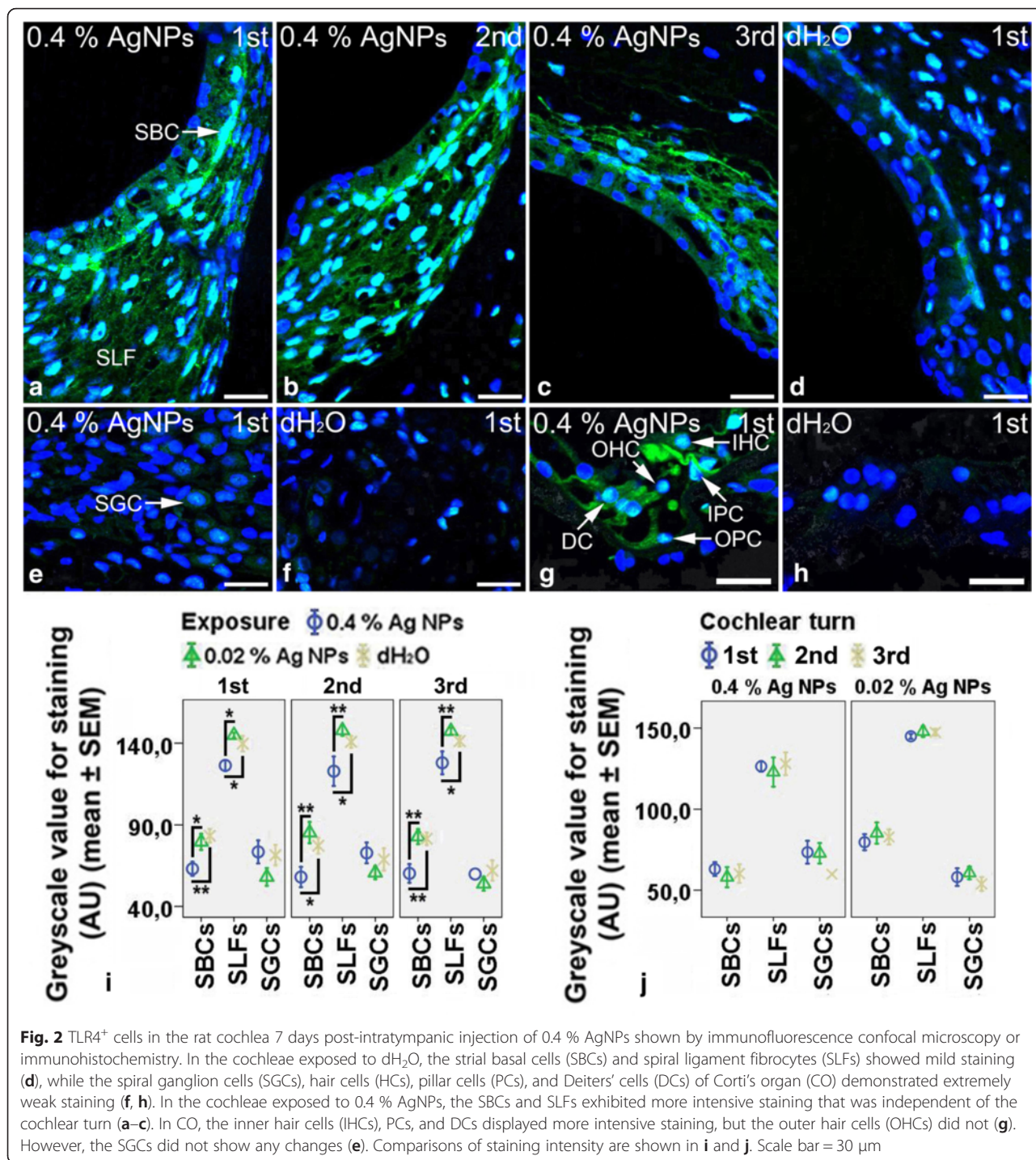


Fig. 2 TLR4⁺ cells in the rat cochlea 7 days post-intratympanic injection of 0.4 % AgNPs shown by immunofluorescence confocal microscopy or immunohistochemistry. In the cochleae exposed to dH₂O, the stria basal cells (SBCs) and spiral ligament fibrocytes (SLFs) showed mild staining (d), while the spiral ganglion cells (SGCs), hair cells (HCs), pillar cells (PCs), and Deiters' cells (DCs) of Corti's organ (CO) demonstrated extremely weak staining (f, h). In the cochleae exposed to 0.4 % AgNPs, the SBCs and SLFs exhibited more intensive staining that was independent of the cochlear turn (a–c). In CO, the inner hair cells (IHCs), PCs, and DCs displayed more intensive staining, but the outer hair cells (OHCs) did not (g). However, the SGCs did not show any changes (e). Comparisons of staining intensity are shown in i and j. Scale bar = 30 μm

turn demonstrated more intensive staining for MCP1. However, the spiral ligament fibrocytes (mainly type III) in the cochleae exposed to 0.4 % AgNPs (Fig. 3a–c) ($p < 0.01$ in the first and third turns and $p < 0.05$ in the second turn, one-way ANOVA) showed more intensive staining for MCP1 that was independent of the cochlear turn ($p > 0.05$, one-way ANOVA). In addition, 0.4 % AgNPs

increased MCP1 staining in the inner pillar cells and Deiters' cells of Corti's organ (Fig. 3g). However, the spiral ganglion cells did not show any changes (Fig. 3e) ($p > 0.05$, one-way ANOVA). Neither 0.4 % nor 0.02 % AgNPs affected the staining of MCP2 in the aforementioned cells in all turns (images not shown) ($p > 0.05$, one-way ANOVA).

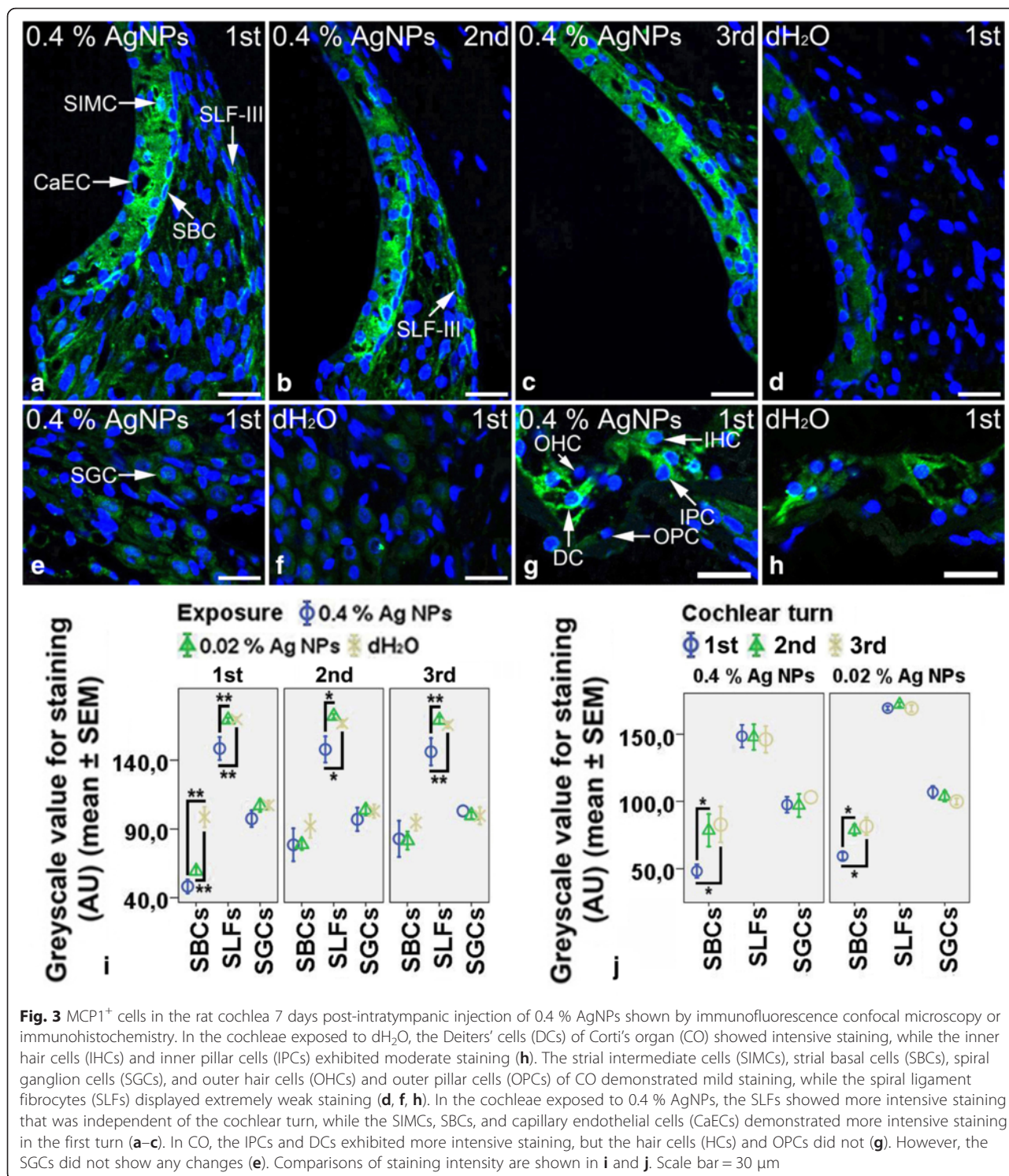


Fig. 3 MCP1⁺ cells in the rat cochlea 7 days post-intratympanic injection of 0.4 % AgNPs shown by immunofluorescence confocal microscopy or immunohistochemistry. In the cochleae exposed to dH₂O, the Deiters' cells (DCs) of Corti's organ (CO) showed intensive staining, while the inner hair cells (IHCs) and inner pillar cells (IPCs) exhibited moderate staining (**h**). The strial intermediate cells (SIMCs), strial basal cells (SBCs), spiral ganglion cells (SGCs), and outer hair cells (OHCs) and outer pillar cells (OPCs) of CO demonstrated mild staining, while the spiral ligament fibrocytes (SLFs) displayed extremely weak staining (**d, f, h**). In the cochleae exposed to 0.4 % AgNPs, the SLFs showed more intensive staining that was independent of the cochlear turn, while the SIMCs, SBCs, and capillary endothelial cells (CaECs) demonstrated more intensive staining in the first turn (**a–c**). In CO, the IPCs and DCs exhibited more intensive staining, but the hair cells (HCs) and OPCs did not (**g**). However, the SGCs did not show any changes (**e**). Comparisons of staining intensity are shown in **i** and **j**. Scale bar = 30 μm

AgNPs had no Effect on the Expressions of Tight Junction-Associated Proteins Including Rac1, Myosin Light Chain, VCAM1, and MAPK Signaling Proteins
 In the cochleae exposed to dH₂O, the strial intermediate cells, strial basal cells, spiral ganglion cells, and hair cells, pillar cells, and Deiters' cells of Corti's organ

showed intensive staining for Rac1 (Additional file 4: Figure S4B, S4D, and S4F), while the spiral ligament fibrocytes (mainly type II) demonstrated moderate staining for Rac1 (Additional file 4: Figure S4B). The spiral ganglion cells and inner pillar cells of Corti's organ exhibited moderate staining for myosin light chain (Additional

file 5: Figure S5D and S5F), while the hair cells, outer pillar cells, and Deiters' cells displayed mild staining for myosin light chain (Additional file 5: Figure S5F). The strial basal cells and spiral ligament fibrocytes showed extremely weak staining for myosin light chain (Additional file 5: Figure S5B). The strial basal cells, spiral ligament fibrocytes, spiral ganglion cells, and hair cells, pillar cells, and Deiters' cells of Corti's organ showed extremely weak staining for VCAM1 (Additional file 6: Figure S6B, S6D, and S6F), JNK (Additional file 7: Figure S8B, S8E, and S8J), and p38 (Additional file 7: Figure S8D, S8H, and S8L). However, the strial intermediate cells, strial basal cells, spiral ligament fibrocytes, spiral ganglion cells, and hair cells, pillar cells, and Deiters' cells of Corti's organ showed intensive staining for Erk1/2 (Additional file 8: Figure S7B, S7D, and S7F). 0.4 % AgNPs had no influence on the staining of Rac1 (Additional file 4: Figure S4A, S4C, and S4E) ($p > 0.05$, independent sample t test), myosin light chain (Additional file 5: Figure S5A, S5C, and S5E), VCAM1 (Additional file 6: Figure S6A, S6C, and S6E), Erk1/2 (Additional file 8: Figure S7A, S7C, and S7E) ($p > 0.05$, independent sample t test), JNK (Additional file 7: Figure S8A, S8E, and S8I), and p38 (Additional file 7: Figure S8C, S8G, and S8K) in the aforementioned cells in all turns.

AgNPs Upregulated the Expressions of Ubiquitin-Editing Proteins A20 and RNF11 Without Affecting the Expressions of Inflammatory Cytokines

In the cochleae exposed to dH₂O, the spiral ganglion cells, inner hair cells, and inner pillar cells of Corti's organ showed mild staining for TNF- α (Additional file 9: Figure S9H and S9N), while the strial basal cells, spiral ligament fibrocytes, outer pillar cells, outer hair cells, and Deiters' cells demonstrated extremely weak staining for TNF- α (Additional file 9: Figure S9B and S9N). The strial intermediate cells, strial basal cells, and spiral ganglion cells exhibited mild staining for TNFR1 (Additional file 9: Figure S9D and S9J), while the spiral ligament fibrocytes, hair cells, pillar cells, and Deiters' cells displayed extremely weak staining for TNFR1 (Additional file 9: Figure S9D and S9P). The strial intermediate cells and strial basal cells showed mild staining for TNFR2 (Additional file 9: Figure S9F), while the spiral ligament fibrocytes, spiral ganglion cells, hair cells, pillar cells, and Deiters' cells demonstrated extremely weak staining for TNFR2 (Additional file 9: Figure S9F, S9L, and S9R). The strial basal cells, spiral ganglion cells, and pillar cells of Corti's organ exhibited intensive staining for IL-1 β , while the spiral ligament fibrocytes (mainly type II) and inner hair cells displayed mild staining for IL-1 β (Additional file 10: Figure S10B, S10D, and S10F). The outer hair cells and Deiters' cells showed extremely weak staining for IL-1 β (Additional file 10:

Figure S10F). 0.4 % AgNPs had no influence on the staining of TNF- α (Additional file 9: Figure S9A, S9G, and S9M), TNFR1 (Additional file 9: Figure S9C, S9I, and S9O), TNFR2 (Additional file 9: Figure S9E, S9K, and S9Q), and IL-1 β (Additional file 10: Figure S10A, S10C, and S10E) ($p > 0.05$, independent sample t test) in the aforementioned cells in all turns.

In the cochleae exposed to dH₂O, the spiral ganglion cells showed intensive staining for IL-10 (Additional file 11: Figure S11F), while the pillar cells of Corti's organ demonstrated mild staining for IL-10 (Additional file 11: Figure S11J). The strial basal cells, spiral ligament fibrocytes, hair cells, and Deiters' cells exhibited extremely weak staining for IL-10 (Additional file 11: Figure S11B and S11I). The spiral ganglion cells and pillar cells of Corti's organ displayed intensive staining for TGF- β (Additional file 11: Figure S11H and S11L), while the strial basal cells, spiral ligament fibrocytes, and inner hair cells demonstrated mild staining for TGF- β (Additional file 11: Figure S11D and S11L). The outer hair cells and Deiters' cells showed extremely weak staining for TGF- β (Additional file 11: Figure S11L). 0.4 % AgNPs had no influence on the staining of IL-10 (Additional file 11: Figure S11A, S11E, and S11I) ($p > 0.05$, independent sample t test) and TGF- β (Additional file 11: Figure S11C, S11G, and S11K) ($p > 0.05$, independent sample t test) in the aforementioned cells in all turns.

In the cochleae exposed to dH₂O, the spiral ganglion cells, inner hair cells, pillar cells, and Deiters' cells of Corti's organ showed intensive staining for A20 (Fig. 4j, n), while the strial basal cells, spiral ligament fibrocytes, and outer hair cells demonstrated mild staining for A20 (Fig. 4d, n). The strial basal cells, spiral ganglion cells, and inner pillar cells of Corti's organ exhibited intensive staining for RNF11, while the spiral ligament fibrocytes, hair cells, and outer pillar cells displayed mild staining for RNF11 (Fig. 4h, l, p). The Deiters' cells showed extremely weak staining for RNF11 (Fig. 4p). In the cochlear lateral wall, 0.4 % AgNPs enhanced the staining of A20 ($p < 0.05$ in the first and second turns and $p > 0.05$ in the third turn at the strial basal cells, $p < 0.05$ in the first and third turns and $p < 0.01$ in the second turn at the spiral ligament fibrocytes, one-way ANOVA) and RNF11 ($p > 0.05$ in the first and third turns and $p < 0.05$ in the second turn at the strial basal cells, $p < 0.01$ in the first turn and $p < 0.05$ in the second and third turns at the spiral ligament fibrocytes, one-way ANOVA) remarkably in the strial basal cells and spiral ligament fibrocytes that were independent of the cochlear turn (Fig. 4a–c, e–g) ($p > 0.05$, one-way ANOVA). In Corti's organ, 0.4 % AgNPs increased A20 staining in the outer hair cells and Deiters' cells (Fig. 4m) and RNF11 staining in the outer pillar cells and Deiters' cells (Fig. 4o). In the spiral ganglion cells and capillary endothelial cells, 0.4 % AgNPs did not alter the staining of

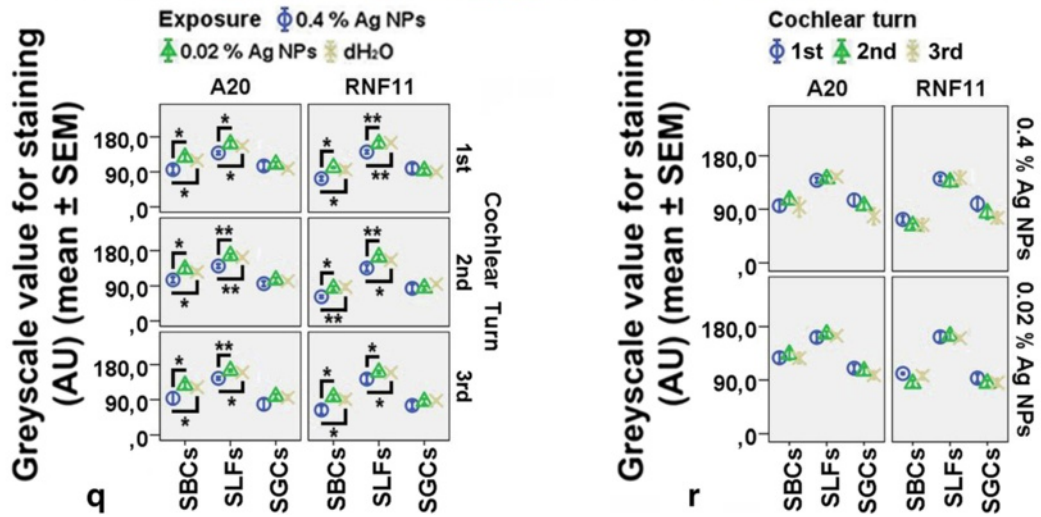
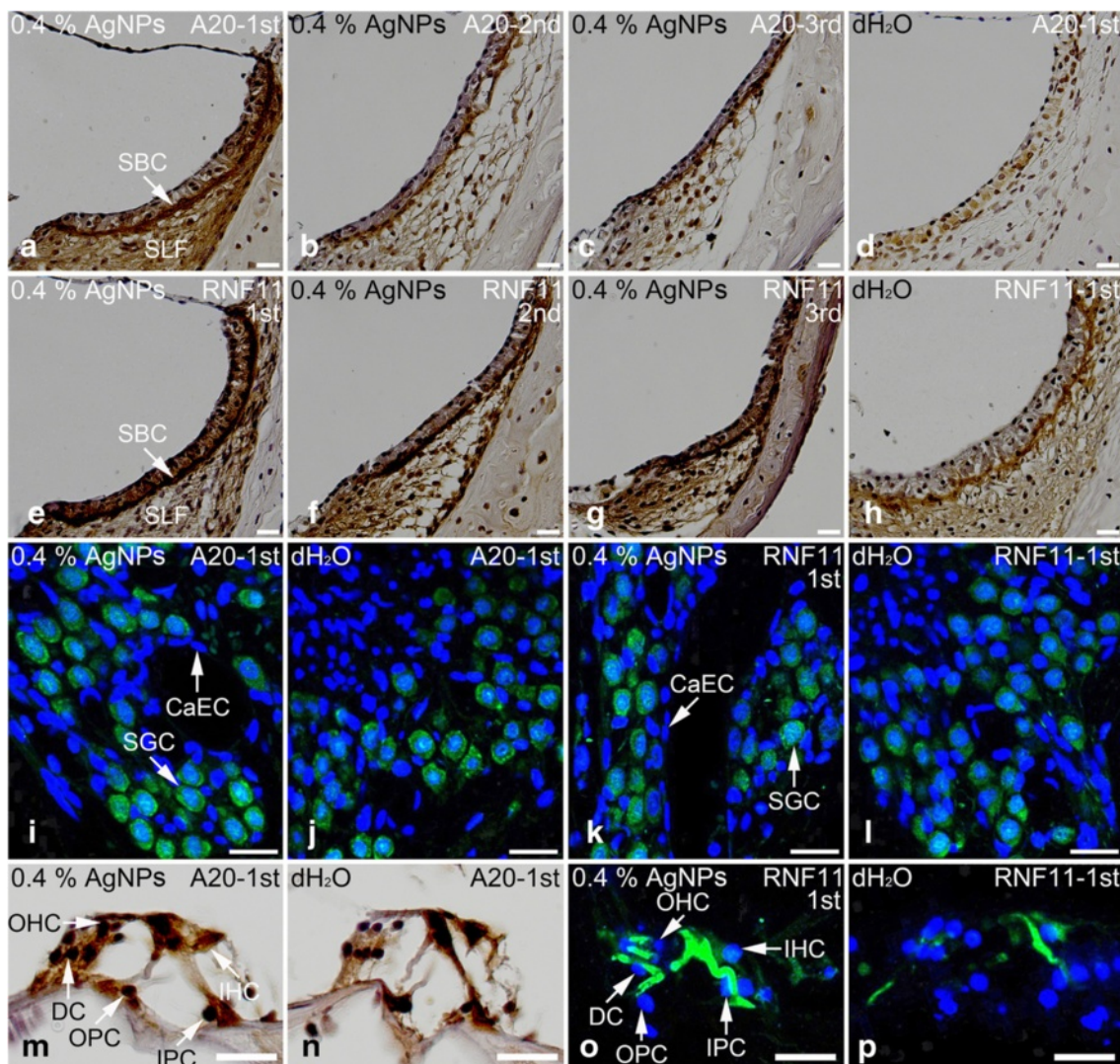


Fig. 4 (See legend on next page.)

(See figure on previous page.)

Fig. 4 A20⁺ and RNF11⁺ cells in the rat cochlea 7 days post-intratympanic injection of 0.4 % AgNPs shown by immunofluorescence confocal microscopy or immunohistochemistry. In the cochleae exposed to dH₂O, the spiral ganglion cells (SGCs), inner hair cells (IHCs), pillar cells (PCs), and Deiters' cells (DCs) of Corti's organ (CO) showed intensive staining for A20 (**j, n**), while the stria basal cells (SBCs), spiral ligament fibrocytes (SLFs), and outer hair cells (OHCs) demonstrated mild staining for A20 (**d, n**). The SBCs, SGCs, and inner pillar cells (IPCs) of CO exhibited intensive staining for RNF11, while the SLFs, hair cells (HCs), and outer pillar cells (OPCs) displayed mild staining for RNF11 (**h, l, p**). The DCs showed extremely weak staining for RNF11 (**p**). In the cochleae exposed to 0.4 % AgNPs, the SBCs and SLFs demonstrated more intensive staining for A20 and RNF11 that was independent of the cochlear turn (**a-c, e-g**). In CO, the OHCs and DCs displayed more intensive staining for A20 (**m**), the OPCs and DCs exhibited more intensive staining for RNF11 (**o**). However, the SGCs and capillary endothelial cells (CaECs) did not show any changes in the staining of A20 and RNF11 (**i, k**). Comparisons of staining intensity are shown in **q** and **r**. Scale bar = 50 μm in **a-h**, 20 μm in **m, n**, and 30 μm in **i-l, o, p**

A20 and RNF11 in all turns (Fig. 4i, k) ($p > 0.05$, post hoc test). 0.02 % AgNPs had no influence on the staining of A20 and RNF11 in the aforementioned cells in all turns (images not shown) ($p > 0.05$, post hoc test).

There were no positive staining in the negative control slides (Additional file 12: Figure S12). The unchanged molecules in the rat cochlea exposed to AgNPs were summarized in Table 1.

Discussion

The current study showed that 0.4 % AgNPs but not 0.02 % AgNPs upregulated the expressions of CD68, TLR4, MCP1, A20, and RNF11 in the stria basal cells, spiral ligament fibrocytes, and non-sensory supporting cells of Corti's organ. 0.4 % AgNPs had no effect on CD44, TLR2, MCP2, Rac1, myosin light chain, VCAM1, Erk1/2, JNK, p38, IL-1 β , TNF- α , TNFR1, TNFR2, IL-10, or TGF- β . The toxicological mechanism of AgNPs is unclear. The Ag⁺ released from AgNPs was thought to be an important mediator involved in the pathological process associated with AgNPs exposure [35]. However, this is actually doubtful because no Ag⁺ remains in either animal or human body after reacting with the Cl⁻ and forming AgCl. The IC₅₀ for AgNO₃ was lower than that for AgNPs [1]. Our unpublished data demonstrated that AgCl did not cause any hearing loss at the second day through the seventh day post-intratympanic injection at the saturated concentration (520 μg/100 g). Therefore, our hypothesis is that the cytokine alteration in the current study is resulted from intact AgNPs rather than the disassociated Ag⁺.

Increasing evidence demonstrate that the inner ear is an active immune organ rather than an 'immunologically

privileged organ' that was generally accepted previously [36]. Cochlear lateral wall including the stria vascularis and spiral ligament has been reported as the primary site harbouring macrophages in the inner ear of human and mouse [37, 38]. In the current study, cells that showed mild staining for CD68 without ramified morphology were identified in the stria vascularis and spiral ligament of rat cochlea exposed to dH₂O, suggesting that the rat cochlea did not have typical tissue-resident macrophages and might have a different immune mechanism from the one in human. Macrophages were reportedly recruited into murine cochlea exposed to noise and ototoxic drugs [39–42]. The current study detected a sparse appearance of ramified CD68-positive cells in the spiral ligament and mononuclear cells in the modiolus of cochlea exposed to 0.4 % AgNPs, implying that either the rat cochlea possessed a different innate immune system from the mouse or the AgNPs triggered different signaling pathways from noise and conventional ototoxic drugs. The sole upregulation of MCP1 without sufficient cooperation with other molecules such as CD44, Rac1, myosin light chain, and VCAM1 might be the reason for failure in recruiting abundant macrophages into the cochlea [43–45]. Moreover, the unchanged levels of Erk1/2, JNK, and p38 did not provide the molecular basis for the adhesion and migration of monocytes [46]. Instead, the expressions of CD68 in the stria basal cells, spiral ligament fibrocytes, and non-sensory supporting cells of Corti's organ were significantly upregulated after 0.4 % AgNPs exposure.

The upregulated CD68 might confer macrophage-like functions on the stria basal cells and spiral ligament fibrocytes and enhance the immune activities of non-sensory supporting cells of Corti's organ. Non-sensory supporting cells of Corti's organ are indicated as microglia-like cells and may determine the fate of the auditory sensory epithelium because microglia are believed to be macrophages in the central nervous system and play an irreplaceable role in immune surveillance [47–49]. CD68 was reportedly involved in vesicular trafficking to deliver the lipids to their proper intracellular compartments [50]. The current study suggested that CD68 might be implicated in the activation of TLR4 via caveolae trafficking operated by lipid raft and caveolin-1 phosphorylation [51]. Previous

Table 1 Unchanged molecules in the rat cochlea exposed to AgNPs

| Functions/properties | Molecules |
|------------------------------------|---|
| Cell recruitment | CD44 |
| Innate immunity | TLR2 |
| Chemotaxis | MCP2 |
| Tight junction-associated proteins | VCAM1, Rac1, and MLC |
| Cellular signaling transduction | Erk1/2, JNK, and p38 |
| Inflammation | IL-1 β , TNF- α , TNFR1, TNFR2 |
| Anti-inflammation | IL-10 and TGF- β |

MLC myosin light chain

research indicated that AgNPs induced the accumulation of hyaluronan, the substrate of TLR4, in the cochlea [3]. TLR4 was also upregulated in the cochlea exposed to 0.4 % AgNPs in the current study. Theoretically, TLR4 activation triggers the NF- κ B signaling pathway and finally upregulates the expressions of inflammatory cytokines including IL-1 β , TNF- α , and its receptors TNFR1 and TNFR2. However, neither the downstream cytokines of macrophages nor TLR4 activation was upregulated in the cochlea exposed to AgNPs. Although it was unlikely that these pathways were never activated, it was predictable that certain cytokines were upregulated at an early stage but suppressed afterwards. This possibility was supported by previous studies showing that AgNPs caused reversible changes to the permeability of biological barriers in the rat inner ear and transient hearing loss that partially recovered as of the seventh day [1, 3].

A20, in the context of RNF11, has been shown to inhibit TLR-mediated inflammatory response, and it induced NF- κ B signaling pathway [16, 17]. The current study showed that A20 and RNF11 were significantly upregulated in the strial basal cells, spiral ligament fibrocytes, and non-sensory supporting cells of Corti's organ of the cochlea exposed to 0.4 % AgNPs, suggesting that A20 and RNF11 might play roles in maintaining cochlear homeostasis and thus preserving hearing [1, 3]. However, the incomplete hearing recovery in the high-frequency range in the AgNP-exposed ear suggested that the protective effects of A20 and RNF11 might be limited.

Conclusions

AgNPs might confer macrophage-like functions on the strial basal cells and spiral ligament fibrocytes and enhance the immune activities of non-sensory supporting cells of Corti's organ through the upregulation of CD68, which might be involved in TLR4 activation. A20 and RNF11 played roles in maintaining cochlear homeostasis via negative regulation of the expressions of inflammatory cytokines. The current study suggested that the rat cochlea might have a different immune mechanism from the one in human and mouse.

Additional files

Additional file 1: Figure S1. CD44⁺ cells in the rat cochlea 7 days post-intratympanic injection of 0.4 % AgNPs shown by immunofluorescence confocal microscopy or immunohistochemistry. In the cochleae exposed to dH₂O, the strial intermediate cells (SIMCs), strial basal cells (SBCs), spiral ligament fibrocytes (SLFs), spiral ganglion cells (SGCs), and outer hair cells (OHCs), pillar cells (PCs), and Deiters' cells (DCs) of Corti's organ (CO) showed intensive staining (B, D, and F), while the inner hair cells (IHCs) demonstrated mild staining (F). 0.4 % AgNPs had no influence on the staining in the SIMCs, SBCs, SLFs, SGCs, and CO (A, C, and E). Comparisons of staining intensity are shown in G and H. Scale bar = 50 μ m in A–D and 20 μ m in E and F. (JPG 4396 kb)

Additional file 2: Figure S2. TLR2⁺ cells in the rat cochlea 7 days post-intratympanic injection of 0.4 % AgNPs shown by immunofluorescence confocal microscopy or immunohistochemistry. In the cochleae exposed to dH₂O, the strial basal cells (SBCs), spiral ligament fibrocytes (SLFs) (mainly type II), spiral ganglion cells (SGCs), and inner hair cells (IHCs) and pillar cells (PCs) of Corti's organ (CO) showed intensive staining (B, D, and F), while the outer hair cells (OHCs) and Deiters' cells (DCs) demonstrated extremely weak staining (F). 0.4 % AgNPs enhanced the staining in the OHCs and DCs but not in the SBCs, SLFs, SGCs, IHCs, and PCs (A, C, and E). Comparisons of staining intensity are shown in G and H. Scale bar = 50 μ m in A–D and 20 μ m in E and F. (JPG 4393 kb)

Additional file 3: Figure S3. MCP2⁺ cells in the rat cochlea 7 days post-intratympanic injection of 0.4 % AgNPs shown by immunofluorescence confocal microscopy or immunohistochemistry. In the cochleae exposed to dH₂O, the strial basal cells (SBCs), spiral ligament fibrocytes (SLFs), spiral ganglion cells (SGCs), and hair cells (HCs), pillar cells (PCs), and Deiters' cells (DCs) of Corti's organ (CO) showed intensive staining (B, D, and F). 0.4 % AgNPs had no influence on the staining in the SBCs, SLFs, SGCs, and CO (A, C, and E). Comparisons of staining intensity are shown in G and H. Scale bar = 50 μ m in A–D and 20 μ m in E and F. (JPG 4614 kb)

Additional file 4: Figure S4. Rac1⁺ cells in the rat cochlea 7 days post-intratympanic injection of 0.4 % AgNPs shown by immunofluorescence confocal microscopy or immunohistochemistry. In the cochleae exposed to dH₂O, the strial intermediate cells (SIMCs), strial basal cells (SBCs), spiral ganglion cells (SGCs), and hair cells (HCs), pillar cells (PCs), and Deiters' cells (DCs) of Corti's organ (CO) showed intensive staining (B, D, and F), while the spiral ligament fibrocytes (SLFs) (mainly type II) demonstrated moderate staining (B). 0.4 % AgNPs had no influence on the staining in the SIMCs, SBCs, SLFs, SGCs, and CO (A, C, and E). Comparisons of staining intensity are shown in G and H. Scale bar = 50 μ m in A–D and 20 μ m in E and F. (JPG 4501 kb)

Additional file 5: Figure S5. Myosin light chain positively stained cells in the rat cochlea 7 days post-intratympanic injection of 0.4 % AgNPs shown by immunofluorescence confocal microscopy or immunohistochemistry. In the cochleae exposed to dH₂O, the spiral ganglion cells (SGCs) and inner pillar cells (IPCs) of Corti's organ (CO) showed moderate staining (D and F), while the inner hair cells (IHCs), outer pillar cells (OPCs), outer hair cells (OHCs), and Deiters' cells (DCs) demonstrated mild staining (F). The strial basal cells (SBCs) and spiral ligament fibrocytes (SLFs) exhibited extremely weak staining (B). 0.4 % AgNPs had no influence on the staining in the SBCs, SLFs, SGCs, and CO (A, C, and E). Scale bar = 50 μ m in A–D and 20 μ m in E and F. (JPG 4602 kb)

Additional file 6: Figure S6. VCAM1⁺ cells in the rat cochlea 7 days post-intratympanic injection of 0.4 % AgNPs shown by immunofluorescence confocal microscopy or immunohistochemistry. In the cochleae exposed to dH₂O, the strial basal cells (SBCs), spiral ligament fibrocytes (SLFs), spiral ganglion cells (SGCs), and hair cells (HCs), pillar cells (PCs), and Deiters' cells (DCs) of Corti's organ (CO) showed extremely weak staining (B, D, and F). 0.4 % AgNPs had no influence on the staining in the SBCs, SLFs, SGCs, and CO (A, C, and E). Scale bar = 30 μ m. (JPG 4582 kb)

Additional file 7: Figure S8. JNK⁺ and p38⁺ cells in the rat cochlea 7 days post-intratympanic injection of 0.4 % AgNPs shown by immunofluorescence confocal microscopy or immunohistochemistry. In the cochleae exposed to dH₂O, the strial basal cells (SBCs), spiral ligament fibrocytes (SLFs), spiral ganglion cells (SGCs), and hair cells (HCs), pillar cells (PCs), and Deiters' cells (DCs) of Corti's organ (CO) showed extremely weak staining for JNK (B, F, and J) and p38 (D, H, and L). 0.4 % AgNPs had no influence on the staining of JNK (A, E, and I) and p38 (C, G, and K) in the SBCs, SLFs, SGCs, and CO. Scale bar = 50 μ m in A–H and 20 μ m in I–L. (JPG 4719 kb)

Additional file 8: Figure S7. Erk1/2⁺ cells in the rat cochlea 7 days post-intratympanic injection of 0.4 % AgNPs shown by immunofluorescence confocal microscopy or immunohistochemistry. In the cochleae exposed to dH₂O, the strial intermediate cells (SIMCs), strial basal cells (SBCs), spiral ligament fibrocytes (SLFs), spiral ganglion cells (SGCs), and hair cells (HCs), pillar cells (PCs), and Deiters' cells (DCs) of Corti's organ (CO) showed intensive staining (B, D, and F). 0.4 % AgNPs had no influence on the staining in the SIMCs, SBCs, SLFs, SGCs, and CO (A, C, and E). Comparisons of staining intensity are shown in G and H. Scale bar = 50 μ m in A–D and 20 μ m in E and F. (JPG 4418 kb)

Additional file 9: Figure S9. TNF- α ⁺, TNFR1⁺, and TNFR2⁺ cells in the rat cochlea 7 days post-intratympanic injection of 0.4 % AgNPs shown by immunofluorescence confocal microscopy or immunohistochemistry. In the cochleae exposed to dH₂O, the spiral ganglion cells (SGCs), inner hair cells (IHCs), and inner pillar cells (IPCs) of Corti's organ (CO) showed mild staining for TNF- α (B and N), while the striae basal cells (SBCs), spiral ligament fibrocytes (SLFs), outer pillar cells (OPCs), outer hair cells (OHCs), and Deiters' cells (DCs) demonstrated extremely weak staining for TNF- α (B and N). The striae intermediate cells (SIMCs), SBCs, and SGCs exhibited mild staining for TNFR1 (D and J), while the SLFs, hair cells (HCs), pillar cells (PCs), and DCs displayed extremely weak staining for TNFR1 (D and P). The SIMCs and SBCs showed mild staining for TNFR2 (F), while the SLFs, SGCs, HCs, PCs, and DCs showed extremely weak staining for TNFR2 (F, L, and R). 0.4 % AgNPs had no influence on the staining of TNF- α (A, G, and M), TNFR1 (C, I, and O), and TNFR2 (E, K, and Q) in the SIMCs, SBCs, SLFs, SGCs, and CO. Scale bar = 30 μ m. (JPG 4651 kb)

Additional file 10: Figure S10. IL-1 β ⁺ cells in the rat cochlea 7 days post-intratympanic injection of 0.4 % AgNPs shown by immunofluorescence confocal microscopy or immunohistochemistry. In the cochleae exposed to dH₂O, the striae basal cells (SBCs), spiral ganglion cells (SGCs), and pillar cells (PCs) of Corti's organ (CO) showed intensive staining, while the spiral ligament fibrocytes (SLFs) (mainly type II) and inner hair cells (IHCs) demonstrated mild staining (B, D, and F). The outer hair cells (OHCs) and Deiters' cells (DCs) exhibited extremely weak staining (F). 0.4 % AgNPs had no influence on the staining in the SBCs, SLFs, SGCs, and CO (A, C, and E). Comparisons of staining intensity are shown in G and H. Scale bar = 50 μ m in A–D and 20 μ m in E and F. (JPG 4326 kb)

Additional file 11: Figure S11. IL-10⁺ and TGF- β ⁺ cells in the rat cochlea 7 days post-intratympanic injection of 0.4 % AgNPs shown by immunofluorescence confocal microscopy or immunohistochemistry. In the cochleae exposed to dH₂O, the spiral ganglion cells (SGCs) showed intensive staining for IL-10 (J). The striae basal cells (SBCs), spiral ligament fibrocytes (SLFs), hair cells (HCs), and Deiters' cells (DCs) exhibited extremely weak staining for IL-10 (B and J). The SGCs and PCs of CO displayed intensive staining for TGF- β (H and L), while the SBCs, SLFs, and inner hair cells (IHCs) demonstrated mild staining for TGF- β (D and L). The outer hair cells (OHCs) and DCs showed extremely weak staining for TGF- β (L). 0.4 % AgNPs had no influence on the staining of IL-10 (A, E, and I) and TGF- β (C, G, and K) in the SBCs, SLFs, SGCs, and CO. Comparisons of staining intensity are shown in M and N. Scale bar = 50 μ m in A–H and 20 μ m in I–L. (JPG 4356 kb)

Additional file 12: Figure S12. Negative control. Scale bar = 50 μ m in A and C, 20 μ m in E, and 30 μ m in B, D, and F. (JPG 3915 kb)

Abbreviations

AgNPs: silver nanoparticles; DAMP: danger/damage-associated molecular pattern; Erk1/2: extracellular signal-regulated kinases 1/2; IL-10: interleukin-10; IL-1 β : interleukin-1 β ; JNK1/2/3: c-Jun N-terminal kinases 1/2/3; MCPs: monocyte chemoattractant proteins; NF- κ B: nuclear factor- κ B; PAMP: pathogen-associated molecular pattern; PRR: pattern recognition receptor; RNF11: RING finger protein 11; SBCs: striae basal cells; SGCs: spiral ganglion cells; SLFs: spiral ligament fibrocytes; TGF- β : transforming growth factor- β ; TLR2/4: toll-like receptors 2/4; TNFRs: tumour necrosis factor receptors; TNF- α : tumour necrosis factor- α ; VCAM1: vascular cell adhesion molecule 1.

Competing Interests

The authors declare that they have no competing interests.

Authors' Contributions

JZ conceived and designed the experiments. HF performed the experiments. HF and JZ analysed the data and wrote the paper. JZ and IP edited the paper. All authors read and approved the final manuscript.

Acknowledgements

This study was supported by the European Union 7th Framework Programme large-scale integrating project NanoValid (contract: 263147).

Received: 3 March 2016 Accepted: 13 April 2016

Published online: 04 May 2016

References

- Zou J, Feng H, Mannerstrom M, Heinonen T, Pyykko I (2014) Toxicity of silver nanoparticle in rat ear and BALB/c 3T3 cell line. *J Nanobiotechnology* 12:52
- Zou J, Hannula M, Misra S, Feng H, Labrador RH, Aula AS et al (2015) Micro CT visualization of silver nanoparticles in the middle and inner ear of rat and transportation pathway after transtympanic injection. *J Nanobiotechnology* 13:5
- Feng H, Pyykko I, Zou J (2015) Hyaluronan up-regulation is linked to renal dysfunction and hearing loss induced by silver nanoparticles. *Eur Arch Otorhinolaryngol* 272:2629–2642
- Termeer C, Benedix F, Sleeman J, Fieber C, Voith U, Ahrens T et al (2002) Oligosaccharides of hyaluronan activate dendritic cells via toll-like receptor 4. *J Exp Med* 195:99–111
- Sloane JA, Batt C, Ma Y, Harris ZM, Trapp B, Vartanian T (2010) Hyaluronan blocks oligodendrocyte progenitor maturation and remyelination through TLR2. *Proc Natl Acad Sci U S A* 107:11555–11560
- Swaidani S, Cheng G, Lauer ME, Sharma M, Mikecz K, Hascall VC et al (2013) TSG-6 protein is crucial for the development of pulmonary hyaluronan deposition, eosinophilia, and airway hyperresponsiveness in a murine model of asthma. *J Biol Chem* 288:412–422
- Tolg C, McCarthy JB, Yazdani A, Turley EA (2014) Hyaluronan and RHAMM in wound repair and the “cancerization” of stromal tissues. *Biomed Res Int* 2014:103923
- Elson G, Dunn-Siegrist I, Daubeuf B, Pugin J (2007) Contribution of Toll-like receptors to the innate immune response to Gram-negative and Gram-positive bacteria. *Blood* 109:1574–1583
- Schmidt M, Raghavan B, Muller V, Vogl T, Fejer G, Tchaptchet S et al (2010) Crucial role for human Toll-like receptor 4 in the development of contact allergy to nickel. *Nat Immunol* 11:814–819
- Jones BW, Means TK, Heldwein KA, Keen MA, Hill PJ, Belisle JT et al (2001) Different Toll-like receptor agonists induce distinct macrophage responses. *J Leukoc Biol* 69:1036–1044
- Castranova V (2004) Signaling pathways controlling the production of inflammatory mediators in response to crystalline silica exposure: role of reactive oxygen/nitrogen species. *Free Radic Biol Med* 37:916–925
- Zhou H, Zhao K, Li W, Yang N, Liu Y, Chen C et al (2012) The interactions between pristine graphene and macrophages and the production of cytokines/chemokines via TLR- and NF- κ B-related signaling pathways. *Biomaterials* 33:6933–6942
- Lee EG, Boone DL, Chai S, Libby SL, Chien M, Lodolce JP et al (2000) Failure to regulate TNF-induced NF- κ B and cell death responses in A20-deficient mice. *Science* 289:2350–2354
- Boone DL, Turer EE, Lee EG, Ahmad RC, Wheeler MT, Tsui C et al (2004) The ubiquitin-modifying enzyme A20 is required for termination of Toll-like receptor responses. *Nat Immunol* 5:1052–1060
- Liew FY, Xu D, Brint EK, O'Neill LA (2005) Negative regulation of toll-like receptor-mediated immune responses. *Nat Rev Immunol* 5:446–458
- Gon Y, Asai Y, Hashimoto S, Mizumura K, Jibiki I, Machino T et al (2004) A20 inhibits toll-like receptor 2- and 4-mediated interleukin-8 synthesis in airway epithelial cells. *Am J Respir Cell Mol Biol* 31:330–336
- Guedes RP, Csizmadia E, Moll HP, Ma A, Ferran C, da Silva CG (2014) A20 deficiency causes spontaneous neuroinflammation in mice. *J Neuroinflammation* 11:122
- Dalal NV, Pranski EL, Tansey MG, Lah JJ, Levey AI, Betarbet RS (2012) RNF11 modulates microglia activation through NF- κ B signalling cascade. *Neurosci Lett* 528:174–179
- Shembade N, Parvatiyar K, Harhaj NS, Harhaj EW (2009) The ubiquitin-editing enzyme A20 requires RNF11 to downregulate NF- κ B signalling. *EMBO J* 28:513–522
- Hollingsworth JW, Li Z, Brass DM, Garantzios S, Timberlake SH, Kim A et al (2007) CD44 regulates macrophage recruitment to the lung in lipopolysaccharide-induced airway disease. *Am J Respir Cell Mol Biol* 37:248–253
- Beck-Schimmer B, Oertli B, Pasch T, Wuthrich RP (1998) Hyaluronan induces monocyte chemoattractant protein-1 expression in renal tubular epithelial cells. *J Am Soc Nephrol* 9:2283–2290

22. Deshmane SL, Kremlev S, Amini S, Sawaya BE (2009) Monocyte chemoattractant protein-1 (MCP-1): an overview. *J Interferon Cytokine Res* 29:313–326
23. Moon SK, Woo JI, Lee HY, Park R, Shimada J, Pan H et al (2007) Toll-like receptor 2-dependent NF-kappaB activation is involved in nontypeable *Haemophilus influenzae*-induced monocyte chemotactic protein 1 up-regulation in the spiral ligament fibrocytes of the inner ear. *Infect Immun* 75:3361–3372
24. Woo JI, Pan H, Oh S, Lim DJ, Moon SK (2010) Spiral ligament fibrocyte-derived MCP-1/CCL2 contributes to inner ear inflammation secondary to nontypeable *H. influenzae*-induced otitis media. *BMC Infect Dis* 10:314
25. Golias C, Tsoutsis E, Matziridis A, Makridis P, Batistatou A, Charalabopoulos K (2007) Review. Leukocyte and endothelial cell adhesion molecules in inflammation focusing on inflammatory heart disease. *In Vivo* 21:757–769
26. Cook-Mills JM (2002) VCAM-1 signals during lymphocyte migration: role of reactive oxygen species. *Mol Immunol* 39:499–508
27. Bruewer M, Hopkins AM, Hobert ME, Nusrat A, Madara JL (2004) RhoA, Rac1, and Cdc42 exert distinct effects on epithelial barrier via selective structural and biochemical modulation of junctional proteins and F-actin. *Am J Physiol Cell Physiol* 287:C327–C335
28. Griffiths GS, Grundl M, Allen JS 3rd, Matter ML (2011) R-Ras interacts with filamin A to maintain endothelial barrier function. *J Cell Physiol* 226:2287–2296
29. Tsukamoto O, Kitakaze M (2013) Biochemical and physiological regulation of cardiac myocyte contraction by cardiac-specific myosin light chain kinase. *Circ J* 77:2218–2225
30. Colombara M, Antonini V, Riviera AP, Mainiero F, Strippoli R, Merola M et al (2005) Constitutive activation of p38 and ERK1/2 MAPKs in epithelial cells of myasthenic thymus leads to IL-6 and RANTES overexpression: effects on survival and migration of peripheral T and B cells. *J Immunol* 175:7021–7028
31. Cheng Q, Fan H, Ngo D, Beaulieu E, Leung P, Lo CY et al (2013) GILZ overexpression inhibits endothelial cell adhesive function through regulation of NF-kappaB and MAPK activity. *J Immunol* 191:424–433
32. Mitchell AJ, Roediger B, Weninger W (2014) Monocyte homeostasis and the plasticity of inflammatory monocytes. *Cell Immunol* 291:22–31
33. Mills CD, Kincaid K, Alt JM, Heilman MJ, Hill AM (2000) M-1/M-2 macrophages and the Th1/Th2 paradigm. *J Immunol* 164:6166–6173
34. Mantovani A, Sica A, Sozzani S, Allavena P, Vecchi A, Locati M (2004) The chemokine system in diverse forms of macrophage activation and polarization. *Trends Immunol* 25:677–686
35. Hadrup N, Lam HR (2014) Oral toxicity of silver ions, silver nanoparticles and colloidal silver—a review. *Regul Toxicol Pharmacol* 68:1–7
36. Harris JP, Tomiyama S (1987) Experimental immune system of the inner ear. *ORL J Otorhinolaryngol Relat Spec* 49:225–233
37. Zhang W, Dai M, Fridberger A, Hassan A, Degagne J, Neng L et al (2012) Perivascular-resident macrophage-like melanocytes in the inner ear are essential for the integrity of the intrastrial fluid-blood barrier. *Proc Natl Acad Sci U S A* 109:10388–10393
38. O'Malley JT, Nadol JB, McKenna MJ Jr (2016) Anti CD163+, Iba1+, and CD68+ cells in the adult human inner ear: normal distribution of an unappreciated class of macrophages/microglia and implications for inflammatory otopathology in humans. *Otol Neurotol* 37:99–108
39. Hirose K, Discolo CM, Keasler JR, Ransohoff R (2005) Mononuclear phagocytes migrate into the murine cochlea after acoustic trauma. *J Comp Neurol* 489:180–194
40. Tornabene SV, Sato K, Pham L, Billings P, Keithley EM (2006) Immune cell recruitment following acoustic trauma. *Hear Res* 222:115–124
41. Sato E, Shick HE, Ransohoff RM, Hirose K (2010) Expression of fractalkine receptor CX3CR1 on cochlear macrophages influences survival of hair cells following ototoxic injury. *J Assoc Res Otolaryngol* 11:223–234
42. Hirose K, Li SZ, Ohlemiller KK, Ransohoff RM (2014) Systemic lipopolysaccharide induces cochlear inflammation and exacerbates the synergistic ototoxicity of kanamycin and furosemide. *J Assoc Res Otolaryngol* 15:555–570
43. Matheny HE, Deem TL, Cook-Mills JM (2000) Lymphocyte migration through monolayers of endothelial cell lines involves VCAM-1 signaling via endothelial cell NADPH oxidase. *J Immunol* 164:6550–6559
44. Sun C, Wu MH, Yuan SY (2011) Nonmuscle myosin light-chain kinase deficiency attenuates atherosclerosis in apolipoprotein E-deficient mice via reduced endothelial barrier dysfunction and monocyte migration. *Circulation* 124:48–57
45. Rom S, Fan S, Reichenbach N, Dykstra H, Ramirez SH, Persidsky Y (2012) Glycogen synthase kinase 3beta inhibition prevents monocyte migration across brain endothelial cells via Rac1-GTPase suppression and down-regulation of active integrin conformation. *Am J Pathol* 181:1414–1425
46. So H, Kim H, Lee JH, Park C, Kim Y, Kim E et al (2007) Cisplatin cytotoxicity of auditory cells requires secretions of proinflammatory cytokines via activation of ERK and NF-kappaB. *J Assoc Res Otolaryngol* 8:338–355
47. Rio C, Dikkes P, Liberman MC, Corfas G (2002) Glial fibrillary acidic protein expression and promoter activity in the inner ear of developing and adult mice. *J Comp Neurol* 442:156–162
48. Ladrech S, Wang J, Simonneau L, Puel JL, Lenoir M (2007) Macrophage contribution to the response of the rat organ of Corti to amikacin. *J Neurosci Res* 85:1970–1979
49. Sun S, Yu H, Yu H, Honglin M, Ni W, Zhang Y et al (2015) Inhibition of the activation and recruitment of microglia-like cells protects against neomycin-induced ototoxicity. *Mol Neurobiol* 51:252–267
50. Ashley JW, Shi Z, Zhao H, Li X, Kesterson RA, Feng X (2011) Genetic ablation of CD68 results in mice with increased bone and dysfunctional osteoclasts. *PLoS One* 6:e25838
51. Jiao H, Zhang Y, Yan Z, Wang ZG, Liu G, Minshall RD et al (2013) Caveolin-1 Tyr14 phosphorylation induces interaction with TLR4 in endothelial cells and mediates MyD88-dependent signaling and sepsis-induced lung inflammation. *J Immunol* 191:6191–6199

Submit your manuscript to a SpringerOpen® journal and benefit from:

- Convenient online submission
- Rigorous peer review
- Immediate publication on acceptance
- Open access: articles freely available online
- High visibility within the field
- Retaining the copyright to your article

Submit your next manuscript at ► springeropen.com